FINAL REPORT NO. 111
February 1, 1964

MASS, MOMENTUM, AND HEAT TRANSFER WITHIN A TURBULENT BOUNDARY LAYER WITH FOREIGN GAS MASS TRANSFER AT THE SURFACE

PART I—CONSTANT FLUID PROPERTIES

by
Robert M. Kendall
Morris W. Rubesin
Thomas J. Dahm
Michael R. Mendenhall

prepared for
OFFICE OF NAVAL RESEARCH, WASHINGTON, D. C.
and
ADVANCED RESEARCH PROJECTS AGENCY, WASHINGTON, D. C.

Contract No. Nonr 3997(00)
ARPA Order No. 322
Project Code No. 2740

Vidya Project No. 9057

RESEARCH DEVELOPMENT

A DIVISION OF Itek CORPORATION

व VIDYA

The word Vidya, taken from the Vedanta philosophy of the Hindus, means knowledge. The symbol used to denote the Vidya organization is the letter "V" from Sanskrit, the ancient language of India.

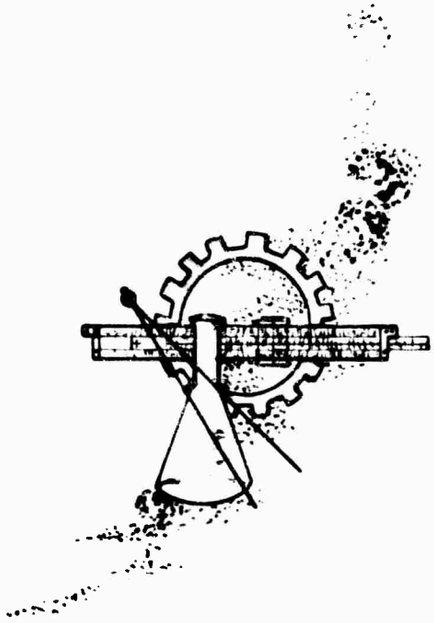

APPLIED MECHANICS
THERMODYNAMICS
NUMERICAL ANALYSIS
PHOTO-OPTICS
IMAGE ANALYSIS
PHYSICS

VIDYA COPY NO 307

FINAL REPORT NO. 111

February 1, 1964

MASS, MOMENTUM, AND HEAT TRANSFER WITHIN A TURBULENT BOUNDARY LAYER WITH FOREIGN GAS MASS TRANSFER AT THE SURFACE

PART I – CONSTANT FLUID PROPERTIES

by

Robert M. Kendall
Morris W. Rubesin
Thomas J. Dahm
Michael R. Mendenhall

prepared for

OFFICE OF NAVAL RESEARCH, WASHINGTON, D. C.
and
ADVANCED RESEARCH PROJECTS AGENCY, WASHINGTON, D. C.

Contract No. Nonr 3997(00)
ARPA Order No. 322
Project Code No. 2740

Vidya Project No. 9057

This research is a part of Project DEFENDER sponsored by the Advanced Research Projects Agency, Department of Defense, and technically administered by the Fluid Dynamics Branch of the Office of Naval Research.

VIDYA

A DIVISION OF Itek CORPORATION

1450 PAGE MILL ROAD • PALO ALTO, CALIFORNIA
TEL: DAVENPORT 1-2455 TWX: 415 492-9270

ABSTRACT

A critical reexamination is made of existing experimental data on the velocity, temperature, and concentration profiles in a low-speed, constant property turbulent boundary layer with surface mass injection. It is found that a model of the boundary layer can be constructed that fits the local profile data as well as the local drag, mass, and heat-transfer coefficients at the surface. The essential features of the model include a "law of the wall" that provides a continuous and smooth profile from the surface to the fully turbulent region and a "wake region" that joins the inner region smoothly and is characterized by an eddy diffusivity that is constant with respect to distance from the wall. Four empirical parameters appear in the analysis: the Prandtl mixing length constant, K; the Clauser eddy diffusivity Reynolds number; an inner region mixing length constant analogous to Rotta's intercept constant; and a value of turbulent Schmidt or Prandtl number. Constant values of these parameters are found to be suitable in predicting data over a wide range of surface blowing or suction and Reynolds number.

BLANK PAGE

TABLE OF CONTENTS

LIST OF FIGURES

LIST OF SYMBOLS

		Units
a_n	parameters defined on page 2-40	L^2/θ
C_f	local skin-friction coefficient	
$\overline{C_f}$	average skin-friction coefficient	
C_H or St	local Stanton number, $q_o/\rho_1 u_1 (h_r - h_o)$	
C_M	local mass-transfer coefficient, $j_o/\rho_1 u_1 (\omega_1 - \omega_c)$	
C_p	specific heat	FL/MT
$\overline{C_p}$	specific heat of gaseous mixture = $\sum C_{p_i} \omega_i$	FL/MT
C_{p_i}	specific heat of specie i	FL/MT
D^*	binary diffusion coefficient in binary gas with corstant properties	L^2/θ
D^*_{ij}	binary diffusion coefficient of specie i in specie j	L^2/θ
D_i^T	thermal diffusion coefficient of specie i	$M/L\theta$
f	stream function defined in Equation (2-122)	
g	parameter defined in Equation (2-112)	
H	boundary-layer shape factor, δ^*/θ	
h	enthalpy of gaseous mixture	FL/M, L^2/θ^2
h_i	enthalpy of specie i	FL/M, L^2/θ^2
h_t	total enthalpy = h + $(u^2/2)$	L^2/θ^2
j_i	mass diffusion flux of specie i caused by molecular motion relative to mean mass flux	$M/L^2\theta$
k	thermal conductivity	$F/\theta T$
k_T	thermal diffusion ratio	
ℓ	mixing length	I
M	Mach number	
m_i	molecular weight of specie i	M/N
Pr	Prandtl number, $\mu C_p/R$	
Pr'	turbulent Prandtl number, ϵ_M/ϵ_H	

q	local convective heat flux	$FL/\theta L^2$
R	universal gas constant per mole	FL/NT
Re_x	Reynolds number gased on length of run	
Re_{δ^*}	Reynolds number based on displacement thickness	
Re_θ	Reynolds number based on momentum thickness	
Re_ξ	Reynolds number based on energy thickness	
r	ratio of actual injection rate at a station to average injection rate over surface	
Sc	Schmidt number, $\nu/$ *	
Sc'	turbulent Schmidt number, ϵ_M/ϵ_D	
T	temperature	T
u	velocity in x-direction	L/θ
u_τ	shear velocity, $\sqrt{\tau_o/\rho_1}$	L/θ
v	velocity in y-direction	L/θ
x	coordinate parallel to surface	L
x_i	mole fraction of specie i	
y	coordinate normal to surface	L
α	binary thermal diffusion factor	
Γ	mass or concentration thickness of full boundary layer	L
Γ_y	mass or concentration thickness contribution of boundary layer between y = 0 and y = y (Eq. (2-46))	L
δ	boundary-layer thickness	L
δ^*	displacement thickness of full boundary layer	L
δ_b	laminar sublayer plus buffer region thickness	L
δ_ℓ	laminar sublayer	L
δ_t	sublayer, buffer layer, and turbulent layer thickness	L
δ^*_y	displacement thickness contribution of boundary layer between y = 0 and y = y (Eq. (2-44)	L

ϵ_D	eddy diffusion coefficient in binary mixture	L^2/θ
ϵ_{D_i}	eddy diffusion coefficient of specie i (defined by Eq. (2-2))	L^2/θ
ϵ_H	eddy thermal conductivity of gaseous mixture (see Eq. (2-11))	L^2/θ
ϵ_M	eddy viscosity or eddy diffusivity	L^2/θ
ζ	injection parameter (defined on p. 1-6)	
η	coordinate normal to surface	
υ	momentum thickness of full boundary layer	L
θ_y	momentum thickness contribution of boundary layer between $y = 0$ and $y = y$ (Eq. (2-45))	L
κ	constant	
μ	viscosity	$M/\theta L$, $F\theta/L^2$
ν	kinematic viscosity	L^2/θ
ξ	thermal boundary-layer thickness of full boundary layer	L
ξ_y	thermal energy thickness contribution of boundary layer between $y = 0$ and $y = y$ (Eq. (2-47))	L
ρ	density	M/L^2
τ	local shear in the boundary layer	F/L^2
ψ_i	rate of mass generation of specie i by chemical reactions per unit volume	$M/L^3\theta$
ω_i	concentration (mass fraction) of specie i	M/M

Subscripts

o	at the surface, or zero mass transfer at the surface
1	at the outer edge of the boundary layer
1-D	one dimensional
a	specie designation is binary system or at interface
b	specie designation in binary system
c	on surface of a cone

s	slip at the surface
t	total

Superscripts

'	turbulent fluctuating quantity
$\bar{}$	time averaged quantity, $\bar{A} = \frac{1}{\theta}\int_0^{\theta} A\, d\theta$
+	normalized as indicated in Equations (2-31) to (2-36)
~	normalized with respect to edge quantity (e.g., $\tilde{T} = \frac{T - T_o}{T_1 - T_o}$, $\tilde{u} = \frac{u}{u_1}$)

Units

F	force
L	length
M	mass
N	number of moles
T	temperature
θ	time

BLANK PAGE

MASS, MOMENTUM, AND HEAT TRANSFER WITHIN A TURBULENT BOUNDARY LAYER WITH FOREIGN GAS MASS TRANSFER AT THE SURFACE

1. INTRODUCTION

The most effective current techniques for thermally protecting missile nose cones or manned reentry vehicles from aerodynamic heating, namely, techniques involving ablation or transpiration cooling, are characterized by a mass transfer of gas through the surface of the body. Because of this mass transfer and the attendant surface roughness of ablating surfaces or porous skins, turbulent boundary layers can be expected to exist on the surfaces of reentry vehicles even at the Reynolds numbers corresponding to rather shallow reentry angles. Thus, an understanding of the behavior of turbulent boundary layers under the conditions of reentry and with simultaneous surface mass transfer is of considerable importance in the design of reentry body thermal protection systems. In addition, this understanding is essential in the prediction of electromagnetic radiation emission or of radar reflectivity from the boundary layer or the initial stages of the wake.

When an examination is made of the published literature on this subject, it becomes apparent that rather tenuous extrapolations of tests of limited scope and of early heuristic theories have been made to predict the behavior of the dynamically complex, chemically reacting flows about the reentry bodies. The work contained in this report constitutes a reexamination of the problem, with the intent of arriving at a model of the t rbulent boundary layer that is entirely consistent with data obtained under successively more complex situations.

1.1 Historical Review

Before a review is made of the historical background of the current research, it will be worthwhile to present a description of the general structure of the turbulent boundary layer as it is presently understood. This will provide the reader with the hindsight the authors enjoyed while performing this cr tical reexamination, and will clarify some of the approaches taken in the analysis. The structure of the turbulent boundary layer is described in detail in References 1 and 2 and is summarized in the following sections.

1.1.1 General description of the turbulent boundary-layer structure

Generally, the boundary layer can be considered to be divided into four successive layers from the surface to the outer edge.

(a) The layer closest to the surface is the "laminar sublayer" or the "viscous layer." This layer is characterized by shear stresses that are predominately caused by molecular viscosity. The flow here need not be steady, but can fluctuate as a result of turbulence in the layers above. Where no mass transfer occurs normal to the surface, the time-averaged shear in this layer is essentially constant with distance from the surface.

(b) The next layer away from the surface is the "buffer layer." In this layer, the shear stress is dependent on both the molecular viscosity and the turbulent motion (Reynolds stresses). Again, with no surface mass transfer, the time-averaged shear stress in this layer is essentially constant with distance from the surface. The term "buffer layer" was employed originally by von Kármán to indicate the presence of this layer between a completely laminar and a completely turbulent layer.

(c) The third layer from the surface is called "fully turbulent region." In this layer, the shear stress is dependent primarily on the turbulent motions. The velocity distributions in this layer have been shown experimentally to be dependent on the local wall conditions, and rather insensitive to the local boundary-layer thickness or pressure gradients. This has led Coles to apply the term "law of the wall" to describe this layer, together with layers (a) and (b), above, References 3 and 4.

(d) The fourth layer is also fully turbulent; however, this layer's characteristics are controlled more by the boundary-layer thickness than the local shear at the wall. The flow in this region is generally characterized by eddies that are similar to those that exist in wakes and, thus, Coles could represent the velocity in this region for nonporous walls by a "law of the wake," Reference 4. Others, References 5 and 6, have applied the term "velocity decrement law" to velocity correlations for this same region.

The relative thickness of the four layers described above are indicated in Figure 1, reproduced from Reference 2. The values shown in this figure correspond to a turbulent boundary layer on a nonporous flat plate in low-speed flow, where the properties in the boundary layer are essentially constant, and where the Blasius skin-friction law is applicable. It reveals that the relative thicknesses of the inner layers diminish with increases in the local length Reynolds number. At $Re_x = 10^8$, the boundary-layer law of

the wall applies over only 5 percent of the thickness of the boundary layer, while the wake region occupies 95 percent of the boundary layer. When consideration is made that heat and mass transfer within the boundary layer with Prandtl numbers and Schmidt numbers less than unity result in larger thicknesses of the diffusional boundary layers relative to the flow or momentum exchange boundary layers, the presence of the wake-type flow becomes even more important and requires consideration at lower Reynolds numbers. Also, surface injection tends to increase the boundary-layer thickness which may force a consideration of the wake layers at lower length Reynolds numbers than indicated in Figure 1.

1.1.2 Early contributions

In the late 1940's and early 1950's, a need arose for more effective cooling systems for missile surfaces experiencing aerodynamic heating through turbulent boundary layers. It was known then, from research with laminar boundary layers, that "transpiration" of gas at a surface was a very effective cooling mechanism, Reference 7. Because a qualitatively similar effectiveness was expected to occur with the turbulent boundary layer, research began on this subject at MIT, and then independently, a few years later, at Convair and the Ames Laboratory of the NACA (now NASA).

The MIT work, under the direction of H. S. Mickley, was largely experimental during its early periods, Reference 8. This excellent work has continued to this day, References 9 through 15 and 17 through 20, and provides the bases for many of the deductions of this report that are discussed in detail later. Reference 9 served as the basis for the empirical parameters of the early heuristic theories described in the following paragraphs.

To satisfy the needs for effective missile cooling systems, the speculative analyses of References 21 and 22 were performed to yield indications of the effect of surface mass transfer of air under supersonic conditions where the then existent MIT data of Reference 9 did not apply directly. Reference 21 employed the classical Prandtl mixing-length theory, with variable density, across the entire boundary layer on a flat plate. Thus, the viscous sublayer, the buffer layer, and the wake regions were not considered. In addition, both the laminar and turbulent Prandtl numbers were set equal to unity in the energy equation. The local shear stress distribution in the boundary layer was modified to account for the surface mass transfer; that is, the local shear stress was expressed as

$$\tau = \tau_o + (\rho v)_o u \qquad (1\text{-}1)$$

The omission of the wake region resulted in the mathematical requirement of a continual increase of shear stress with distance away from the wall[1] even with the known boundary condition that the average shear stress must approach zero at the outer edge of the boundary layer. Implicit here was the hope that the equally erroneous ever increasing mixing length, $\ell = ky$, somehow compensated to yield adequate velocity distribution near the outer edge of the boundary layer. The closed-form solution for the velocity distribution in the turbulent region obtained in this analysis could, by an adjustment of the arbitrary constants of integration, be made to fit the compressible analog of the classic logarithmic velocity distribution for the case of zero blowing, that is, Reference 23. Thus, an additional implied assumption was made that the "constants" of integration were not dependent, themselves, on the blowing rate.

An analysis based on the identical physical assumptions as in Reference 21 was performed independently in Reference 24, except that the latter investigation was restricted to constant fluid properties. Again, Reference 9 was used as the experimental basis for comparison. It was found that the theory generally predicted the trends in the data on boundary-layer growth and skin friction (to $\approx$ 25 percent); however, the predicted and measured velocity profiles disagreed considerably in shape.

To account for the Prandtl numbers other than unity in the heat-transfer rates, Reference 22 added a laminar sublayer to the fully turbulent outer region, again characterized by the Prandtl mixing-length theory and the shear distribution represented in Equation (1-1). The omission of a buffer layer caused a discontinuity in the slope of the velocity profile to occur at the interface of the sublayer and fully turbulent regions. It was found that the thickness of the sublayer was an important parameter, and recourse to the low-speed data of Reference 9 was made to define a realistic hypothesis for the sublayer thickness. The results of Reference 22, while yielding quantitative results on the expected reduction in surface heat-transfer rates that agreed fairly well with subsequent experimental data, Reference 25, never yielded satisfying results concerning the velocity and temperature profiles over the entire boundary layer or of the temperature or enthalpy recovery factor. The theory showed an ever increasing value of recovery factor with

[1] The term u in Equation (1-1) increases monotonically with distance from the surface.

increasing length Reynolds number that was not evident in the zero and finite blowing-rate data. Significantly, no consistent Mach number effect was evident in the theoretical results, and the tests of Reference 25 did not contribute information regarding these Mach number effects, as they were conducted at a single Mach number, M = 2.7. Later it was indicated, Reference 26, that the theory of Reference 22 agreed to about ±25 percent with the skin-friction data obtained at M = 5.1 from boundary-layer velocity surveys. This agreement appears, in retrospect, to have been fortuitous because the skin-friction data were obtained from an extrapolation of velocity distribution measurements toward the surface, usually a rather inaccurate technique with probes as large as the conventional impact pressure tubes (see Analysis).

Theories similar to Reference 22 were developed for the case of injection of a single foreign gas into undissociated air, References 27 and 28. These theories were further restricted, however, to changes in the physical properties of the binary mixture caused only by concentration variations of the individual gases and did not include chemical reactions, temperature, or compressibility effects. In general, these theories indicated the marked effectiveness of light gas to reduce heat transfer and skin friction at the surface but, in general, possessed the shortcomings of Reference 22. Further, Reference 28 only yielded the relationship between heat transfer and skin friction, but not an explicit value of either term.

When the skin-friction data of Reference 29 were obtained, it was found that the results agreed qualitatively with the theory of Reference 27, in that the transpiration of lighter gases was more effective in reducing skin friction. The data also showed that the theories of References 21 and 22 failed to predict quantitatively the Mach number effect indicated in the data, and that the agreement of the predictions of Reference 22 with earlier data was fortuitous, as the data were obtained at a Mach number of 2.7 where agreement happened to occur, see Figure 2 reproduced from Reference 29. This latter effect occurred because the data of Reference 9, the basis of arbitrary constants in Reference 22, showed a lesser reduction in skin friction with gas injection than the later data of Reference 15. The data of Reference 26, therefore, are inconsistent with these general results.

An analysis by Ness, Reference 31, extended the work of Reference 27 to include variations of the properties in the boundary layer caused by temperature variations as well as by concentration distributions. The gases considered were undissociated air and a light, chemically inert injected foreign gas. Ness used the two-layer formulation of References 22 and 27 with

essentially the same sublayer thickness criterion. Numerical values of surface skin friction and heat-transfer rates were evaluated for the particular case of helium injection into air up to Mach numbers of 4.

For light gas injection where Schmidt numbers can vary between about 0.2 to 1.6 in the sublayer, Ness argues that the turbulent Schmidt number must be equal to the Schmidt number based on molecular transport properties at the interface of the two layers, Reference 32. His argument is based on the mathematical result that if the turbulent Schmidt number is a fixed value lying between the extreme values of the Schmidt number in the sublayer, a maximum in the concentration of the light gas at the wall occurs when the velocity ratio at the edge of the sublayer is varied at constant, but large, values of the injection parameter ζ.[2] The concentration at the wall varies monotonically if Ness' criterion cited above is applied. Why Ness finds a maximum in concentration of the light gas at the wall with varying sublayer velocity ratio an unacceptable anomaly is not clear. As the velocity ratio is increased with increased skin friction, the resistance of the boundary layer to mass transfer tends to increase, causing a rise in surface concentration for the increased flow rates corresponding to constant ζ. On the other hand, the increased flow rate also results in an increased light gas concentration at the edge of the sublayer which increases the molecular Schmidt number in the sublayer that, in turn, tends to drop the boundary-layer resistance to mass transfer. Thus, two simultaneous, but opposite, effects are occurring so that it is not inconceivable that a maximum in concentration actually occurs. Thus, Ness' argument cannot be accepted a priori but must be tested against the concentration profile data that exist It will be shown later that the assumption of a laminar Schmidt number equal to 0.2 and a turbulent Schmidt number equal to 0.75 yields excellent agreement with concentration profile data; and since this is in contradiction to Ness' criterion for the value of the turbulent Schmidt number, it can be concluded that his criterion is not a necessary condition.

In view of the above discussion, some caution must be exercised in accepting Ness' numerical results which indicate a correspondence to the Mach number effect found in Reference 29. In fact, Ness' analysis reduces to that of Reference 22 for air injection, where little, if any, Mach number effect is noted, see Figure 2. It is believed that the results of Reference 31 may be fortuitous and introduced through the arbitrary choice of the variation of

[2]The injection parameter

$$\zeta = \frac{\rho_o u_o}{\rho_1 u_1 (C_f/2)}$$

the turbulent Schmidt number. Again, Reference 31 possesses all the defects cited earlier for two-layer models of the turbulent boundary layer; for example, ever increasing temperature recovery factor with increasing Reynolds number.

Regardless of the limitations of the data cited and of the two-layer theories, the practical needs in the design of ablation bodies have led to the use of results of these investigations to define the heat flow blocking effect by the injected gases, for example, Reference 33.

1.1.3 Recent contributions

The recent publication by Pappas and Okuno, Reference 34, extends the work of Reference 29 to local heat-transfer rate measurements while helium, air, and Freon-12 are injected from the surface of a 15° included angle cone. The results of this test indicate further anomalies not evident in the previously discussed theories. These can be summarized as follows:

(a) No particular Mach number effect is shown in plots of St/St_o versus $\rho_o v_o/\rho_1 u_1\ St_o$ for air injection. This agrees with the theory of Reference 27, yet the skin-friction data of Reference 29 do not agree with the same theory. The implication here is that the theoretical prediction of the modified Reynolds analogy is not correct.

(b) The data show little variation of dropoff in Stanton number with Reynolds number which is inconsistent with the theory of Reference 27 for helium injection.

(c) At subsonic speeds, the recovery factor for helium injection increases from the zero injection value of 0.84 to a maximum value near 1.35 and then decreases with increasing injection. At supersonic speeds, the recovery factors for all the injection gases initially decrease from the zero injection value and then increase at higher injection rates to values greater than unity. None of these effects are evident in the existent theories. It is believed (Ref. 35) that thermal diffusion in the sublayer may be causing these recovery-factor effects.

The general result of these data is that the light gases are not relatively as effective in reducing heat-transfer rates as has hitherto been expected from the theories cited above. These data are not entirely consistent with the heat-transfer measurements of Bartle and Leadon, Reference 36, where a Mach number effect on heat-transfer data is still noted. For injected gases other than nitrogen, there is insufficient detail in Reference 36 to make direct comparison with the data of Pappas and Okuno.

1.2 Curr[illegible] Approach

In general, it can be deduced from the survey cited above that several major discrepancies exist between the data obtained to date and existing theory dealing with air or foreign gas injection into a turbulent air boundary layer. In addition, certain unresolved differences exist between different sets of data. The use of these theories to predict the behavior of turbulent boundary layers on ablating reentry bodies requires extrapolation that borders on mere guessing.

It is the intent of the current research, therefore, to create a newer model of turbulent boundary layer that is consistent with successively more complex experimental results. In the following paragraphs the broader aspects of this model will be described in order that the details of the analysis presented in Section 2 can be viewed in their proper perspective.

As has been previously noted (Section 1.1.1), the boundary layer can be divided into essentially four parts, the first three of which are characterized by the "law of the wall." Because the characteristics of this portion of the boundary layer have been found to be almost exclusively dependent on wall conditions, it is possible to formulate its solution in terms of a "one-dimensional" initial value problem. The initial values are those that characterize the conditions at the wall which, in general, vary from one point on the wall to another. The term "one-dimensional" is appropriate in the mathematical sense that the solution proceeds out (in one dimension, y) from a specified wall point.

The fourth region of the boundary layer (as enumerated in Section 1.1.1) is strongly dependent on the history of the boundary layer and on local free-stream conditions and gradients. Thus, the solution of this portion of the boundary-layer problem is characterized by a "two-dimensional" boundary value problem. The boundary values are conditions at some initial plane normal to the flow direction, conditions on a plane parallel to the wall in the free stream beyond the extent of the boundary layer, and conditions at the interface between this region and the inner "law of the wall" region.

In the analysis presented in the next section, these two regimes will be studied, first individually and then in concert, to establish a "solution" for the complete boundary layer. The establishment of this "solution" is dependent, in large measure, on the physical assumptions which will be made to obtain a tractable set of mathematical relations for each of these two regimes. These are briefly summarized in the following table:

Regime	Mathematical Characteristics	Assumptions
"Law of the wall"	"One-dimensional" initial-value problem	1. Mixing length representative of the variation of turbulent transport properties. 2. Rate of increase of mixing length based on local properties in the boundary layer
Wake Regime	"Two-dimensional" boundary-layer problem	1. Molecular transport effects negligible. 2. Turbulent transport properties are functions of the streamwise coordinate, x, only. 3. Clauser parameter, $\epsilon_M/u_1\delta^*$, invariant. 4. Invariant turbulent Schmidt and Prandtl numbers.

The advantages realized by dividing the solution into two distinct regimes are manifold, if consideration is given to the complexities of a single unified solution. It is indeed fortunate that such a division not only reduces an otherwise intractable mathematical problem into two reasonable straightforward problems, but also is consistent with the physical character of the boundary layer. The assumptions used in the wake regime, although reasonably valid therein, are totally invalid in the law of the wall regime. Likewise the "one-dimensional" assumption of the law of the wall regime, although good therein, cannot be extended into the wake regime. Thus, the complexities of one regime are avoided in the solution of the other, resulting in a profound reduction in the overall complexity of the total problem.

In previous work, boundary-layer studies have emphasized the "law of the wall" regime, usually ignoring the contributions of the wake regime. The principal difference between these analyses has involved the chosen representation of the variation of the turbulent transport effects. In the present work these various techniques have been evaluated in light of the existing data with a particular emphasis on their application under conditions of surface mass addition. The choice of a "mixing length" model was based primarily on its initial successful application under these conditions. The selected analytical representation of the mixing length, although original, is a consequence of a generalization and rationalization of existing representations. Based on the data evaluated, the two constants of this representation do not

vary with surface mass addition or Schmidt (or Prandtl) number nor with application to velocity, temperature, or concentration gradients. Because the consequent mathematical formulation is an initial-value problem, its solution is conceptually simple.

Solutions for the outer portion of the boundary layer (the wake regime), with one notable exception, do not exist per se. There are various velocity profile generalizations which have been evolved and successfully applied (e.g., Coles, Ref. 3; Black and Sarnecki, Ref. 37; and Kendall, Ref. 17; the latter two being inspired by the former) but these techniques are not supported by any particular physical rationale relating to the turbulent transport properties which dictate the profiles. The exception is the work of Clauser (Ref. 6). Based on observations with regard to the variation of the turbulent viscosity within the boundary layer, he proposed a simplification and a generalization, namely, that the turbulent viscosity coefficient was a function of the streamwise coordinate only, and that this functional dependence could be specified as

$$\frac{\bar{\epsilon}_M}{u_1 \delta^*} = \text{constant}$$

that is, the turbulent viscosity is proportional to the product of the free-stream velocity and the boundary-layer displacement thickness. In his original work, Clauser restricted his solution to velocity profiles on impervious walls. In the analysis to follow, the technique has been extended to concentration and temperature profiles as well as velocity profiles, all under condition of surface mass addition. The procedure involves the formulation of a similarity solution, much akin to the classical solutions of the laminar boundary layer. Some of the requisites for a truly similar (turbulent) boundary-layer solution are found to be more palatable than their conterparts in the laminar boundary layer. In particular, a constant value of the transpiration ratio $\rho_o v_o / \rho_1 v_1$ is required rather than its inverse decay with boundary-layer thickness as prescribed for laminar similarity solutions.

The remaining requirements of the solution of the entire boundary layer involve the coupling of the inner and outer solutions and generalizations of the results obtained for specified boundary conditions. This is again an almost purely mathematical effort and requires no further physical assumptions, beyond those already discussed. A total of four <u>invariant</u> constants are utilized: the Clauser parameter, the turbulent Prandtl (or Schmidt) number, and the two constants of the mixing length expression.

In checking for consistency between theory and experiment, emphasis has been placed on velocity, temperature, and gas specie concentration profiles in addition to overall surface transfer coefficients, such as the skin friction coefficient or Stanton number. The work reported in this report is limited to the case where the fluid properties in the boundary layer are essentially constant. The excellent agreement of the proposed boundary-layer model with much of the data obtained at low speeds and with small quantities of foreign gas injection is quite encouraging. Even the initial objectives of this program cannot be considered to be complete, however, until the boundary-layer model is adapted to be consistent with existing data on the following:

(a) Boundary-layer velocity profiles obtained at supersonic speeds with air injection at the surface.

(b) Surface transfer coefficients in supersonic flow with foreign gas injection in moderate and large quantities.

(c) Surface transfer coefficients deduced in sonic or supersonic flows where intense chemical activity and high surface mass transfer takes place.

Ultimately, the theoretical model of the boundary layer will have to be tested against future experiments in high-speed chemically reacting boundary layers where local profile data are obtained.

BLANK PAGE

2. ANALYSIS

2.1 Basic Boundary-Layer Equations

Because of the complexity of the ultimate goals of this study, it is imperative that the considerably more restrictive objectives of the initial work reported herein be brought into proper perspective. To aid in the establishment of this perspective, this section will present the basic boundary-layer equations which are appropriate to the general solutions ultimately sought. A sequence of restrictions will subsequently be imposed upon these general relations in order to arrive at the basic set of relations which will be considered in detail in this report. In the various developments which will be presented in the subsequent sections of this report, means of relaxing many of these restrictions will be discussed. Initially, therefore, the boundary-layer relations presented will include effects of compressibility, chemical reactions between multiple components, unequal binary diffusion coefficients, thermal diffusion and its reciprocal partner, the DuFour effect, and temperature and concentration-dependent physical properties.

2.1.1 General two-dimensional mass, momentum, and energy equations

In the derivation of the equations presented here, the standard definitions of time-averaged turbulent quantities and relative order of magnitude are employed, for example, References 23 and 38. Because the turbulent transport terms are expressed in the Bousinesq form, that is, employing eddy viscosity, eddy diffusion, and eddy conductivity, all the terms in the equations are time-averaged quantities and no need exists for using a superscript bar to distinguish the time-averaged quantities. The reader is cautioned to remember, however, that ρv represents $\overline{\rho v}$, not $\overline{\rho}\,\overline{v}$.

The equations derived are essentially identical to those derived in References 38 and 39 for flow over a flat plate with uniform free-stream conditions, except that the diffusion flux used here is in a more general form including the effects of thermal diffusion (Soret effect) and unequal binary diffusion coefficients. The diffusion introduced by pressure gradients and body forces are the only physical phenomena that are neglected. In the order of magnitude arguments, terms of the following type have been eliminated: (1) triple correlations, (2) derivatives of turbulent correlations parallel to the wall, and (3) correlations involving turbulent components of molecular transport mechanisms.

2.1.1.1 Conservation of specie and mass equations

A mass balance of an individual specie in a unit volume results in the relationship

$$\frac{\partial}{\partial x}(\rho u \omega_i) + \frac{\partial}{\partial y}(\rho v \omega_i) = \frac{\partial}{\partial y}\left(\rho \epsilon_{D_i} \frac{\partial \omega_i}{\partial y} - j_i\right) + \psi_i \qquad (2\text{-}1)$$

where ψ_i represents the rate of mass generation of species i per unit volume due to chemical reactions. ϵ_{D_i} is defined in terms of the correlation of the fluctuating components of concentration and normal velocity, that is,

$$\rho \epsilon_{D_i} = - \frac{\overline{(\rho v)' \omega_i'}}{\partial \omega_i / \partial y} \qquad (2\text{-}2)$$

and j_i is the mass diffusion rate of species i due to molecular processes. This latter term can be related to the gradient of species i (as well as gradients of other species), the family of binary diffusion coefficients, D^*_{ij} appropriate to the boundary-layer system, and the multicomponent thermal diffusion coefficients D_i^T through the Stefan-Maxwell relations, Equation 8.1-3 of Reference 39,

$$\frac{\partial x_i}{\partial y} = \sum_j \frac{x_i x_i}{\rho D^*_{ij}} \left(\frac{j_j + D_j^T \frac{\partial \ln T}{\partial y}}{\omega_j} - \frac{j_i + D_i^T \frac{\partial \ell n T}{\partial y}}{\omega_i} \right) \qquad (2\text{-}3)$$

When Equation (2-1) is summed over all the species in the system, and it is remembered that

$$\sum_i \left(\rho_e \epsilon_{D_i} \frac{\partial \omega_i}{\partial y} - j_i \right) = 0 \qquad (2\text{-}4)$$

because of the definition of "mass diffusion" and that

$$\sum_i \psi_i = 0 \qquad (2\text{-}5)$$

because of a conservation of atomic species, there results

$$\frac{\partial \rho u}{\partial x} + \frac{\partial \rho v}{\partial y} = 0 \qquad (2\text{-}6)$$

since $\sum \omega_i = 1$. Equation (2-6) is the familiar overall continuity equation.

When Equation (2-6) is considered together with Equation (2-1), there results

$$\rho u \frac{\partial \omega_i}{\partial x} + \rho v \frac{\partial \omega_i}{\partial y} = \frac{\partial}{\partial y}\left(\rho \epsilon_{D_i} \frac{\partial \omega_i}{\partial y} - j_i\right) + r_i \tag{2-7}$$

2.1.1.2 Momentum equation

For the case of a uniform free-stream condition, the momentum equation can be written as follows:

$$\rho u \frac{\partial u}{\partial x} + \rho v \frac{\partial u}{\partial y} = \frac{\partial}{\partial y}\left[\rho(\nu + \epsilon_M) \frac{\partial u}{\partial y}\right] \tag{2-8}$$

where the eddy viscosity is defined in terms of the Reynolds stresses of turbulent flow by

$$\rho \epsilon_M = - \frac{\overline{(\rho v)' u'}}{(d\bar{u}/dy)} \tag{2-9}$$

2.1.1.3 The energy equation

The energy equation for this general system can be written as

$$\rho u \frac{\partial h_t}{\partial x} + \rho v \frac{\partial h_t}{\partial y} = \frac{\partial}{\partial y}\left[\rho(\epsilon_M + \nu) \frac{\partial \frac{u^2}{2}}{\partial y} + \left(\frac{k}{\bar{c}_p} + \rho \epsilon_H\right) \frac{\partial h}{\partial y}\right.$$
$$+ \sum_i \left(\rho \epsilon_{D_i} \frac{\partial \omega_i}{\partial y} - j_i\right) h_i - \left(\rho \epsilon_H + \frac{k}{\bar{c}_p}\right) \sum_i h_i \frac{\partial \omega_i}{\partial y}$$
$$\left. - \frac{RT}{\rho} \sum_i \sum_j \frac{x_j D_i^T}{m_i D_{ij}^*} \left(\frac{j_i}{\omega_i} - \frac{j_j}{\omega_j}\right)\right] \tag{2-10}$$

where the DuFour effect, the flux of heat caused by thermal diffusion, is given in terms of the diffusion fluxes of the pertinent species in the final term, and the turbulent enthalpy transport coefficient is defined by

$$-\rho\epsilon_H = \frac{\sum_i \omega_i \overline{(\rho v)' h_i'}}{\sum_i \omega_i (dh_i/dy)} \tag{2-11}$$

2.1.2 Binary, non-reacting system

If the boundary layer is constrained to a binary non-reacting system (species a and b), considerable simplification results. The relations for mass transfer, Equations (2-7) and (2-3), become

$$\rho u \frac{\partial \omega_i}{\partial x} + \rho v \frac{\partial \omega_i}{\partial y} = \frac{\partial}{\partial y}\left(\rho\epsilon_D \frac{\partial \omega_i}{\partial y} - j_i\right) \tag{2-12}$$

with

$$\frac{d\omega_a}{dy} = -\frac{j_a}{\rho D^*_{ab}} - \omega_a\omega_b\alpha \frac{\partial \ell n\, T}{\partial y} \tag{2-13}$$

The heat-transfer equation becomes

$$\rho u \frac{\partial h_t}{\partial x} + \rho v \frac{\partial h_t}{\partial y} = \frac{\partial}{\partial y}\left[\rho(\epsilon_M + \nu) \frac{\partial \frac{u^2}{2}}{\partial y} + \left(\frac{k}{\bar{c}_p} + \rho\epsilon_H\right)\frac{\partial h}{\partial y} + \left(\rho\epsilon_D \frac{\partial \omega_a}{\partial y} - j_a\right)(h_a - h_b) - \left(\rho\epsilon_H + \frac{k}{\bar{c}_p}\right)\frac{\partial \omega_a}{\partial y}(h_a - h_b) - RT \frac{\dot{m} j_a \alpha}{m_a m_b}\right] \tag{2-14}$$

where the parameter α is related to the thermal diffusion coefficient in Equations 8.1-17 and 8.1-10 of Reference 39 by

$$\alpha \equiv \frac{k_T}{x_a x_b} = \frac{1}{x_a x_b}\left(\frac{m^2}{\rho m_a m_b} \frac{D_a^T}{D^*_{ab}}\right) \tag{2-15}$$

and is, in general, relatively invariant with concentration (in contrast to the rather large variations of D_i^T).

If, additionally, the boundary layer is constrained to the case of constant properties, negligible viscous dissipation, no thermal diffusion, and only trace amounts of foreign gases, the final simplified two-dimensional relations are obtained. These are for mass and energy, respectively

$$u \frac{\partial w_i}{\partial x} + v \frac{\partial w_i}{\partial y} = \frac{\partial}{\partial y} \left[(\epsilon_D + D^*_{ab}) \frac{\partial w_i}{\partial y} \right] \tag{2-16}$$

$$u \frac{\partial T}{\partial x} + v \frac{\partial T}{\partial y} = \frac{\partial}{\partial y} \left[\left(\frac{\epsilon_H}{c_p} + \frac{k}{\rho c_p} \right) \frac{\partial T}{\partial y} \right] \tag{2-17}$$

2.1.3 The one-dimensional mass, momentum, and energy equations

The general two-dimensional boundary-layer relations described in the preceding subsections are such a complex set of simultaneous, non-linear, partial differential equations that their complete solution including even the simplest phenomenological development of the turbulent transport properties (ϵ_M, ϵ_D, and ϵ_H) has yet to be performed. Many of the complicating factors in this equation are significant only in the region close to the wall. It is in this region that the molecular transport properties are of consequence and it is here that the turbulent transport properties are most variable. To seek a two-dimensional solution in this region seems unwarranted, particularly in light of the extensive empirical evidence that it is characterized by a "law of the wall." Since the mathematical statement of the "law of the wall,"

$$\text{local state and local normal fluxes} = f\left(\begin{matrix}\text{wall state, wall fluxes, thermodynamic} \\ \text{properties of the fluids, } y\end{matrix}\right)$$

is identical with the implied solution of a one-dimensional initial value problem, it is apparent that the two assumptions are compatible. Thus, it is pertinent to look at the relations that will result when a one-dimensional assumption is introduced.

The general two-dimensional continuity equation which is

$$\frac{\partial \rho u}{\partial x} + \frac{\partial \rho v}{\partial y} = 0 \tag{2-6}$$

reduces to

$$\frac{d\rho v}{dy} = 0 \tag{2-18}$$

which is solved to yield

$$\rho v = (\rho v)_o = \rho_o v_o$$

since turbulent correlations vanish at the surface, $(\overline{\rho' v'})_o = 0$. Here, $\rho_o v_o$ can be considered as a parameter that may vary with x.

The one-dimensional assumption leads to the following forms for the mass, momentum, and energy equations:

$$\rho_o v_o \left(\omega_i - \omega_{i_o}\right) = \rho \epsilon_D \frac{d\omega_i}{dy} - j_i + j_{i_o} + \int_o^y \psi_i \, dy \tag{2-19}$$

$$\rho_o v_o u = \rho(\nu + \epsilon_M) \frac{du}{dy} - \tau_o \tag{2-20}$$

$$\rho_o v_o (h_t - h_o) = \rho(\epsilon_M + \nu) \frac{d(u^2/2)}{dy} + \left(\frac{k}{\bar{c}_p} + \rho\epsilon_H\right) \frac{dh}{dy}$$

$$+ \sum_i \left(\rho \epsilon_{D_i} \frac{d\omega_i}{dy} - j_i\right) h_i - \left(\rho\epsilon_H + \frac{k}{\bar{c}_p}\right) \sum_i h_i \frac{d\omega_i}{dy}$$

$$- \frac{RT}{\rho} \sum_i \sum_j \frac{x_j D_i^T}{m_i D_{ij}^*} \left(\frac{j_i}{\omega_i} - \frac{j_j}{\omega_j}\right) + q_o \tag{2-21}$$

where the wall shear τ_o is, in general, a function of x, as is q_o which is defined by

$$q_o = \rho_o v_o (h_{\text{injectant}} - h_o) + q_{\text{supplied}}$$

where $h_{\text{injectant}}$ is the enthalpy of the injectant evaluated at some plane at or below the surface and q_{supplied} is heat crossing the same plane as a consequence of conduction or radiation. It should be emphasized that h_o is the enthalpy of the gas mixture adjacent to the surface as contrasted to the enthalpy of the pure injectant.

If the boundary layer is restricted to a binary nonreactive system, these equations become

$$\rho_o v_o \left(\omega_i - \omega_{i_o}\right) = \rho \epsilon_D \frac{d\omega_i}{dy} - j_i + j_{i_o} \tag{2-22}$$

$$\rho_o v_o u = \rho(\nu + \epsilon_M) \frac{du}{dy} - \tau_o \tag{2-23}$$

$$\rho_o v_o (h_t - h_o) = \rho(\epsilon_M + \nu) \frac{d(u^2/2)}{dy} + \left(\rho\epsilon_H + \frac{k}{\bar{c}_p}\right) \frac{dh}{dy}$$

$$+ \left(\rho\epsilon_D \frac{d\omega_a}{dy} - j_a\right)(h_a - h_b) - \left(\frac{k}{\bar{c}_p} + \rho\epsilon_H\right) \frac{d\omega_a}{dy} (h_a - h_b)$$

$$- RT \frac{m j_a \alpha}{m_a m_b} + q_o \tag{2-24}$$

with

$$j_a = -\rho D^*_{ab} \left(\frac{d\omega_a}{dy} - \omega_a \omega_b \alpha \frac{d\ \ell n\ T}{dy}\right)$$

and if further the boundary layer is constrained to an essentially one-component system containing only trace amounts of foreign species and having essentially constant properties, the final relations are obtained.

$$\left.\begin{aligned} v_o \left(\omega_a - \omega_{a_o}\right) &= (\epsilon_D + D^*_{ab}) \frac{d\omega_a}{dy} + \frac{j_o}{\rho} \\ \text{or} \\ v_o \left(x_a - x_{a_o}\right) &= (\epsilon_D + D^*_{ab}) \frac{dx_a}{dy} + \frac{N_o m}{\rho} \end{aligned}\right\} \tag{2-25}$$

$$v_o u = (\nu + \epsilon_M) \frac{du}{dy} - \frac{\tau_o}{\rho} \tag{2-26}$$

$$v_o (T - T_o) = \frac{(\epsilon_M + \nu)}{c_p} \frac{d(u^2/2)}{dy} + \left(\epsilon_H + \frac{k}{\rho c_p}\right) \frac{dT}{dy} + \frac{q_o}{\rho c_p} \tag{2-27}$$

The last three relations of the equations above can be expressed in terms of a new set of variables as follows:

$$1 + v_o^+ x^+ = \left(\frac{1}{Sc} + \frac{\epsilon_M}{\nu}\ \frac{1}{Sc'}\right)\ \frac{dx^+}{dy^+} \tag{2-28}$$

$$1 + v_o^+ u^+ = \left(1 + \frac{\epsilon_M}{\nu}\right)\ \frac{du^+}{dy^+} \tag{2-29}$$

$$1 + v_o^+ T^+ = \left(\frac{1}{Pr} + \frac{\epsilon_M}{\nu}\ \frac{1}{Pr'}\right)\ \frac{dT^+}{dy^+} \tag{2-30}$$

where the viscous dissipation term has been ignored in the energy relation. The non-dimensional variables that are utilized above are defined by

$$y^+ = \frac{y u_\tau}{\nu} \tag{2-31}$$

$$u^+ = \frac{u}{u_\tau} \tag{2-32}$$

$$u_\tau = \sqrt{\tau_o/\rho} = u_1\sqrt{C_f/2} \tag{2-33}$$

$$x^+ = \left(\frac{x_a - x_{a_o}}{x_{a_1} - x_{a_o}}\right)\ \frac{u_\tau/u_1}{C_M} = \tilde{x}\ \frac{u_\tau}{u_1 C_M} \tag{2-34}$$

$$T^+ = \left(\frac{T - T_o}{T_1 - T_o}\right)\ \frac{u_\tau}{u_1 C_H} = \tilde{T}\ \frac{u_\tau}{u_1 C_H} \tag{2-35}$$

$$v_o^+ = \frac{v_o}{u_\tau} \tag{2-36}$$

the Prandtl and Schmidt numbers by

$$Pr = \frac{c_p \mu}{k} \tag{2-37}$$

$$Pr' = \frac{\epsilon_M}{\epsilon_H} \tag{2-38}$$

$$Sc = \frac{\nu}{D} \tag{2-39}$$

$$Sc' = \frac{\epsilon_M}{\epsilon_D} \tag{2-40}$$

In addition, the momentum, mass, and energy transfer coefficients are defined by

$$\frac{C_f}{2} = \frac{\tau_o}{\rho u_1^2} \tag{2-41}$$

$$C_M \quad \frac{mN_o}{\rho u_1 \left(x_{a_1} - x_{a_o}\right)} = \frac{j_o}{\rho u_1 \left(\omega_{a_1} - \omega_{a_o}\right)} \tag{2-42}$$

$$C_H = \frac{-q_o}{\rho u_1 c_p (T_1 - T_o)} \tag{2-43}$$

The solution of the basic equations, either one- or two-dimensional, can be divided into two major aspects. The first is the adequate specification of the physical parameters, of particular importance being the various eddy transport properties. The second and equally important aspect involves the mathematical procedures for solution for various imposed boundary conditions.

2.1.4 Integral boundary-layer equations for constant fluid properties

Because of the physical requirement for a knowledge of the turbulent transport coefficients, it is desirable to present the boundary-layer equations in a fashion permitting the experimental evaluation of these parameters. A way of obtaining these parameters from mean value data is through use of integral boundary-layer equations. These equations have been derived for the constant property boundary layers and are summarized below. These relations are presented in terms of the internal or partial values ($y < \delta$) of the displacement, momentum, mass, and enthalpy thicknesses. These thicknesses are defined, respectively, as

$$\delta_y^* = \int_o^y (1 - \tilde{u})\, dy \tag{2-44}$$

$$\theta_y = \int_o^y \tilde{u}(1 - \tilde{u})\, dy \tag{2-45}$$

$$\Gamma_y = \int_0^y \tilde{u}(1 - \tilde{x})\, dy \tag{2-46}$$

$$\xi_y = \int_0^y \tilde{u}(1 - \tilde{T})\, dy \tag{2-47}$$

The integral relations become for the momentum equation

$$\nu + \epsilon_M = \frac{u_1}{d\tilde{u}/dy}\left\{\frac{C_f}{2} - \frac{d\theta_y}{dx} + \tilde{u}\,\frac{v_o}{u_1} - (1 - \tilde{u})\,\frac{d\delta_y^*}{dx} - \frac{\sigma_y}{u_1}\,\frac{du_1}{dx}\left[2 + \frac{\delta_y^*}{\sigma_y} + (1 - \tilde{u})\left(\frac{\delta_y^*}{\theta_y} - \frac{y}{\theta_y}\right)\right]\right\} \tag{2-48}$$

for the energy equation

$$\frac{k}{\rho c_p} + \epsilon_H = \frac{u_1}{d\tilde{T}/dy}\left\{C_H - \frac{d\xi_y}{dx} - \xi_y\,\frac{d\,\ell n(T_o - T_1)}{dx} + \tilde{T}\,\frac{v_o}{u_1} - (1 - \tilde{T})\,\frac{d\delta_y^*}{dx} - \frac{\xi_y}{u_1}\,\frac{du_1}{dx}\left[1 - (1 - \tilde{T})\left(\frac{y}{\xi_y} - \frac{\delta_y^*}{\xi_y}\right)\right]\right\} \tag{2-49}$$

and for the mass equation

$$D^* + \epsilon_D = \frac{u_1}{d\tilde{x}/dy}\left\{C_M - \frac{d\Gamma_y}{dx} - \Gamma_y\,\frac{d\,\ell n(x_o - x_1)}{dx} + \tilde{x}\,\frac{v_o}{u_1} - (1 - \tilde{x})\,\frac{d\delta_y^*}{dx} - \frac{\Gamma_y}{u_1}\,\frac{du_1}{dx}\left[1 - (1 - \tilde{x})\left(\frac{y}{\Gamma_y} - \frac{\delta_y^*}{\Gamma_y}\right)\right]\right\} \tag{2-50}$$

When $y \geq \delta$ these relations reduce to the more conventional integral boundary-layer equations. These are as follows for momentum, energy, and mass conservation, respectively:

$$\frac{C_f}{2} = \frac{d\theta}{dx} - \frac{v_o}{u_1} + \frac{\theta}{u_1}\,\frac{du_1}{dx}\,(2 + H) \tag{2-51}$$

$$C_H = \frac{d\xi}{dx} - \frac{v_o}{u_1} + \frac{\xi}{T_o - T_1}\,\frac{d(T_o - T_1)}{dx} + \frac{\xi}{u_1}\,\frac{du_1}{dx} \tag{2-52}$$

$$C_M = \frac{d\Gamma}{dx} - \frac{v_o}{u_1} + \frac{\Gamma}{x_o - x_1}\,\frac{d(x_o - x_1)}{dx} + \frac{\Gamma}{u_1}\,\frac{du_1}{dx} \qquad (2\text{-}53)$$

where the shape factor, H, is equal to the ratio of the displacement thickness to the momentum thickness (δ^*/θ).

2.2 Solution of the One-Dimensional Boundary-Layer Equations

In this section, the solutions of one-dimensional boundary-layer equations presented in the preceding section will be developed. These solutions are primarily dependent on the development of an appropriate model of turbulence and its coupling with the one-dimensional equations. Certain basic considerations will be discussed with regard to the formulation of a universal "law of the wall." Subsequently, the more empirical models of turbulence will be considered, specifically, the pragmatic mixing length concept. A functional dependence of the mixing length on the various boundary-layer variables will be postulated based on certain limiting criteria and on dimensional arguments.

This postulated mixing length relation will be used to predict profiles of velocity, temperature, and concentration throughout the one-dimensional portion of the boundary layer. Extensive re-evaluation of the existing data was required in order to establish the significance of these comparisons. Because of the importance of these evaluations, they will be described in reasonable detail.

2.2.1 The law of the wall

Mathematically it is required that $y \ll \delta$ for the one-dimensional boundary-layer equations developed in the preceding section to be strictly applicable. In practice, however, this "one-dimensional" regime includes three regions of interest which extend over a significant portion of the boundary-layer thickness as indicated in Figure 1. These regions include the laminar "sublayer" wherein molecular transport mechanisms prevail, the transitional regime, and the turbulent core of the velocity profile (the log-law regime). Inspection of the basic one-dimensional equations for mass, heat, or momentum transfer indicates that a solution can be obtained for a specified set of surface conditions, provided only that the variation of the various thermodynamic and transport properties, both molecular and turbulent, be known. The turbulent viscosity, thermal conductivity, and diffusion coefficients are by far the most elusive of these properties. With the possible exception of these turbulent properties, the required properties are functions of local conditions (including normal fluxes). Thus, the assumptions implicit

in the acceptance of the one-dimensional equations are consistent with the empirically accepted "law of the wall." The implication of the "law" is that all properties of the boundary layer within its regime are functions of the normal coordinate from the wall and properties at the wall, for example,

$T = f(y, T_o, q_o, \tau_o, v_o,$ physical properties of mainstream and injected gases)

For this generalization to apply, however, it is necessary that the turbulent transport properties be the function of the same set of variables. It should be emphasized that there is no obvious analytical logic which would indicate this simplified dependence. In the region $y \ll \delta$, the equations governing the turbulent components of velocity cannot be reduced to a one-dimensional set, rather a three-dimensional set persists. The solution of this set requires initial conditions both at the wall and at two mutually perpendicular planes normal to the wall. Considerable data exist, however, which indicate that a "law of the wall" represents the mean flow and that properties within the realm of this law are functions only of the normal coordinate and the wall state. Clauser, Reference 40, was one of the first to make extensive use of this fact under conditions of severe adverse pressure gradients. The implications of these facts are significant in that they indicate the direction possible solutions should take.

2.2.1.1 The turbulent transport properties

Because of the current lack of understanding of turbulent mechanisms, "theoretical" predictions of the variation of turbulence near the wall must rely on empirical input into relations based on some phenomenological dependence. Because of the generality of the ultimate goals of this analysis and of the strong desire to approximate the physical situation, certain prerequisites were established for the turbulent transport relations. These were:

(a) The relations must indicate a continuous variation of the turbulent transport properties from the wall to the fully turbulent region.

(b) The relations must be generally applicable to mass, momentum, and energy transport.

(c) The relations must be extendable to compressible real gas property flow.

(d) The relations should be suitable for transpired and untranspired boundary layers without any, or a minimum, modification of form.

Two basic types of viscous layer hypotheses have been proposed in the past. The first type predicts the variation of turbulent viscosity from the

wall to the fully turbulent regime. Reichardt, Rannie, and Deissler have, in References 41 through 43, for example, proposed such variations. The second type of hypothesis relates to a variation of mixing length from the wall into the fully turbulent portion of the boundary layer. Rotta, von Kármán, and van Driest (Refs. 44 to 46) have adopted this procedure.[3] Since data indicate that surface mass addition strongly affects the eddy viscosity profile, it was found that the first type of hypotheses could not be simply modified to predict this variation. On the other hand, the success of the pragmatic mixing length theory in predicting profiles in the fully turbulent portion of the boundary layer with surface mass addition has been noted (e.g., Refs. 13 and 17). It has generally been concluded that the slope of the linear relation between mixing length and distance from the wall is insensitive to surface mass addition. As a consequence of this apparent generality of the mixing length approach, it was adopted for the present studies.

2.2.1.2 The mixing length postulate

The basic mixing length postulate can be expressed as

$$\overline{(\rho v)'u'} = \rho \ell^2 \left(\frac{du}{dy}\right)^2 = \rho \epsilon_M \frac{du}{dy} \qquad (2\text{-}54)$$

where the mixing length, ℓ, is a combination of various correlations, but retains some relationship to the scale of turbulence. Prandtl proposed that this length will, in its simplest form, be related to the distance from a wall, at least in the region of development of turbulence. His proposition that

$$\frac{d\ell}{dy} = \text{constant} = \kappa \qquad (2\text{-}56)$$

---

[3]It is, of course, obvious that the turbulent viscosity and mixing length postulates are simply related and that it would be possible to cast the former in terms of the latter. When properties are constant and the surface is impervious, the relation becomes

$$\ell^+ = \frac{\epsilon_M}{\nu}\left(1 + \frac{\nu}{\epsilon_M}\right)^{1/2}$$

or when $\epsilon_M >> \nu$

$$\ell^+ = \epsilon_M/\nu$$

has been tested under a variety of conditions and found to be quite adequate in the fully turbulent portion of the law of the wall regime.

As the wall is approached, however, this simple relation is no longer appropriate and, in fact, it can be shown theoretically that

$$\left.\begin{aligned} &\lim_{y\to o} \ell \to 0 \\ &\lim_{y\to o} \frac{d\ell}{dy} \to 0 \end{aligned}\right\} \qquad (2\text{-}57)$$

This is a consequence of the Reichardt-Elrod criterion (see Refs. 41 and 47, Appendix A) which states that

$$\lim_{y\to o} \overline{u'v'} \to 0 \ , \quad \lim_{y\to o} \frac{d\overline{u'v'}}{dy} \to 0 \ , \quad \lim_{y\to o} \frac{d^2\overline{u'v'}}{dy^2} \to 0 \qquad (2\text{-}58)$$

and in addition that

$$\lim_{y\to o} \frac{d^3\overline{u'v'}}{dy^3} \to 0 \qquad (2\text{-}59)$$

if the flow is independent of the spanwise coordinate and if axial variations of mean flow parameters can be ignored at the wall. The expression for the mixing length decay (Eq. (2-57)) is required by Equation (2-58) but also encompasses Equation (2-59).

Thus, two criteria have been specified, namely, Prandtl's hypothesis which will be taken as appropriate in the fully turbulent portion of the "law of the regime" and the Reichardt-Elrod criterion as expressed by Equation (2-57).

When the mixing length postulate, Equation (2-54), is introduced into the constant property one-dimensional momentum (Eq. (2-29)), there results

$$\ell^{+2}\left(\frac{du^+}{dy^+}\right)^2 + \left(\frac{du^+}{dy^+}\right) = 1 + v_o^+ u_o^+$$

or

$$\frac{du^+}{dy^+} = \frac{-1 + \sqrt{1 + 4\ell^{+2}\left(1 + v_o^+ u^+\right)}}{2\ell^{+2}} \qquad (2\text{-}60)$$

where $\ell^+ = \ell u_\tau/\nu$. Equation (2-60) can be integrated by finite difference techniques, given the form of ℓ^+. In addition, Equations (2-28) and (2-30) can be simultaneously integrated with Equation (2-60) to yield the desired non-dimensional concentration and temperature distributions, given the form of ℓ^+, and the variation (if any) of turbulent Prandtl and Schmidt numbers.

2.2.2 The momentum boundary layer without surface mass addition

Since experimental data must serve as the principal basis of the appropriate mixing length relation and since the majority of the available boundary-layer data are for the case of no surface mass addition, it is appropriate to consider this simpler case first. In this section the various relations which have been postulated for the mixing length will be evaluated in light of the data and the various criteria developed in the preceding section.

2.2.2.1 Previous mixing length representations

Based on experimental data, several functional representations of the mixing length have been generated which satisfy the criterion proposed in Section 2.2.1, along with others that do not. Some of the better known relations are included in Table I. This table also indicates the ranges of validity for the various expressions and their compliance (or noncompliance) with various criteria.

For the purposes of comparison, the empirical constants for each of these expressions have been re-evaluated consistent with the following requirements:

(a) The mixing length constant $\kappa = 0.44$.

(b) A value of u^+ of 16.2 at $y^+ = 100$.

These values are consistent with a universal log-law velocity profile of the form

$$u^+ = 5.2 \log_{10} y^+ + 5.8 \qquad (2\text{-}61)$$

where the constant 5.2 ($\log_e 10/\kappa$, $\kappa = 0.44$) has been selected based on evaluation of impervious wall velocity profiles from a variety of investigators, of particular significance in this regard being the data of Reference 50 (see Fig. 16 of that reference). The lower values of κ generally employed have been derived based on massed data plots such as Figure 4 of Reference 40. With such plots, the departures of u^+ from linearity above the curve at large values of $\log y^+$ (the wake effect) and below the curve at low values of $\log y^+$ (Laminar flow effects) tend to prejudice the

selection of the linear representations. On the other hand, individual profile plots (e.g., Fig. 5 of Ref. 40) tend to support the higher value of κ used here. At a value of y^+ of 100 there is rather uniform agreement amongst various investigators as to the value of u^+. It was for this reason that this intercept was chosen as a basis, the value of u^+ of 16.2 being a representative average of the amassed profile data (see Refs. 3 and 40). In Table I, six flow postulates are considered. They have been selected, not with an eye toward completeness, but rather in an effort to present the range of postulates available. Historically, the two-layer Prandtl-Taylor model must be taken as the point of departure for all subsequent models. It takes on greater significance in this study since it has been used almost exclusively as a basis for past mixing length studies of the transpired turbulent boundary layer. The van Kármán three-layer profile prediction was introduced in order to improve the u^+ relation in the range of y^+ from about 5 to 30. In so doing, however, it provides no particular insight into the mechanisms in this transitional range. Rotta, by perturbing the original mixing length expansion to account for a constraining effect of the laminar sublayer and by including the contribution of the molecular transport properties beyond the sublayer, achieved continuity of shear and velocity without introducing undue complication. Reichardt postulated a direct expression for the evaluation of the turbulent viscosity which was consistent with the Reichardt-Elrod criterion. Similarly, van Driest proposed a mixture length expression, also consistent with this criterion. The mixing length expression utilized in the current work, and developed in a more general form in the next subsection, is shown in Table I in its reduced form for the case of constant properties and no transpiration. Additional models and their comparisons are discussed in References 1 and 2. For each model given in Table I, the requisite mixing length expression is presented, if the original representation of the model was in some alternate form.

As would be expected, the three multiple layer models for the law of the wall fail to satisfy all the continuity tests. From the limiting expression for mixing length as the wall is approached, it can be argued that all of the models given satisfy the Reichardt-Elrod criterion, if the criterion is limited to the requirement that ℓ^+ and $d\ell^+/dy^+$ approach zero at the wall, but only the continuous representations do so in a non-degenerate fashion. The van Driest representation of ℓ^+ includes an inflection point which distinguishes it from the other models. The model, to be developed in Section 2.2.2.2, appears to combine the displacement effect of Rotta with the exponential decay of van Driest.

This latter model has been used as a standard of comparison in the formulation of Figure 3 wherein the differences between the prediction of u^+ by the various techniques are amplified. It is apparent that the three single layer models agree rather well and any selection betweeen them should be based on grounds other than this comparison.

2.2.2.2 Proposed mixing length representation

The discussion of Section 2.2.1 leads to two generalizations, one based on experimental evidence, the other on theoretical considerations. These are

$$\frac{d\ell}{dy} \to \kappa \quad \text{as} \quad y \quad \text{increases} \tag{2-62}$$

$$\lim_{y \to o} \frac{d\ell}{dy} \to 0 \quad \text{and} \quad \lim_{y \to o} \ell \to 0 \tag{2-63}$$

Several means of expressing a relation covering the full range of y and including these limiting criteria have been presented in Table I. Since physically these relations are concerned with the transition from laminar to turbulent flow, it is advantageous in considering extensions of mixing length theory to establish some physical logic for the selected relation. Unfortunately, the understanding of the transitional process has not reached a state permitting any quantitive specification. Therefore, the selected model may be based only on qualitative understanding of the process, dimensional considerations, and the above limiting criteria. These criteria are immediately satisfied by a simple implicit relation of the form

$$\frac{d\ell}{dy} \propto (\kappa y - \ell) \tag{2-64}$$

which implies that the rate of increase of the mixture length is proportional to the difference between value postulated by Prandtl (κy) and its actual value. This rate of increase should also be augmented by the local applied shear and retarded by the local viscosity. Using these parameters to nondimensionalize the above relation yields

$$\frac{d\ell}{dy} \propto (\kappa y - \ell) \sqrt{\frac{\tau/\rho}{\nu}} \tag{2-65}$$

For constant shear through the boundary layer (no surface mass addition), this relation becomes

$$\frac{d\ell^+}{dy^+} = \kappa y^+ - \ell^+$$

$$= \frac{\kappa y^+ - \ell^+}{y_a^+} \qquad (2\text{-}66)$$

where y_a^+ is a dimensionless constant of proportionality. Integrating this relation yields

$$\ell^+ = \kappa \left\{ y^+ - y_a^+ \left[1 - \exp\left(- \frac{y^+}{y_a^+} \right) \right] \right\} \qquad (2\text{-}67)$$

which for large y^+ reduces to Rotta's expression, namely,

$$\ell^+ = \kappa \left(y^+ - y_a^+ \right) \qquad (2\text{-}68)$$

Table I presents Equation (2-67) along with five of the more conventional relations previously suggested. In addition, this expression served as the basis of comparison in Figure 3 where it was found to be in essential agreement with other continuous models. Because of its conceptual simplicity and its apparent combination of the better features of Rotta's and van Driest's models, Equation (2-66) has been chosen as the basis for the data comparisons of the next subsection. In general form, Equation (2-65) permits inclusion of the change in shear through the boundary layer introduced by surface mass injection in a physically reasonable manner.

2.2.2.3 Comparison of proposed model with data

The adequacy of any turbulent boundary-layer technique is measured by the degree to which the method reproduces the experimental data, when an accounting is made of the uncertainties which may exist in these data. The uncertainties in experimental data which would yield errors in a universal-velocity profile $u^+(y^+)$ are

(a) Uncertainties in friction factor.

(b) Uncertainties in the measured local velocities.

It is common knowledge that experimental velocities determined by pressure probes are subject to errors of unknown magnitude when the probes are in the near vicinity of a wall, as in the viscous sublayer. In addition, the effect of local turbulence can be significant (as will be noted later). To

some extent, errors in measured velocities using hot-wire anemometers are correctible, but are still subject to some uncertainty. Friction factors determined from the integral momentum equation (Eq. (2-51)), are subject to errors primarily because they require the presumption of two-dimensional flow (no spanwise variations) and the differentiation of experimental data, which amplifies inherent errors. This problem is greatly magnified for transpiration data, as will be seen later, in that the friction factor is interpreted by a small difference of two relatively large uncertain numbers, that is, $d\theta/dx - v_o/u_1$. For the purpose of comparing the various mixing length techniques to experimental data, the authors have chosen the following data sources as subject to a minimum of criticism:

(1) Data of Laufer (Ref. 48)

These data were achieved for fully developed turbulent flow in pipes. Velocities were measured by hot-wire anemometers, and friction factors were interpreted from the measured pressure gradient. The major uncertainty here is the point in the universal velocity distribution where flow in a pipe departs from the characteristics of a flat plate and the origin and description of the wake.

(2) Data of Klebanoff (Ref. 49)

These data were achieved for an artificially thickened turbulent boundary layer on a flat plate. Velocities were measured by hot-wire anemometers, and turbulent shears were measured in the boundary layer near the wall from which the surface friction factor could be indirectly determined, that is, when $v_o = 0$, $\partial p/\partial x = 0$

$$\frac{\partial \tau}{\partial y} = 0$$

for small y, or

$$\tau_w \cong \tau = \rho \overline{u'v'}$$

for small y but where $\epsilon_m >> \nu$.

(3) Data of Smith and Walker (Ref. 50)

These data were measured for turbulent boundary layers on a flat plate. Velocities were determined by pressure probes. Friction factors were determined with a floating element flush with the plate surface.

The analytical, universal velocity distribution without transpiration computed using Equations (2-60) and (2-67) is compared with the above data

in Figures 4(a), 4(b), and 4(c).[4] It may be concluded that this technique for computing velocity distributions does a good job of representing the available data, particularly in view of the data of Klebanoff, and those of Smith and Walker.

In addition, it is possible to compare the predictions of various turbulence parameters involving derivatives of the velocity profile with data. These comparisons are presented in Figures 5 through 7. Figure 5 compares the predicted turbulent shear variation with data as obtained by Laufer. In Figure 6, the eddy viscosity, as obtained from Schubauer's presentation (Fig. 6 of Ref. 51) of the interpreted data of Laufer and Klebanoff, are compared with the predictions of the model. Finally, in Figure 7, predictions of two related functions, the energy dissipation function and the turbulent energy production are compared with the values interpreted from the data of Laufer and Klebanoff and presented by Schubauer. In all cases, the comparisons are excellent.

It should be noted that, to this point, comparisons with data have been based primarily on surface shear data obtained in some direct fashion at each station, that is, turbulent shear measurements by floating elements, turbulence correlations, or pressure gradients in pipe flow. Thus, the uncertainties recounted at the beginning of this subsection have been avoided in the verification of the proposed law-of-the-wall representation for the case where $v_o = 0$. In general, this verification would apply equally well to the other continuous models compared in Figure 3, Reichardt or van Driest.

That the simple model proposed in Section 2.2.2.2 accurately predicts events in the range of the "law of the wall" seems well-established for the constant property. impervious wall boundary layer. The success of the model when extended to more general boundary layers will be considered next.

2.2.3 The one-dimensional momentum boundary layer with surface mass addition

Using the preceding discussion on the momentum boundary layer without surface mass addition as a basis, this section will introduce the complicating factors associated with surface mass addition. In the past, this extension has been performed most successfully by use of the mixing length concept, its success having led to its adoption in the present study. A thorough evaluation of the existing data under conditions of surface mass addition will be

---

[4] Direct comparison of the flat-plate relations can be made with pipe flow when attention is confined to the region close to the wall, $y/r \ll 0.1$.

presented in the following sections along with the general comparison of these data with the predictions of the postulated mixing length relations.

2.2.3.1 Previous mixing length representations

The fact that mixing-length theory is readily applicable to the case of transpiration, as previously stated, has been demonstrated, for example, by Rubesin, Kendall, and Mickley and Davis, References 22, 17, and 15. Although these authors have assumed a two-layer approach similar to the Prandtl-Taylor model and thus do not satisfy the current ground rules of a continuous velocity gradient, their successes require some consideration. Therefore, prior to developing a model consistent with the specified ground rules for this study, a brief review of the previous developments will be presented in the following paragraphs.

For the so-called laminar sublayer ($\epsilon_M/\nu = 0$, $\ell^+ = 0$), the solution for the momentum equation is

$$u^+ = \frac{1}{v_o^+}\left(e^{v_o^+ y^+} - 1\right) \tag{2-69}$$

In the two-layer model this solution is presumed to apply over the range

$$0 \leq y^+ \leq y_a^+$$

where y_a^+ is the non-dimensional thickness of the "laminar sublayer" and will, in general, be a function of v_o^+, the mass-transfer parameter.

For the values of y^+ greater than y_a^+, the quantity ϵ_M/ν is assumed to be much greater than 1, allowing Equation (2-29) to be

$$\frac{du^+}{dy^+} = \frac{1 + v_o^+ u^+}{\ell^{+2}\dfrac{du^+}{dy^+}} = \frac{1}{\kappa^2 y^{+2}}\,\frac{1 + v_o^+ u^+}{\dfrac{du^+}{dy^+}} \tag{2-70}$$

whose solution, with appropriate limits of integration, yields

$$u^+ = \frac{1}{v_o^+}\left[\left(e^{v_o^+ y_a^+/2} + \frac{v_o^+}{2\kappa}\ln\frac{y^+}{y_a^+}\right)^2 - 1\right] \tag{2-71}$$

for

$$y_a^+ < y^+ < \infty$$

Several postulates have been made with regard to the variation of the laminar sublayer thickness, y_a^+, with transpiration. Rubesin (Ref. 22) assumed two types of conditions from which two forms of this variation could be determined, that is, postulate 1

$$u_a^+ y_a^+ = \text{constant} \tag{2-72}$$

This assumes the Reynolds number based on sublayer thickness and the interface velocity is a constant and is analogous to a transition Reynolds number. This assumption yields, from Equation (2-69)

$$\frac{y_a^+}{y_{a_o}^+}\left(e^{v_o^+ y_a^+} - 1\right) = v_o^+ y_{a_o}^+ \tag{2-73}$$

where the subscript, o, on y_a^+ refers to the value without surface mass addition. An alternative assumption, postulate 2, is

$$u_a^+ = \text{constant}$$

which yields

$$\frac{y_a^+}{y_{a_o}^+} = \frac{\ell n\left(1 + v_o^+ y_{a_o}^+\right)}{v_o^+ y_{a_o}^+} \tag{2-74}$$

Van Driest, Reference 2, assumed that the Reynolds number based on the thickness of the laminar sublayer and the local shear velocity was invariant, that is,

$$\frac{y_a\sqrt{\frac{\tau_a}{\rho}}}{\nu} = \text{constant} = \frac{y_{a_o}\sqrt{\frac{\tau_o}{\rho}}}{\nu} = y_{a_o}^+ = y_a^+\sqrt{\frac{\tau_a}{\tau_o}}$$

$$= y_a^+\left(1 + v_o^+ u_a^+\right)^{1/2} = y_a^+ e^{v_o^+ y_a^+/2} \tag{2-75}$$

or

$$\frac{y_a^+}{y_o^+} e^{v_o^+ y_a^+/2} = 1 \qquad (2\text{-}76)$$

Kendall (Ref. 17) found that the variation of the laminar sublayer thickness required for Equation (2-71) to fit his data in the turbulent core was remarkably similar to that postulated by van Driest (Eq. (2-76)) and the second postulate of Rubesin, Equation (2-74). Both of these theoretical postulates yielded essentially identical values of laminar sublayer thickness as indicated in Figure 8.

2.2.3.2 Proposed mixing length representation and resultant predictions

Since the above relations depend on the existence of a purely laminar sublayer up to y_a^+ to form the relation for y_a^+, their extension to the techniques permitting a continuous decay of turbulence all the way to the wall is not well defined. Fortunately, the extension of the technique proposed in Equation (2-65) is quite straightforward. This relation becomes

$$\frac{d\ell^+}{dy^+} = \frac{\kappa y^+ - \ell^+}{y_a^+} \frac{\sqrt{\tau/\rho}}{\sqrt{\tau_o/\rho_o}} \qquad (2\text{-}77)$$

where the effect of transpiration manifests itself in the locally variable shear ratio. With Equation (2-26), this expression becomes, for the constant property boundary layer

$$\frac{d\ell^+}{dy^+} = \frac{\kappa y^+ - \ell^+}{y_a^+} \left(1 + v_o^+ u^+\right)^{1/2} \qquad (2\text{-}78)$$

Because of the implicit nature of Equation (2-78), it is intractable in closed form for $v_o^+ \neq 0$. Since the use of a computer had long since been accepted, this did not result in any significant complication of the solution procedure.

The results obtained when Equation (2-78) is combined with Equation (2-60) and the indicated integration is carried forward numerically are presented in Figure 9 for a range of values of the blowing parameter v_o^+ and $y_a^+ = 11.83$, its value for the zero surface mass-transfer case. Before an assessment can

be made of the accuracy of this inner region prediction technique, including the assumption of a constant y_a^+, it will be necessary to demonstrate means of obtaining the local skin friction to be used in the dimensionless parameters u^+ and y^+. This is the topic of the next section.

2.2.3.3 Evaluation of available friction factor data

As was noted in the preceding section, values of the local wall shear are required to normalize velocity profile data if these data are to be compared directly with the predictions of the law of the wall. Most of the existing skin-friction data for cases with transpiration have been evaluated employing the integral momentum equation for two-dimensional flow, namely:

$$\frac{C_f}{2} = \frac{d\theta}{dx} - \frac{v_o}{u_1} + (2 + H)\frac{\theta}{u_1}\frac{du_1}{dx} \qquad (2\text{-}79)$$

wherein the sum and difference between experimentally determined parameters are required. This is rather an inaccurate procedure when the positive and negative terms are both large and of the same magnitude. Although the accuracy of friction factors interpreted from data by use of Equation (2-79) is reduced when v_o/u_1 is positive, it is enhanced when v_o/u_1 is negative, that is, for the cases of suction. Thus, the suction data of Dutton, Reference 16, becomes an important basis of comparison.

For positive values of v_o/u_1, the data obtained at MIT under the direction of H. S. Mickley represent an extensive source of two-dimensional data. Before comparisons are made with these data, however, it is well to subject it to some scrutiny, as is done in the next paragraphs.

A series of reports and doctoral dissertations containing transpiration data have been originated at MIT, authored by Mickley, Stewart, Squyres, Gessner, Curl, Davis, Kendall, Smith, Goodwin, and Butensky (Refs. 9 through 15 and 17 through 20). These sources contain data for heat, mass, and momentum transfer under the influence of transpiration into incompressible turbulent boundary layers on a flat porous plate. With one exception, all reported friction factors were determined from velocity profiles and the integral momentum equation. In detail, uncertainties in this method of evaluation of the friction factors arise for the following reasons:

(1) Lack of knowledge of <u>local</u> transpiration rates in the vicinity of the survey probe, in contrast to the reported average compartment transpiration rates.

(2) The influence of three-dimensional wind-tunnel flow effects when evaluations are based on the presumption of two-dimensional flow.

(3) As blowing rate increases, the gradient in the momentum thickness ($d\theta/dx$) approaches the blowing-rate parameter, v_o/u_1, and the calculated friction factor is the result of a small difference in two large numbers, each with some error, Equation (2-79).

(4) The determination of the gradient of the momentum thickness along the plate requires differentiation of experimental data.

For these reasons, an attempt has been made here to report momentum data in an alternate form, in order to distinguish differences in experimental results, and in the hope of determining experimental friction factors in light of all of the available data. To this end, the following format for data presentation was adopted. The momentum integral, Equation (2-79), when integrated with respect to x, yields

$$\frac{\bar{C}_f}{2} Re_x = Re_\theta - \frac{\rho_1 u_1}{\mu} \int_0^x \frac{v_o}{u_1} dx + \frac{\rho_1 u_1}{u_1} \int_0^x \theta(2 + H) \frac{d \ell n\, u_1}{dx} dx \quad (2\text{-}80)$$

The terms on the right side of the above equation can be evaluated directly from velocity profile data, the surface injection rate distribution, and the velocity gradient along the surface. No differentiation of experimental profile data is required and the attendant uncertainties of such an operation are avoided in the comparisons that follow. Although $(\bar{C}_f/2)Re_x$ cannot be considered a universal relationship independent of such factors as the location of the boundary-layer transition, the strength of boundary-layer trips, and the streamwise pressure gradients, this relationship is quite useful in the comparison of data all taken with similar equipment and flow conditions.

The drag parameter $(\bar{C}_f/2)Re_x$ for some of the MIT data is presented in Figures 10(a) through (d). It is seen that a significant spread in the data exists between and within the data sources. This spread is likely to be due, primarily, to the uncertainty in the local blowing rate, that is, in the blowing rate along the axial plane in which the velocity profiles were measured, in contrast to the spanwise average blowing rate that was the actual quantity measured. For cases in which concentration or temperature profiles were measured simultaneously (or at least for the same operating conditions) with the velocity profiles, mass or energy balances can be performed on the system in order to establish the consistency of the reported blowing rates.

For cases in which concentration profiles were measured, the following overall mass balance can be written on a given specie:

$$\int_0^x v_o \left(x_{i_2} - x_{i_1}\right) dx = \int_0^\delta u \left(x_i - x_{i_1}\right) dy \qquad (2\text{-}81)$$

where x_{i_2} is the mole fraction of the species i in the undiluted injectant and x_{i_1} is its mole fraction in the free stream. Equation (2-81) presumes that the mole density of this mixture is essentially constant (i.e., temperature and pressure are constant for a mixture of perfect gases)[5]. In terms of the mass thickness (Eq. (2-46) at $y = \delta$) this becomes

$$\frac{1}{u_i}\left(x_{i_2} - x_{i_1}\right) \int_0^x v_o \, dx = \Gamma_i \left(x_{i_o} - x_{i_1}\right) \qquad (2\text{-}82)$$

since x_{i_2} and x_{i_1} were constant with distance along the plate for the available data.

Similarly, an overall energy balance in low speed flow with constant C_p results in

$$\xi(T_o - T_1) - \frac{1}{u_1} \int \frac{\Sigma \dot{q}}{\rho C_p} dx = \frac{1}{u_1} \int_0^x v_o (T_2 - T_1) dx \qquad (2\text{-}83)$$

where $\Sigma\dot{q}$ = sum of electrical heat input less losses per unit surface area, and T_2 is the temperature of the pure injectant prior to its contact with the surface heating units.

The right-hand side of Equation (2-82) was plotted against its left-hand side (Ref. 17), using the helium data of that reference. The resultant curve has been duplicated here as Figure 11. The slope of the line best fitting these data is 1.10. Thus, if all other parameters of Equation (2-82) are presumed accurate, it is possible to conclude that

$$\frac{v_{o_{actual}}}{v_{o_{measured}}} \approx 1.1$$

---

[5]For the available data this assumption is less restrictive than the constant mass density assumption introduced in the theoretical development.

for cases when v_o is approximately constant. The required presumption is relatively sound since no differentiation or extrapolation is required to obtain the necessary parameters. For this reason the blowing rates reported in Reference 17 include this correction factor.

In Figure 12(a), the right-hand side of Equation (2-83) was plotted against its left-hand side for one run of Squyres (Refs. 9 and 10). When heat losses are ignored it is seen that the slope of the curve is 1.38 indicating, for approximately constant v_o,

$$\frac{v_{o_{actual}}}{v_{o_{measured}}} = 1.38$$

Equation (2-83) indicates that inclusion of heat losses would further increase this factor. In Figure 12(b), a similar plot was prepared for one run of Reference 12. It is seen that a fairly good energy balance is obtained for these latter data. The effect of heat losses is also indicated based on the original estimates of Curl in Reference 12. He considers the loss calculation to be accurate only to within ± 50 percent, however. The indicated values of the ratio $v_{o_{actual}}$ to $v_{o_{measured}}$ are 0.89 and 0.95 for the balances, excluding and including heat losses, respectively.

It might appear unusual that this parameter varies so significantly from one set of data to another, since nonuniformities in blowing distribution and/or three-dimensional effects would normally be considered a characteristic of the apparatus. In each instance, however, changes were made between individual experiments in the configuration of the porous wall and the adjacent side walls.

As a consequence of these determinations, the transpiration rates of Squyres were "corrected" for the particular run studied. The consequent values of $\bar{C}_f \, Re_x$ were also modified and replotted in Figure 13. There results a significant improvement in the correspondence of these data with those of the other investigators. This lends credance to the postulated error mechanism.

It is apparent that, with the exception of the no-blowing data, a straight line is the only justifiable curve through the assessed data. The resultant relations will be of the form

$$Re_x \frac{\bar{C}_f}{2} = a \, Re_x^{\,b} \qquad (2\text{-}84)$$

yielding on differentiation of the entire left side

$$\frac{C_f}{2} = ab\ Re_x^{b-1} \tag{2-85}$$

The following table summarizes the results obtained using the straight lines indicated in Figures 10(a), (b), (d), (e), and 13:

v_o/v_1	a	b	ab	b-1
0.000	5.50×10^{-2}	0.768	4.23×10^{-2}	-0.232
.001	3.26×10^{-2}	.784	2.55×10^{-2}	- .216
.002	8.24×10^{-2}	.689	5.67×10^{-2}	- .311
.003	2.21×10^{-2}	.762	1.68×10^{-2}	- .238
.004	2.26×10^{-1}	.595	1.34×10^{-1}	- .405

Although a number of tests have been performed at nominal transpiration ratios of 0.005, the data when presented in the form of Figure 10 scatter wildly. As an example of this difficulty, one run from Reference 17 is plotted in Figure 14. It is obvious that the evaluation of a slope from these data is impossible. It should be emphasized that the magnitude of the ordinate of the plotted points represent on the average only about 3 percent of the experimentally determined Re_θ.

When velocity gradients exist, another integral form of the momentum equation is more convenient than Equation (2-81) in the evaluation of data, namely:

$$\int \frac{C_f}{2} \cdot u_1^{2+\bar{H}}\, dx = \theta u_1^{2+\bar{H}} - \int \frac{v_o}{u_1} u_1^{2+\bar{H}}\, dx + \int (H - \bar{H}) \theta u_1^{1+\bar{H}}\, du_1 \tag{2-86}$$

where the final term can usually be ignored if the shape factor, H, does not vary much from an average value, $\bar{H}$. This relation was used with two runs of Davis, specifically those runs which he used to define the friction factor at a v_o/u_1 of 0.005. The results are shown in Figure 15. Again the same scatter is noticed, and any conclusion with regard to actual values of friction factor must be seriously questioned.

Tewfik (Ref. 35) also used the momentum equation to evaluate friction factors at transpiration ratios to 0.003. His determinations indicated the same difficulties described here for the MIT data. It seems apparent that

these determinations have also been affected by feedback of downstream perturbations of the flow field. Such perturbations have been found significant in other experiments (Ref. 14). For this reason, the values of skin friction determined in the midrange of his test section are considered most reliable.

It is thus apparent that the values of skin friction, determined by the momentum equation, for transpiration ratios, v_o/u_1, in excess of 0.003 are subject to considerable uncertainty utilizing boundary-layer integrals.

Because of the above uncertainties, an alternate method of skin-friction evaluation was attempted in Reference 17. It was based on interpretations of the dynamic pressure measurements of the pitot probe in the vicinity of the wall. Basically, two assumptions were made. The first was that

$$\left(\frac{\overline{u^2}}{2}\right)_{\text{measured}} = \int_{y-\delta_p/2}^{y+\delta_p/2} \left(\frac{u^2}{2}\right)_{\text{undisturbed}} dy \qquad (2\text{-}87)$$

where δ_p was the probe height and y was the distance of the midplane of the probe from the wall. The second presumption was that the velocity profile ultimately approached the wall according to the laminar wall law relation (Eq. (2-69)). The technique is described in detail in Appendix B.

It is concluded in Appendix B that the procedure does indeed yield valid friction factors and that the accuracy of the technique does not degenerate as the mass addition rate is increased. It should be emphasized that the procedure is independent of any assumption with regard to the growth (or decay) or turbulence near the wall except that reasonably monatonic behavior is anticipated. On the contrary, such profile analysis procedures as those proposed by Clauser (Ref. 40) require the pre-knowledge of the "law of the wall" turbulent velocity distribution. Since the law of the wall is significantly affected by surface mass addition, the application of the Clauser procedure here will be valid only where the law of the wall with surface mass addition is verified by such independent friction-factor determinations as were discussed in this subsection.

In Figure 16 the friction factors developed in Reference 17 by use of the technique described in Appendix B are presented, together with those values obtained from the momentum equation (see the table following Eq. (2-85)). In addition, a curve based on the data of Smith and Walker (Ref. 50) is also shown along with the Schultz-Grunow correlation curve. The general agreement is well within that expected. In order to present the results of these

evaluations in a more useful fashion, Figure 17 was prepared based on a sequence of cross plots of the data of Figure 16. This latter figure might be considered the "conclusion" of this evaluation of available friction-factor data for the turbulent boundary layer with surface mass addition. Values will be taken from this figure in the next section to formulate the nondimensional velocity profile parameters and their subsequent comparison with the proposed law of the wall.

2.2.3.4 Comparison of proposed model with data

Probably the most meaningful test of the proposed law of the wall relations is its "direct" comparison with measured profile data. This comparison had to await the prior establishment of the friction factors appropriate to these measured profiles. This was done in the preceding subsection and resulted in a generalized plot of friction factor as a function of the Reynolds number and the blowing ratio (Fig. 17). In the comparisons to follow, friction factors will be obtained from this figure for all flat-plate profiles.

A series of comparisons are presented in Figures 18(a) and (b) using the blowing data of Kendall and Gessner and the suction data of Dutton. For the suction profiles, essentially asymptotic condition prevailed and thus

$$\frac{C_f}{2} \rightarrow \frac{v_o}{u_1} \quad \text{as} \quad \frac{d\theta}{dx} \rightarrow 0$$

assuring rather good accuracy in the determination of friction factors for these data. The quality of all the comparisons is seen to be good. The deviations noted in the range of y^+ up to 30 are most likely due to probe and turbulence corrections, the former effect being significant only for y^+ less than 10 (see Fig. B-4). Turbulence contributions to the dynamic pressure measurements cannot be evaluated without introducing multiple assumptions but appear to approximate the noted discrepancy (based on the $\overline{u'u'}$ correlation data of Refs. 48, 49, and 19).[6]

[6]A mixing length model was proposed, namely

$$\overline{u'u'} = \ell_u^2 \left(\frac{du}{dy}\right)^2$$

where

$$\ell_u^+ \approx y^+ \left(\frac{\ell^+}{Ky^+}\right)^{1/2}$$

Using this model good agreement was obtained with all available data.

Certain additional data have been reported by Tewfik (Ref. 35). The woven screen used in these experiments produced definite roughness effects. The electromesh screen used at MIT did not produce these effects and thus direct comparison is difficult. Using the data obtained without blowing it was noted that the required value of y_a^+ for the proposed model (Eq. (2-6f)) was 6.86 (as compared to 11.825). Using this value, a comparison was made with one of the profiles reported in Reference 35, the results being shown in Figure 19. The comparison is quite satisfactory. The reduction of the effective laminar sublayer thickness by wall roughness is in accord with the supposition of Rotta. It is significant, however, that blowing does not appear to lessen this roughness effect.

Final conclusions with regard to the adequacy of the proposed wall law model will be reserved until after concentration and temperature profile comparisons are presented. To this point a certain internal consistency has been established between the chosen model, the measured profiles, and the evaluated friction-factor data. The weak link is of course the accuracy of the friction-factor data. Mass-transfer and heat-transfer coefficients are more directly determined and thus will serve as a better basis for the final assessment of the model.

2.2.4 The one-dimensional diffusion and thermal boundary-layer equations with surface mass addition

2.2.4.1 Mixing length form of equations

When viscous dissipation and chemical reactions do not occur, and when the foreign gas is present in trace quantities so that properties are essentially constant across the boundary layer, the diffusion and energy equations in the inner portion of the boundary layer can be written as follows:

$$\frac{dx^+}{dy^+} = \frac{Sc\left(1 + v_o^+ x^+\right)}{1 + \frac{Sc}{Sc'}\,\ell^{+2}\,\frac{du^+}{dy^+}} \tag{2-88}$$

$$\frac{dT^+}{dy^+} = \frac{Pr\left(1 + v_o^+ T^+\right)}{1 + \frac{Pr}{Pr'}\,\ell^{+2}\,\frac{du^+}{dy^+}} \tag{2-89}$$

In these equations, the mixing length term and the velocity gradient are obtained in numerical form from previous numerical integrations of Equations (2-78) and (2-60). Integration of Equations (2-88) and (2-89) can proceed numerically once values of the turbulent Prandtl and Schmidt numbers (Pr' and Sc') are specified.

The MIT data of Curl and Kendall were used to evaluate the turbulent Prandtl and Schmidt numbers employed in the numerical work of this study. If in the above diffusion equation it is assumed that the turbulent eddy transport is much larger than the molecular transport and v_o^+ is set equal to zero, it can be shown readily that

$$x^+ = (Sc')u^+ + \text{const} \tag{2-90}$$

In Kendall's experiment, Reference 17, he introduced a helium-air mixture into an air boundary layer at such small mass injection rates that an equation of the form of Equation (2-90) would be expected to hold over a portion of the boundary layer. When his concentration data are plotted against the local dimensionless velocity as in Figure 20, it is found that a straight-line relationship holds quite well for the data and that the turbulent Schmidt number can be represented by 0.75. The dimensionless velocity range used here is such that molecular viscosity effects can be neglected and, yet, the one-dimensional character of the flow should still apply. Under conditions of blowing, where one-dimensional eddy transport prevails, the turbulent Schmidt number can be expressed as

$$Sc' = \frac{1 + v_o^+ u^+}{1 + v_o^+ x^+} \frac{dx^+}{du^+} \tag{2-91}$$

Kendall found that he could not evaluate his data with blowing as accurately as the very small (essentially zero) blowing data described above; therefore, in the present work, the small increase in turbulent Schmidt number exhibited by the data at the increased blowing rates will be ignored. Turbulent Prandtl numbers, in the neighborhood of the wall, were found from the temperature distribution data of Curl and Gessner in a manner similar to that shown in Figure 20. It was found that a Prandtl number of 0.75 fitted the data well. Again, under the conditions of transpiration, these data contained serious uncertainties in friction factor and heat-transfer coefficients and in the velocity and temperature distributions in the inner portions of the boundary layer where these one-dimensional equations can be expected to apply.

For the purposes of this study, therefore, the turbulent Prandtl and Schmidt numbers were assumed constant, independent of surface mass transfer, and each equal to 0.75. These simplifications facilitated the integration of the diffusion and energy equations, the results of which are shown in the next section.

2.2.4.2 Comparison of concentration and temperature distributions with data

The theoretical parametric predictions of the law of the wall nondimensional concentration (Sc = 0.21, Sc' = 0.75) and temperature (Pr = 0.7, Pr' = 0.75) profiles are presented in Figures 21 and 22, respectively. The significance of these figures will become apparent in the data comparisons that follow and in the later stages of the analysis.

The theoretical predictions corresponding to the experimental concentration profiles of Kendall (using his reported friction and mass-transfer factors) are compared with his data in Figure 23. The departure of the experimental data from the theory, in its range of applicability, is well within the uncertainty of Kendall's reported mass-transfer factors; that is, adjustment of the reported mass-transfer factors of less than 10 percent is required for the predicted distributions to agree with the normalized experimental concentration profiles for the three blowing rates shown. Note that the wall pressure profile technique, discussed in Appendix B, was used to determine the experimental friction factors needed in these dimensionless coordinates.

The theoretical predictions corresponding to the temperature distribution data of Curl are shown, along with the data, in Figure 24. The ordinate in this figure is the dimensionless temperature parameter defined by Equation (2-35). It will be noted that two sets of data are given for largest blowing rate where $v_o^+ = 0.168$. The differences in these data are the Stanton numbers (C_H) employed in the correlations; the data indicated by square symbols are based on the directly measured Stanton numbers as reported, and the data represented by diamond symbols are based on Stanton numbers with the heat-loss correction excluded. The better agreement of the latter representation should not be considered significant, rather the difference between the two curves should be considered as one measure of the effect of the uncertainties in the heat-transfer coefficient data. It should be noted that the direct determination of heat-transfer coefficient is linearly dependent on the <u>local</u> transpiration ratio. This potentially represents the most significant source of uncertainty. The increasing deviations of the data from the predictions

as the wall is approached are no doubt due to the relatively large gradients of temperature close to the wall and other wall-probe interactions.

It can be concluded from the above comparisons of data and theory that the law-of-the-wall predictions of temperature distributions (employing Pr = 0.7 and Pr' = 0.75) and helium concentration distribution (using Sc = 0.21 and Sc' = 0.75) are quite satisfactory when consideration is given to the possible uncertainties in the data.

2.2.5 Conclusions regarding law of the wall

A law of the wall was developed in the previous sections that produced continuous profiles of velocity in the laminar, transitional, and fully turbulent regimes near the wall under the conditions of nonzero surface mass transfer and a constant density in the boundary layer. Profiles of the concentration of trace elements and small temperature variations were also evaluated. The theoretical model employs a mixing-length formulation that continuously approaches the Prandtl requirement, $d\ell/dy \rightarrow K$, in the fully turbulent region and the Elrod criteria at the wall. In addition, the mixing-length formulation contain factors that can be treated as constants, independent of the surface blowing rate.

When the theoretical model is compared to velocity profile data, after skin-friction factors have been established to permit expressing the profiles in dimensionless form characteristic of a wall law, it is found that there is rather good agreement over a considerable range of surface mass transfer. Further, temperature and concentration profiles were predicted and compared with data, after turbulent Prandtl and Schmidt were evaluated from zero-blowing data and assumed unchanged by surface mass transfer. The good agreement of the latter comparisons further established the usefulness of the currently proposed model, at least in the vicinity of the wall.

As stated earlier, wall laws are expressed in terms of the local surface shear. The history of the boundary-layer growth up to the point in question does not appear explicitly, but only through the value of the local shear. To establish the position of this local shear on the surface of a body, it is necessary to first establish the local boundary-layer thickness. This is accomplished by linking the law of the wall described in the previous sections with a flow model applicable to the outer portion of the boundary layer. This is accomplished in the following sections of this report.

2.3 Solution of the Two-Dimensional Boundary-Layer Equations (Law of the Wake)

As outlined in the Introduction, the turbulent boundary layer is characterized by two regions; the inner region that is essentially one dimensional and the outer region that is two dimensional. A general solution of the outer, two-dimensional region would require an understanding of turbulence mechanisms beyond the current state of knowledge and an ingeneous handling of the inner boundary conditions to provide a continuous match with the inner region. Fortunately, an empirical discovery by Clauser, Reference 6, that the eddy viscosity is essentially constant across the outer portion of a boundary layer, but varies from station to station, opens new avenues for an analytical representation of the wake region. In fact, as will be shown presently, the old standby in laminar boundary-layer theory of local similarity can be employed in this portion of the turbulent boundary layer. The novel requirements here with respect to laminar boundary-layer solutions are that the inner boundary conditions of the two-dimensional region must be established through a matching process with the inner one-dimensional law of the wall and that the eddy viscosity varies with the distance along the surface.

It will be noticed in the following development that the solution of the two-dimensional region can be achieved through the use of similarity arguments. Because some of the requirements for strict similarity are not universally realized, it is necessary to think in terms of "local" similarity much as the investigators did with laminar boundary layers that truly are not similar. This mathematical inexactness obviates the need for extreme thoroughness in the matching of the inner and outer flow, a process that would involve iterative procedures of significant complexity. Matching here is accomplished by extending the two-dimensional solution to the surface and employing a fictitious slip velocity there. This slip velocity becomes a variable that can be adjusted in the matching procedure needed to couple the flow solution for the inner and outer solution. The matching procedure will be described in detail in Section 2.4. In this section a description is given of the two-dimensional boundary-layer solution.

The basic incompressible boundary-layer equations for which a similarity solution is sought are the continuity equation, Equation (2-6), reduced to

$$\frac{\partial u}{\partial x} + \frac{\partial v}{\partial y} = 0$$

at constant density and the momentum equation, Equation (2-8), with the inviscid flow pressure gradient term retained

$$u \frac{\partial u}{\partial x} + v \frac{\partial u}{\partial y} = \bar{\epsilon}_m \frac{\partial^2 u}{\partial y^2} + u_1 \frac{du_1}{dx} \tag{2-93}$$

Here $\bar{\epsilon}_m$ is the total kinematic viscosity acting in the fully developed turbulent (or wake) region of the boundary (i.e., $\epsilon_m + \nu$ has been replaced by $\bar{\epsilon}_m$). The form of the third term in Equation (2-93) indicates an anticipation of employing the Clauser criterion that

$$\frac{\bar{\epsilon}_m}{u_1 \delta^*} = \text{const} = 0.018 \tag{2-94}$$

namely, the dependence of $\bar{\epsilon}_m$ on x through δ^* and u_1 but an independence of the normal coordinate y.

The first step in the formulation of a similarity solution involves a selection of certain similarity forms for the dependent and independent variables. For the present, these are chosen as

$$\tilde{u} = \frac{u - u_s}{u_1 - u_s} \tag{2-95}$$

$$\tilde{v} = \frac{v - v_o}{v_1 - v_o} \tag{2-96}$$

and

$$\tilde{y} = \frac{y}{\delta} \tag{2-97}$$

where u_s is the apparent wall-slip velocity and v_1 is the normal component of velocity existing at points beyond the boundary layer, that is, for y greater than δ. In general, v_1 is a function of y as well as x, but can be related to the other parameters of the solution by use of the continuity equation, that is,

$$v - v_o = - \frac{\partial}{\partial x} \int_o^y u \, dy \tag{2-98}$$

which for $y \geq \delta$ yields

$$v_1 - v_o = u_1 \frac{d\delta^*_{sim}}{dx} + \delta^*_{sim} \frac{du_1}{dx} - y \frac{du_1}{dx} \qquad (2\text{-}99)$$

Here δ^*_{sim} is employed to represent the displacement thickness of the entire similarity flow region from $y = 0$ to $y = \delta$ and with slip at the surface. It should be noted that by integrating Equation (2-98) over the range of y down to the wall, a region of the boundary is being considered where the outer flow solution does not correspond to the real flow. To account for this, a distinction is made between the displacement thickness evaluated from the similarity solution δ^*_{sim} and the displacement thickness applicable to the real flow, δ^*.

Consider first the transformation of the independent variables x and y to $\tilde{x}$ and $\tilde{y}$.

$$\tilde{x} = x \qquad (2\text{-}100)$$

$$\tilde{y} = \frac{y}{\delta} \qquad (2\text{-}97)$$

The transformation equations become

$$\frac{\partial}{\partial x} = \frac{\partial}{\partial \tilde{x}} - \frac{\tilde{y}}{\delta} \frac{d\delta}{dx} \frac{\partial}{\partial \tilde{y}} \qquad (2\text{-}101)$$

and

$$\frac{\partial}{\partial y} = \frac{1}{\delta} \frac{\partial}{\partial \tilde{y}} \qquad (2\text{-}102)$$

When the continuity equation is transformed according to Equations (2-101) and (2-102) and the dependent variables are replaced by the definitions (2-95) and (2-96), there results

$$(u_1 - u_s)\left(\frac{\partial \tilde{u}}{\partial \tilde{x}} - \frac{\tilde{y}}{\delta} \frac{d\delta}{dx} \frac{\partial \tilde{u}}{\partial \tilde{y}}\right) + \tilde{u} \frac{d}{dx}(u_1 - u_s) + \frac{du_s}{dx} + \left[u_1 \frac{d\delta^*_{sim}}{dx} + (\delta^*_{sim} - \tilde{y}\delta) \frac{du_1}{dx}\right] \frac{1}{\delta} \frac{\partial \tilde{v}}{\partial \tilde{y}} - \tilde{v} \frac{du_1}{dx} = 0 \qquad (2\text{-}103)$$

Similar transformations convert the momentum equation to

$$\left[(u_1 - u_s)\hat{u} + u_s\right]\left[\hat{u}\,\frac{d}{dx}(u_1 - u_s) + \frac{du_s}{dx} + (u_1 - u_s)\left(\frac{\partial\hat{u}}{\partial\tilde{x}} - \frac{\tilde{y}}{\delta}\,\frac{d\delta}{dx}\,\frac{\partial\hat{u}}{\partial\tilde{y}}\right)\right]$$

$$+\left\{\left[u_1\,\frac{d\delta^*_{sim}}{dx} + \delta\left(\frac{\delta^*_{sim}}{\delta} - \tilde{y}\right)\frac{du_1}{dx}\right]\tilde{v} + v_o\right\}\frac{(u_1 - u_s)}{\delta}\,\frac{\partial\hat{u}}{\partial\tilde{y}}$$

$$= \frac{\bar{\epsilon}_m(u_1 - u_s)}{\delta^2}\,\frac{\partial^2\hat{u}}{\partial y^2} + u_1\,\frac{du_1}{dx} \qquad (2\text{-}104)$$

If similarity exists, that is, $\hat{u}$ is a function of $\tilde{y}$ only, the axial variation of $\hat{u}$ at constant $\tilde{y}$ must vanish. Incorporating this similarity assumption into the above relations and further rearranging them results in a continuity equation of the form

$$-\left[(u_1 - u_s)\,\frac{1}{\delta}\,\frac{d\delta}{dx}\right]\tilde{y}\,\frac{d\hat{u}}{d\tilde{y}} + \left[\frac{d}{dx}(u_1 - u_s)\right]\hat{u} + \left(\frac{du_o}{dx}\right) + \left(-\frac{du_1}{dx}\right)\tilde{v}$$

$$+\left(\frac{u_1}{\delta}\,\frac{d\delta^*_{sim}}{dx} + \frac{\delta^*_{sim}}{\delta}\,\frac{du_1}{dx}\right)\frac{d\tilde{y}}{dv} - \left(\frac{du_1}{dx}\right)\tilde{y}\,\frac{d\tilde{y}}{d\tilde{y}} = 0 \qquad (2\text{-}105)$$

and a momentum equation of the form

$$\left(u_s\,\frac{du_s}{dx} - u_1\,\frac{du_1}{dx}\right) + \left[\frac{d}{dx}u_s(u_1 - u_s)\right]\hat{u} - \left[u_s(u_1 - u_s)\,\frac{1}{\delta}\,\frac{d\delta}{dx}\right]\tilde{y}\,\frac{d\hat{u}}{d\tilde{y}}$$

$$+\left[(u_1 - u_s)\,\frac{d}{dx}(u_1 - u_s)\right]\hat{u}^2 - \left[(u_1 - u_s)^2\,\frac{1}{\delta}\,\frac{d\delta}{dx}\right]\hat{u}\tilde{y}\,\frac{d\hat{u}}{d\tilde{y}}$$

$$+\left[\frac{(u_1 - u_s)}{\delta}\,\frac{d(\delta^*_{sim}u_1)}{dx}\right]\tilde{v}\,\frac{d\hat{u}}{dy} - \left[\frac{du_1}{dx}(u_1 - u_s)\right]\tilde{y}\tilde{v}\,\frac{d\hat{u}}{d\tilde{y}} + \left[\frac{v_o(u_1 - u_s)}{\delta}\right]\frac{d\hat{u}}{d\tilde{y}}$$

$$= \left[\frac{\bar{\epsilon}_m(u_1 - u_s)}{\delta^2}\right]\frac{d^2\hat{u}}{d\tilde{y}^2} \qquad (2\text{-}106)$$

In order to achieve similarity, the axially dependent coefficients of the variables in the above equations must be in constant ratio to avoid the inconsistency of an x dependence. If the Clauser parameter is modified to

$$\frac{\epsilon_m}{u_1 \delta^*_{sim}}$$

(a relative minor change) and is presumed constant, it is required that the following parameters be axially invariant (or at least very slowly varying)

$$\frac{u_s}{u_1}, \quad \frac{v_o}{u_1}, \quad \frac{d\bar{\delta}}{dx}, \quad \frac{\bar{\delta}}{u_1}\frac{du_1}{d\bar{\delta}}, \quad \frac{\delta^*_{sim}}{\delta}$$

The first two parameters require a linear dependence of the fictitious slip velocity and the normal surface mass transfer velocity on the free-stream velocity at the edge of the boundary layer. For a flat plate, the latter parameter would indicate the requirement of a constant blowing rate along the plate. The third parameter indicates a linear growth of the boundary layer. The fourth parameter, when combined with the third, results in a requirement on the allowed free-stream velocity distribution, namely -

$$u_1 = (ax + b)^m$$

where a, b, and m are constants. The fifth parameter indicated is not really independent as can be discerned from the definition of the displacement thickness expressed in terms of the similarity variables

$$\frac{\delta^*_{sim}}{\delta} = \left(1 - \frac{u_s}{u_1}\right) \int_0^1 (1 - \theta) d\tilde{y} \qquad (2\text{-}107)$$

The value of the definite integral is itself dependent on v_o/u_1 and u_s/u_1; thus, the requirement of constant δ^*_{sim}/δ is automatically satisfied by constant v_o/u_1 and u_s/u_1 and no new requirement is imposed.

The effect of expressing the Clauser parameter in terms of δ^*_{sim} rather than δ^* is approximately 5 percent (i.e., $\epsilon_m/u_1\delta^* = 0.018 \rightarrow \epsilon_m/u_1\delta^*_{sim} = 0.019$) since the ratio of the two displacement thicknesses was, for the entire range of data studied, approximately 0.95. In the numerical work reported here, this modification was <u>not</u> employed and an iterative technique was introduced to correct the solutions. It soon became obvious that this iteration was not warranted and that the constancy of the modified Clauser parameters was as readily justifiable as was the constancy of the original parameter.

Because of the requirement that u_s/u_1 be constant, no loss in generality results from replacing $\hat{u}$ with u/u_1 or $\tilde{u}$. Also, the requirement that δ^*_{sim}/δ be constant permits redefining $\tilde{y}$ as y/δ^*_{sim}. These redefinitions result in considerable algebraic simplification in the transformed continuity equation

$$\frac{\delta^*_{sim}}{u_1}\frac{du_1}{dx}(\tilde{u}-\tilde{v}) - \frac{d\delta^*_{sim}}{dx}\tilde{y}\frac{d\tilde{u}}{d\tilde{y}} + \left(\frac{d\delta^*_{sim}}{dx} + \frac{\delta^*_{sim}}{u_1}\frac{du_1}{dx}\right)\frac{d\tilde{y}}{d\tilde{y}} - \frac{\delta^*_{sim}\tilde{y}}{u_1}\frac{du_1}{dx}\frac{d\tilde{y}}{d\tilde{y}} = 0 \qquad (2\text{-}108)$$

and in the transformed momentum equation

$$-\frac{\delta^*_{sim}}{u_1}\frac{du_1}{dx} + \frac{v_o}{u_1}\frac{d\tilde{u}}{d\tilde{y}} + \left(\frac{d\delta^*_{sim}}{dx} + \frac{\delta^*_{sim}}{u_1}\frac{du_1}{dx}\right)\tilde{v}\frac{d\tilde{u}}{d\tilde{y}} - \tilde{y}\frac{d\delta^*_{sim}}{dx}\tilde{u}\frac{d\tilde{u}}{d\tilde{y}}$$

$$+\frac{\delta^*_{sim}}{u_1}\frac{du_1}{dx}\left(\tilde{u}^2 - \tilde{y}\tilde{v}\frac{d\tilde{u}}{d\tilde{y}}\right) = \frac{\epsilon_m}{u_1\delta^*_{sim}}\frac{d^2\tilde{u}}{d\tilde{y}^2}$$

These simultaneous differential equations, one of the first and the other of the second order, can be combined into a single third-order equation. This is done by solving the continuity equation for $\tilde{v}$ and introducing it into the momentum equation. Before doing this, however, it is well to introduce certain simplified nomenclature by means of the following definitions:

$$a_1 = \frac{d\delta^*_{sim}}{dx}$$

$$a_2 = \frac{C_f}{2} \equiv \frac{\tau_o}{\rho u_1^2}$$

$$a_3 = \frac{u_s}{u_1}$$

$$a_4 = \frac{v_o}{u_1}$$

$$a_5 = \frac{\delta^*_{sim}}{u_1}\frac{du_1}{dx}$$

$$a_6 = \frac{\epsilon_m}{u_1\delta^*_{sim}}$$

An expression for the $\tilde{v}$ can be obtained by integrating the continuity equation once with respect to $\tilde{u}$ and rearranging, yielding

$$\tilde{v} = \frac{(a_1 + a_5) \int \tilde{y}\, d\tilde{u} - a_5 \tilde{y}\tilde{u}}{a_1 + a_5 - a_5 \tilde{y}} \tag{2-110}$$

when this relation is introduced into the momentum equation the following third-order differential equation is obtained

$$a_6 \frac{d^2\tilde{u}}{d\tilde{y}^2} + \left[(a_1 + a_5) \int \tilde{u}\, d\tilde{y} - a_4\right] \frac{d\tilde{u}}{d\tilde{y}} + a_5(1 - \tilde{u}^2) = 0 \tag{2-111}$$

The integral in the coefficient of the second term in Equation (2-111) can be eliminated by introducing a stream-function related term, namely

$$g' = \frac{dg}{d\tilde{y}} = \tilde{u} \tag{2-112}$$

In terms of this variable, Equation (2-111) becomes

$$a_6 g''' + \left[(a_1 + a_5)g - a_4\right] g'' + a_5(1 - g'^2) = 0 \tag{2-113}$$

and the following boundary conditions apply:

$$\tilde{y} = 0 \qquad g = \int_0^{\tilde{y}} \tilde{u}\, d\tilde{y} = 0$$
$$g' = \tilde{u}_s = a_3 \tag{2-114}$$

and

$$\tilde{y} \to \infty \,^{7} \qquad g' = \tilde{u} \to 1$$

With the exception of the term containing a_4 which relates to surface mass addition, this equation is identical to the one presented by Clauser in Reference 6.

Before the techniques employed in the solution of the problem described in Equations (2-113) and (2-114) are discussed, it is convenient to relate the dependent variable g with the actual shear at the wall and with the

---

[7] See also Equation (2-121).

displacement thickness. The momentum equation for the two-dimensional solution with slip, Equation (2-93), reduces to the following equation as $y \to 0$

$$u_s \frac{\partial u_s}{\partial x} + v_o \frac{\partial u}{\partial y} = \frac{1}{\rho} \frac{\partial \tau}{\partial y} + u_1 \frac{du_1}{dx} \tag{2-115}$$

For $u_s = a_3 u_1$, Equation (2-115) becomes

$$\frac{\partial \tau}{\partial y} = \rho a_3 u_1 \frac{du_1}{dx} - \rho u_1 \frac{du_1}{dx} + \rho v_o \frac{\partial u}{\partial y} \tag{2-116}$$

which when integrated with respect to y yields

$$\tau - \tau_s = \rho u_1 \frac{du_1}{dx} \left(a_3^2 - 1\right) y + \rho v_o (u - u_s) \tag{2-117}$$

In the actual boundary layer, no slip occurs and the corresponding expression for the local shear is

$$\tau - \tau_o = \rho v_o u \tag{2-118}$$

For the same shear condition away from the surface in the real boundary layer as in the one with slip, the following relationship is required at $y = 0$

$$\tau_o + \rho v_o u_s = \tau_s = \rho \bar{\epsilon}_m \left(\frac{\partial u}{\partial y}\right)_s \tag{2-119}$$

In terms of the g function, Equation (2-119) can be rewritten as

$$\frac{C_f}{2} = \frac{\tau_o}{\rho u_1^2} = -\frac{v_o}{u_1} \frac{u_s}{u_1} + \frac{\epsilon_m}{u_1 \delta^*_{sim}} \left(\frac{\partial \tilde{u}}{\partial \tilde{y}}\right)_s$$

or

$$g''(0) = \frac{a_2 + a_3 a_4}{a_6} \tag{2-120}^{a}$$

Also

$$\delta^*_{sim} = \int_{\delta}^{y>\delta} (1 - \tilde{u}) dy$$

---

[a] Note that the additional local similarity requirement that $C_f/2$ be constant is introduced here.

or

$$1 = \int_{\delta}^{y>\delta} (1 - \tilde{u})d\tilde{y} = \tilde{y} - g$$

$$g = \tilde{y} - 1 \qquad (2\text{-}121)$$

at large $\tilde{y}$. Equation (2-121) represents an additional boundary condition for large $\tilde{y}$ in Equation (2-114).

To avoid the iterations inherent in the numerical integration of the boundary-value problem discussed by Equations (2-113) and (2-114), the basic problem is transformed to an initial value problem through the transformations

$$\left.\begin{aligned} f &= c_1 g \\ \xi &= c_2 \tilde{y} \end{aligned}\right\} \qquad (2\text{-}122)$$

where c_1 and c_2 are constants. Restricting Equation (2-113) to no main stream acceleration, that is, a flat plate with $a_5 = 0$, the transformations (2-122) result in

$$Af'' - Bff'' = f''' \qquad (2\text{-}123)$$

with the boundary conditions

$$\begin{aligned} \xi = 0 \qquad & f = 0 \\ & f' = D \\ & f'' = C \\ \xi \to \infty \qquad & f = F \\ & f' = E \end{aligned} \qquad (2\text{-}124)$$

where the parameters A, B, C, D, E, and the function F are defined by

$$\begin{aligned} A &= \frac{a_4}{c_2 a_6} & D &= \frac{c_1}{c_2} a_3 \\ B &= \frac{a_1}{c_1 c_2 a_6} & E &= \frac{c_1}{c_6} \\ C &= \frac{c_1}{c_2^2} \frac{a_2 + a_3 a_4}{a_5} & F &= c_1 \left(\frac{\xi}{c_6} - 1 \right) \end{aligned} \qquad (2\text{-}125)$$

It can be seen that if an arbitrary set A, B, C, and D is specified then a complete initial value problem has been formulated. The solution of this problem will yield the parameter E and, from the definitions, the function F. It is seen that knowledge of these latter two quantities permits the evaluation of c_1 and c_2 and subsequently the evaluation of the remaining parameters. From this process there results a self consistent set of values for the parameters a_3, a_4/a_6, a_1/a_6, and a_2/a_6 without recourse to iterating the solution of the differential equation. Thus, in terms of physical quantities a consistent set is found between $C_f/2$, v_o/u_1, u_s/u_1, and $d\delta^*_{sim}/dx$.

Equation (2-123) was solved using a standard Runge-Kutta routine. To test this parametric procedure, it was applied to the Blasius problem. For this case of a laminar boundary layer a_6 is no longer a constant; however,[9]

$$\frac{a_1}{a_6} = \text{const} = Re_{\delta^*} \frac{d\, Re_{\delta^*}}{d\, Re_x} = c_2 A \tag{2-126}$$

and

$$\frac{a_1}{a_6} = \text{const} = \frac{C_f}{2} Re_{\delta^*} = \frac{c_2^2}{c_1} C \tag{2-127}$$

Also, with zero mass addition and surface slip, there results $a_3 = a_4 = 0$. Thus, the problem is defined as an initial value problem when A, B, and C are arbitrarily selected. Two independent sets of A, B, and C were utilized and both yielded

$$\frac{C_f}{2} = 0.33205\, Re_x^{-1/2} \tag{2-128}$$

the classical laminar boundary-layer solution.

In the numerical work associated with the similarity portion of the boundary-layer, values of A, B, C, and D were arbitrarily assigned. It was found that 72 independent solutions were adequate to provide solutions covering the following ranges:

---

[9] If after Equation (2-106), $\bar{\epsilon}_m$ is considered axially independent, the resultant set of axially independent parameters is a_3 and $u_1\delta^*_{sim}$ times a_1, a_2, a_4, a_5, and a_6.

$$0.3 < u_s/u_1 < 1.0$$

$$-0.003 < v_o/u_1 < 0.005$$

and a wide variety of values of $C_f/2$ and $d\delta^*/dx$. How these results are related to the "law-of-the-wall" regio' will be described in detail in the next section.

2.4 Matching Procedure for Solutions of the Laws of the Wall and the Wake

In the previous sections, solutions of the laws of the wall and wake were found having the following functional relationships

$$\text{Law of the wall} \quad u^+ = F(y^+, v_o^+) \tag{2-129}$$

$$\text{Law of the wake} \quad \tilde{u} = G(\tilde{y}, v_o/u_1, C_f/2, u_s/u_1, d\delta^*/dx) \tag{2-130}$$

The four parametric terms on the right of Equation (21-30) (other than $\tilde{y}$) are not randomly variable but were found to be grouped in self consistent sets in which two of the parameters may be considered independent.

Several matching procedures are possible to link these solutions, however, the one described here is thought to be the most straightforward in concept.

The matching procedure is begun by selecting arbitrarily one of the sets of parameters

$$\frac{v_o}{u_1}, \quad \frac{C_f}{2}, \quad \frac{u_s}{u_1}, \quad \frac{d\delta^*}{dx}$$

found to be self co t. The profile results of the two-dimensional similarity solution i en plotted as $\tilde{u}$ versus $\tilde{y} = y/\delta^*_{sim}$. Knowledge of $C_f/2$ and v_o/u_1 permits the direct evaluation of v_o^+ from Equations (2-33) and (2-36) as

$$v_o^+ = \frac{v_o}{u_1\sqrt{C_f/2}} \tag{2-131}$$

Identification of v_o^+ permits establishing the particular unique relationship of u^+ versus y^+ corresponding to Equation (2-130) for the inner region. At this point a particular y^+_{match} and, thus, u^+_{match} is tentatively chosen as the match point. Since the value of $\bar{\epsilon}_m/\nu$ increases continuously

from unity at $y^+ = 0$ all along the inner solution, chosing y^+_{match} also yields a value of $(\bar{\epsilon}_m/\nu)_{match}$. Since the outer region was assumed to have a constant value of $\bar{\epsilon}_m$, it is the value of $(\bar{\epsilon}_m/\nu)_{match}$ that is applicable over the entire outer region. From Equation (2-94) it can be shown that

$$Re_{\delta^*_{sim}} = \frac{u_1 \delta^*_{sim}}{\nu} = \frac{\left(\bar{\epsilon}_m/\nu\right)_{match}}{a_3} \tag{2-132}$$

Utilizing this information, it is easy to relate the coordinates of the inner and outer flows, namely,

$$\tilde{u} = u^+\sqrt{c_f/2} \tag{2-132}$$

and

$$\tilde{y} = \frac{y^+}{\sqrt{Re_{\delta^*_{sim}}}\sqrt{c_f/2}} \tag{2-134}$$

The value of y^+_{match} is moved about iteratively until $\tilde{u}_{match}$ and $\tilde{y}_{match}$ lie on the $\tilde{u}(\tilde{y})$ curve of the outer flow solution.[10]

The resulting curve of $\tilde{u}(\tilde{y})$ is then utilized to evaluate local boundary-layer thickness characteristics needed in subsequent correlations. The displacement thickness of the combined boundary layer is given by

$$\frac{\delta^*}{\delta^*_{sim}} = \int_0^{\tilde{y}_{match}} (1 - \tilde{u})\, d\tilde{y} + \int_{\tilde{y}_{match}}^{\infty} (1 - \tilde{u})\, d\tilde{y} \tag{2-135}$$

and the momentum thickness is given by

$$\frac{\theta}{\delta^*_{sim}} = \int_0^{\tilde{y}_{match}} \tilde{u}(1 - \tilde{u})\, d\tilde{y} + \int_{\tilde{y}_{match}}^{\infty} \tilde{u}(1 - \tilde{u})\, d\tilde{y} \tag{2-136}$$

---

[10] Although the matching method is described as a graphical process, in actual practice the procedure was programed to be performed by the computer. A mismatch in the local shear also results; however, this has been estimated as less than 0.5 percent of the local shear.

The integrals utilize the velocity distribution appropriate to the inner and outer layers of the boundary layer. Equations (2-135) and (2-136) combined with Equation (2-132) yield the displacement and momentum thickness boundary layer appropriate to the blowing parameter, v_o/u_1, and skin-friction coefficient $C_f/2$, in the Equation (2-131).

2.5 Evaluation of Reynolds Numbers Based on the Length of Run

The previous section described the technique for establishing the relationships

$$\frac{C_f}{2} = f_1\left(Re_\theta, \frac{v_o}{u_1}\right) \tag{2-137}$$

$$H = \frac{\delta^*}{\theta} = f_2\left(R_\theta, \frac{v_o}{u_1}\right) \tag{2-138}$$

for the entire boundary layer. To relate the skin-friction coefficient with the Reynolds number based on the length of run, use is made of the integral form of the momentum Equation (2-51). For a flat plate, this equation becomes

$$\frac{C_f}{2} + \frac{v_o}{u_1} = \frac{dR_\theta}{dR_x} \tag{2-139}$$

For constant v_o/u_1 and turbulent flow from the leading edge, this equation can be integrated conveniently to yield

$$Re_x = \int_0^{R_\theta} \frac{dR_\theta}{\frac{C_f}{2} + \frac{v_o}{u_1}} \tag{2-140}$$

The integral in Equation (2-140) was evaluated numerically from the results indicated by Equation (2-137). In the vicinity of the leading edge it was necessary to extrapolate to R_θ smaller than given by the numerical examples worked out. This was accomplished by first deriving an exponential equation for $C_f/2$ in terms of Re_θ from the small Re_θ numerical results and, thus, using this equation for extrapolating the very small values of R_θ.

If one accepts the argument that Equations (2-137) and (2-138) are the basis of a local similarity even under conditions where streamwise pressure

gradients occur, the entire momentum equation, Equation (2-51), can be solved numerically to also yield the growth of the boundary layer on two-dimensional bodies other than flat plates. It would be preferable, however, to expand the set of independent parameters to include the local pressure gradient parameter, a_s, and then enter the integral momentum equation.

2.6 Solution of the Energy and Diffusion Equations

The solutions of the energy and diffusion equations follow nearly the same course as did the solution of the momentum equations, except that the matching of the innner and outer solutions is accomplished at a known position in the boundary layer where momentum matching was already established. The restriction to the constant property case in the current analysis permits separating the solutions of the individual equations and utilizing the existing momentum solution to solve the energy and diffusion equations. In the more general case, these scalar conservational equations would have to be coupled with the momentum equation and simultaneous solution of the three equations would be required.

The basic energy conservation equation for a constant property boundary layer is

$$u \frac{\partial T}{\partial x} + v \frac{\partial T}{\partial y} = \frac{\bar{\epsilon}_m}{Pr'} \frac{\partial^2 T}{\partial y^2} \qquad (2\text{-}141)$$

where the Prandtl number, Pr', is defined here as the overall ratio of momentum to energy transfer coefficients, that is,

$$Pr' = \frac{\epsilon_m + \nu}{\epsilon_H + \frac{k}{\rho C_p}} = \frac{\bar{\epsilon}_m}{\epsilon_H + \frac{k}{\rho C_p}} \qquad (2\text{-}142)$$

again replacing the sum of $\epsilon_m + \nu$ by $\bar{\epsilon}_m$. The value of Pr' in the two-dimensional region is obtained from the one-dimensional energy solution at the y_m^+ determined in the matching of the one- and two-dimensional momentum solutions. Generally, at the match point the contribution of the molecular mechanisms is negligible compared to the turbulent processes and

$$Pr' \cong \frac{\epsilon_m}{\epsilon_H} \qquad (2\text{-}143)$$

Continuity of $\bar{\epsilon}_m$, Pr', temperature, and temperature derivatives across the match point assures a continuity in the heat flux at that point. For the diffusion equations, all relations would be identical with x_a replacing T and Sc' replacing Pr'. Here,

$$Sc' = \frac{\epsilon_m + \nu}{\epsilon_D + D} \tag{2-144}$$

When the outer flow is considered, it is convenient to define the dependent variable as

$$\bar{T} = \frac{T - T_1}{T_o - T_1} = 1 - \tilde{T} \tag{2-145}$$

When Equation (2-145) is inserted into Equation (2-141) and the transformations, Equations (2-101) and (2-102), are utilized, there results

$$\frac{a_6}{Pr'} \frac{d^2\bar{T}}{d\tilde{y}^2} + \left[(a_1 + a_5)g - a_4\right] \frac{d\bar{T}}{d\tilde{y}} - a_7\tilde{u}\bar{T} = 0 \tag{2-146}$$

where

$$a_7 = \frac{\delta^*_{sim}}{T_o - T_1} \frac{dT_o}{dx} \tag{2-147}$$

Similar expressions for the diffusion equation are

$$\frac{a_6}{Sc'} \frac{d^2\bar{X}}{d\tilde{y}^2} + \left[(a_1 + a_5)g - a_4\right] \frac{d\bar{X}}{d\tilde{y}} - a_8\tilde{u}\bar{X} = 0 \tag{2-148}$$

where

$$a_8 = \frac{\delta^*_{sim}}{x_{i_o} - x_{i_1}} \frac{dx_{i_o}}{dx} \tag{2-149}$$

The boundary conditions on these equations are the requirement of a match with the inner region at $\tilde{y}_{match}$ and that $\bar{T} \to 0$ and $\bar{X} \to 0$ as $y \to \infty$. In both of the above equations, it was assumed the free-stream properties, T_1 and x_{i_1}, are invariant with distance along the surface of the body. For consistency with the previous momentum equation solutions, a_5 must be set equal to zero.

For the case of a constant surface temperature, $a_7 = 0$, and Equation (2-146) reduces to

$$\frac{d^2\bar{T}}{d\tilde{y}^2} + \frac{Pr'}{a_6}(a_1 g - a_4)\frac{d\bar{T}}{d\tilde{y}} = 0 \qquad (2\text{-}150)$$

When Equation (2-150) is integrated with respect to $\tilde{y}$, there results

$$\frac{d\bar{T}}{d\tilde{y}} = \left(\frac{d\bar{T}}{d\tilde{y}}\right)_{match} e^{-\int_{\tilde{y}_{match}}^{\tilde{y}} \frac{Pr'}{a_6}(a_1 g - a_4)d\tilde{y}} \qquad (2\text{-}151)$$

which, when integrated again, yields

$$\bar{T} - \bar{T}_{match} = \left(\frac{d\bar{T}}{d\tilde{y}}\right)_{match} \int_{\tilde{y}_{match}}^{\tilde{y}} e^{-\int_{\tilde{y}_{match}}^{\tilde{y}} \frac{Pr'}{a_6}(a_1 g - a_4)d\tilde{y}} d\tilde{y} \qquad (2\text{-}152)$$

At the upper boundary condition, there results

$$-\frac{\bar{T}_{match}}{\left(\frac{d\bar{T}}{d\tilde{y}}\right)_{match}} = \int_{\tilde{y}_{match}}^{\infty} e^{-\int_{\tilde{y}_{match}}^{\tilde{y}} \frac{Pr'}{a_6}(a_1 g - g_4)d\tilde{y}} d\tilde{y} = I_1 \qquad (2\text{-}153)$$

Since $g(\tilde{y})$ is known from the solution of the momentum equation, the integral in Equation (2-153) can be evaluated directly from the chosen self-consistent set of $d\delta^*/dx$, $C_f/2$, u_s/u_1, v_o/u_1, and the known match point.

From the solution of the inner region $T^+(y^+, v_o^+)$, and the definition, Equation (2-35), it is seen that that

$$\bar{T} = 1 - \frac{C_H}{\sqrt{C_f/2}} T^+ \qquad (2\text{-}154)$$

and

$$\frac{d\bar{T}}{d\tilde{y}} = - C_H R_{\delta^*_{sim}} \frac{dT^+}{dy^+} \tag{2-155}$$

From a combination of Equations (2-153) through (2-155), it is found that

$$C_H = \frac{\sqrt{\frac{C_f}{2}}}{I_1 \sqrt{\frac{C_f}{2}} Re_{\delta^*} \left(\frac{dT^+}{dy^+}\right)_{match} + T^+_{match}} \tag{2-156}$$

All the terms of the right member of Equation (2-156) are readily found from the prescribed values of $C_f/2$ and v_o/u_1 and y^+_{match} established in the momentum solution. From Equations (2-154) through (2-156) evaluation of $\bar{T}_{match}$ and $(d\bar{T}/d\tilde{y})_{match}$ can be made and with these quantities, the temperature distribution through the boundary layer is given by Equation (2-152) and the numerical inner flow solution $T^+(y^+)$. The energy thickness (energy decrement thickness) is found by numerically integrating the following

$$\frac{\xi}{\delta^*_{sim}} = \int_0^{\tilde{y}_{match}} \tilde{u}\bar{T}\, d\tilde{y} + \int_{\tilde{y}_{match}}^{\infty} \tilde{u}\bar{T}\, d\tilde{y} \tag{2-157}$$

over the two regions of the boundary layer. The length Reynolds number corresponding to C_H and ξ found in this manner is the same corresponding to the $C_f/2$ used as a parameter in the above procedure.

For the case of constant v_o/u_1, along a plate, the most common injection distribution utilized in the existing experiments, a change in x_o, the molar concentration at the surface, occurs with distance along the surface. This change in x_o results in the requirement for a non-zero value of a_8 (Eq. (2-149)) in Equation (2-148). Under this condition, Equation (2-148) cannot be solved in closed form and numerical integration is required. To avoid iterations in the integrations, advantage is taken of the homogeneous nature of Equation (2-148) to express

$$\bar{X} = \alpha p(\tilde{y}) \tag{2-158}$$

where at large $\tilde{y}$

$$p(\tilde{y}) = 0$$

$$p'(\tilde{y}) = 1$$

Equation (2-148) thus becomes

$$\frac{a_8}{Sc'}\frac{d^2p}{d\tilde{y}^2} + \left[(a_1 + a_5)g - a_4\right]\frac{dp}{d\tilde{y}} - a_8\tilde{u}p = 0 \qquad (2\text{-}159)$$

which can be integrated for specified values of $C_f/2$ and v_o/u_1 and assumed values of a_8. The boundary conditions that must be satisfied at $\tilde{y}_{match}$ (continuity of concentration and its derivative) require that

$$\alpha = \frac{\sqrt{\frac{C_f}{2}}\,Re_{\delta^*_{sim}}\left(x^+\right)'_{match}}{-p'_{match}x^+_{match} + p_{match}\sqrt{\frac{C_f}{2}}\,Re_{\delta^*}\left(x^+\right)'_{match}} \qquad (2\text{-}160)$$

The value of C_M is found conveniently from

$$\therefore\ C_M = \frac{\sqrt{\frac{C_f}{2}}\,(1 - \alpha p_{match})}{x^+_{match}} \qquad (2\text{-}161)$$

Both α and C_M, expressed above, are dependent on the choice of a_8 utilized in Equation (2-159). The unique value of a_8 appropriate to the solution is found iteratively from the requirement that over a plate with uniform blowing

$$Re_\Gamma = (Re_x)\left(C_M + \frac{v_o}{u_1}\right) \qquad (2\text{-}162)$$

where

$$\frac{Re_\Gamma}{Re_{\delta^*_{sim}}} = \int_0^{\tilde{y}_{match}} \tilde{u}\bar{x}\,d\tilde{y} + \int_{\tilde{y}_{match}}^{\infty} \tilde{u}\bar{x}\,d\tilde{y} \qquad (2\text{-}163)$$

is evaluated numerically. The parameter a_8 is iterated until the Re_Γ found from Equations (2-162) and (2-163) agree.

A similar situation to the above occurs for the energy boundary layer on a porous plate dissipating a constant heat flux with a uniform coolant gas injection. Here a_7 is no longer zero and has to be iterated so that

$$\frac{Re_\xi}{Re_x} = \frac{q}{\rho_1 u_1 C_p} \qquad (2\text{-}164)$$

where q is the net energy supplied to the wall, for example, electrical heating less radiation losses plus bulk convection $(\rho v_o C_p (T_2 - T_1))$.

BLANK PAGE

3. RESULTS AND DISCUSSION

In the preceding section a set of analytical procedures was developed for the prediction of the profiles of velocity, temperature, and concentration in a turbulent boundary layer. The results predicted by the "law-of-the-wall" relations were compared with data in order to establish the validity of that portion of the model. For the outer (or wake) region of the boundary layer a locally similar solution was devised. When this latter solution is coupled with the inner "wall law" solution the complete profile predictions result. These profiles can subsequently serve as the basis for integral solutions of the boundary layer.

In this section the predictions for the complete profiles will be compared with data and the subsequent results of the integral solutions will be presented, compared with data, and discussed.

However, one new postulate was introduced in the analysis of the outer region of the profile that should be evaluated prior to the presentation of the results obtained. This postulate is related to the Clauser parameter and its constancy under conditions of surface mass transfer.

The experimental variation of eddy viscosity across a boundary layer where significant surface blowing occurs is shown in Figure 25 along with hot-wire data taken over a smooth, solid plate (the filled-in symbols). The eddy viscosity corresponding to data with blowing was evaluated by employing Equation (2-48) and velocity profiles from Reference 17. Although this latter technique was not expected to be very accurate, rather good agreement was obtained with the more accurate hot-wire data. The data for the blowing case exhibit a scatter that lies almost equally above and below the more accurate data. A value of the Clauser parameter, $\epsilon_m/u_1\delta^*$, of 0.018 agrees quite well with both sets of data for $0.2 < y/\delta < 0.6$. Above $y/\delta = 0.6$ the parameter drops off, primarily due to intermittency, that is, the fraction of the time the boundary layer is turbulent at a particular value of y/δ. That this is the case is seen by the "corrected" data shown on Figure 25 which were obtained by dividing the eddy viscosity values by the values of the intermittency factors given in Reference 51. The most significant conclusion that can be drawn from this figure is that $\epsilon_m/u_1\delta^*$ can be considered to be independent of surface blowing and this is the basis of Equation (2-94).

A comparison is made in Figure 26 between experimental velocity profiles measured over smooth, non-porous plates, and the predicted results of the current analysis. The theoretical predictions shown are evaluated at the value of Re_θ that corresponded to the data. This basis of comparison on

the local boundary-layer thickness avoided those uncertainties that occur when the length-of-run Reynolds number is employed, namely, accounting for the effects of the position of natural transition downstream of the plate leading edge or of boundary-layer trips. In Figure 26(a) the velocity profile comparison is made with the data of Reference 51. Except for the data points quite close to the surface, the prediction for velocity at a given distance from the surface is within a few percent of the data. In the inner region, the difference between the prediction and the data becomes as large as 10 percent where the absolute values of the velocity are much smaller. No systematic difference between the analytical results and the data can really be expected because the Re_θ were matched; however, the prediction over-predicts and under-predicts in four alternate regions indicating a generally good agreement with the data over the whole of the boundary layer rather than favoring one boundary-layer region over the other. The comparison shown in Figures 26(b) and (c) with the data of References 52 and 11 indicates essentially an identical behavior.

In Figure 27, similar velocity profile comparisons are made with data obtained over porous plates where surface blowing or suction occurred. Again, the theoretical and experimental values of Re_θ were matched. In Figure 27(a) comparison of the analytical results is made with the data of References 16 and 17, which data cover a large range of uniform blowing and suction conditions. Again, the general agreement between the analysis and the blowing data is quite good, the differences in velocity being of the order of a few percent, except for the inner 2 percent of the boundary-layer thickness where the prediction is about 10 percent lower than the data. The significance of the latter observation is tempered when it is remembered that the probe size was rather large compared to the distance away from the surface in this region so that data errors can be expected to be larger here. The comparison with the suction data, the data points indicated by square symbols, is also very good. Except for one data point, differences of less than 4 percent occur over the entire boundary layer. The data of Reference 11, shown in Figure 27(b), show the same general agreement with the predictions as do the data of Reference 17 discussed previously. In the immediate vicinity of the wall, the differences between the data and predictions become quite large and, again, probe size effects could be important here as well as the dynamic pressure contributions of turbulence discussed in Section 2.2.3.4.

It can be concluded from Figures 26 and 27 that the analysis does quite a good job in predicting the shapes of velocity profiles under conditions of zero mass transfer, blowing, and suction.

A comparison of the analytical prediction of temperature distributions with data is presented in Figure 28. These data taken from Reference 12, apply for the case of zero blowing and for $v_o/u_1 = 0.004$ and the predictions are based on matching the analytical with the local measured values of Re_σ. The agreement between the predictions and the data is within 3 percent over the entire boundary, except for the innermost points. From this figure it can be concluded that the proposed analytical model predicts these limited number of cases of temperature distribution data quite well under the conditions of zero mass transfer or with blowing.

The distribution of helium that was injected into a boundary layer, Reference 17, is compared in Figure 29 with the prediction given by the present analysis. Again, the measured Re_θ is used as the matching criterion for the analysis. Data are presented for a case with very little blowing, $v_o/u_1 = 0.000113$, and one with rather large blowing, $v_o/u_1 = 0.00545$. For the low blowing case, the agreement between the analysis and the experiment is within 5 percent, except for the data points right next to the surface. Again, probe size may have an influence here. At the higher blowing rate, the data are generally lower than the predicted profile, with a maximum difference of about 10 percent. Generally, the differences are much lower than this maximum figure. It can be concluded, therefore, that the proposed technique does a satisfactory job in predicting concentration distributions.

The analytical results for the model of turbulent boundary layer utilized in this analysis are presented in terms of dimensionless transfer coefficients and shape factors as functions of Reynolds numbers and transpiration rates in Figures 30 through 36.

Figure 30 shows the local skin-friction coefficient on a flat plate with uniform injection as a function of the Reynolds number based on the momentum thickness. The transpiration rate, v_o/u_1, is shown as a parameter of the individual curves. For the curves representing suction, negative v_o/u_1, a limiting line is shown where the local suction rate is just equal to the local skin-friction coefficient, which then results in a constant boundary-layer thickness beyond that point (line of asymptotic suction solutions). The curves shown of this figure reveal that outward transpiration, positive v_o/u_1, reduces the local skin friction Re_θ relationship, with the reduction being greater at the larger values of Re_θ. Suction increases the skin-friction coefficient. These results are qualitatively compatible with past findings.

In Figure 30(b) the $v_o/u_1 = 0$ line from Figure 30(a) is reproduced along with the recent data from Smith and Walker, Reference 50. The maximum difference between the data and the prediction is 5 percent over the Reynolds number range 3×10^3 to 5×10^4 while the bulk of these data agree with the prediction to a few percent.

The theoretically predicted variation of the boundary-layer form factor, $H = \delta^*/\theta$, is shown in Figure 31(a) as a function of the momentum-thickness Reynolds numbers at a variety of transpiration rates. The curves on the figure reveal that H varies quite markedly with both Reynolds number and transpiration rate. Consideration of this variation is of considerable importance in the evaluation of the turbulent boundary-layer growth on a surface possessing a streamwise pressure gradient, see Equation (2-51).

In Figure 31(b) the predicted variation of H under zero transpiration is compared with the data of Reference 50. This comparison indicates that the boundary-layer model proposed herein satisfactorily represents the form factor under conditions of zero transpiration to within about 4 percent. The inadequacy of power law formulations that predict constant values of H with Reynolds number is evident here.

When the von Kármán integral equation is evaluated on a flat plate utilizing the $C_f/2(Re_\theta)$ relationships of Figure 30, the curves of $C_f/2(Re_x)$ shown in Figure 32 result for a boundary-layer turbulent from the leading edge. The values of $C_f/2(Re_\theta)$ utilized at very low Re_θ were obtained from logarithmic extrapolations of the curves of Figure 30(a). It should be noted that the $v_o/u_1 = 0$ line is within a few percent of the Kármán-Schoenherr relationship over the entire range of Reynolds numbers shown. Again, the increased effectiveness of uniform transpiration at the higher Reynolds numbers is evident.

Similar curves to those described above for the heat-transfer coefficient (Stanton number) and the mass-transfer coefficient with uniform transpiration on a flat plate are presented in Figures 33 to 36. The heat-transfer coefficients apply for a laminar Prandtl number of 0.71 and a turbulent Prandtl number of 0.75. The mass-transfer coefficients apply for laminar and turbulent Schmidt numbers of 0.2 and 0.75, respectively. Again, the effect of increased transpiration is greater at the higher Reynolds numbers.

Another way of demonstrating the effect of surface mass transfer on the local skin-friction coefficient is shown in Figure 37. In this coordinate system, C_f/C_f^* is plotted against $v_o/u_1(C_f/2)^*$ where the (*) refers to no-blowing conditions at the same Reynolds number. The effect of [illegible]th Reynolds

number is largely eliminated on such a plot, as is indicated in the current results and those of Reference 22. The current results are essentially the same as those of the pioneer paper by Dorrance and Dore, Reference 21, and slightly lower than the results of Rubesin, Reference 22.

There has been some argument as to the appropriateness of the coordinate system employed in Figure 37 because the term $v_o/u_1\sqrt{C_f/2^*}$ is more consistent with the law of the wall, Reference 54. This parameter was used as the abscissa of the curves shown in Figure 38 and a decided Reynolds number effect is introduced. From a correlation viewpoint, therefore, the coordinates of Figure 37 are more appropriate. Apparently the wake region has a significant effect in the Reynolds number and blowing parameter range shown.

In the evaluation of skin friction on bodies other than a flat plate, the effect of surface mass transfer at constant values of Re_γ is required and this is shown in Figure 39. Again, the choice of the coordinates eliminate the large Reynolds number dependence. At a given value of the blowing parameter, the reduction in skin friction shown in this figure is less than that shown in Figure 37. This is consistent for a boundary layer whose thickness grows at a rate slightly less than linear with distance along a plate.

Figure 40 shows the effect of surface mass transfer on the local mass-transfer coefficient. The curves are generally similar to the skin-friction results shown in Figures 37 and 39. Again, similar results for the local heat-transfer coefficient are given in Figure 41.

The effect of surface mass transfer on the coefficients of diffusion and heat transfer can best be shown by the Reynolds analogy factors $C_f/2C_M$ (dashed lines) and $C_f/2C_H$ (solid lines) indicated in Figure 42. Whereas in Figure 37 there was little to be gained by using the current analysis in place of the early heuristic theories, in this figure it is noted that the heat transfer at the highest blowing rate is only 0.4 that given by Reference 21 (where $Pr = 1$, $Pr_t = 1$) and 0.5 of that given by Reference 22 (where $Pr = 0.75$, $Pr_t = 1$). These major differences result largely from the more precise boundary-layer profiles employed in the current analysis. Of interest also is that at zero mass transfer the Reynolds analogy for heat transfer agrees quite well with the old Colburn value of $Pr^{2/3}$. As surface mass transfer increases the Reynolds analogy factor drops significantly, indicating a lesser effect of blowing on heat transfer than on skin friction. Because of the very low Schmidt number ($Sc = 0.21$) for helium at small concentrations, diffusing in air, the Reynolds analogy factor for diffusion is

much lower than that for heat transfer, although not as low as $Sc^{2/3}$ at zero blowing. Again, surface mass transfer reduces this factor significantly, indicating the lesser sensitivity of the mass transfer or diffusion coefficient to surface mass transfer. For the diffusion coefficients, the coordinates employed in Figure 42 do not completely eliminate the Reynolds number effect.

4. CONCLUDING REMARKS

The results of this report demonstrate that a model of the turbulent boundary layer with surface mass addition can be established, that is, in excellent agreement with profile data for velocity, temperature, and concentration in constant property boundary layers (low speed, small temperature and concentration differences between surface and free stream). A uniquely interesting result of this analysis is that the four parameters employed, namely: (1) the Prandtl mixing length parameter K; (2) the Clauser eddy diffusivity Reynolds number; (3) the inner mixing length parameter y_a^+, analogous to Rotta's intercept parameter; and (4) the turbulent Prandtl or Schmidt number, can be treated as constants independent of the rate of surface mass transfer and Reynolds number.

This agreement with the data, restricted though they may be to essentially constant properties, is sufficiently encouraging to suggest the next step in this work. Velocity profile data have been obtained in boundary layers in supersonic flow with inert gas mass transfer at the surface, References 56 and 55. It would be a logical next step in this research to determine the modifications needed in the present theory to permit its extension to include the effects of variable fluid properties and so yield agreement with the existing data. In accomplishing this extension, it will be worthwhile to examine the applicability of several of the provocative ideas of Reference 57 toward solving the current problem. Another phase of any extensions of this work must be the planning of definitive experiments wherein chemical reactions occur as a consequence of the surface mass transfer. Profile data do not exist at present for such conditions and it is only upon such data that sound extensions of this work can be based.

BLANK PAGE

REFERENCES

Hinze, J. O.: Turbulence. McGraw-Hill Book Co., Inc., New York, 1959.

Kestin, J. and Richardson, P. D.: Heat Transfer Across Turbulent, Incompressible Boundary Layers. Int. J. Heat Transfer, vol. 6, pp. 147-189, 1963.

Coles, D.: The Law of the Wall in Turbulent Shear Flow. 50 Jahre Grenzschichtforschimz (Ed. H. Görtler and W. Tollmian), Braunschweiz: F. Viewez and Sohn, pp. 153-163.

Coles, D.: The Law of the Wake in Turbulent Boundary Layer. J. Fluid Mech., vol. 1, 1956, pp. 191-226.

Ludwiez, H. and Tillman, W.: Investigations of the Wall Shearing Stress in Turbulent Boundary Layers. NACA TM 1285, 1950.

Clauser, F. H.: The Turbulent Boundary Layer. Advances in Applied Mechanics IV, 1956.

Eckert, E. R. G.: Heat Transfer and Temperature Profiles in Laminar Boundary Layers on a Sweat Cooled Wall. Tech. Rep. No. 5646, Air Material Command, Nov. 3, 1947.

Stewart, W. E.: Interaction of Heat, Mass, and Momentum Transfer. Doctoral Thesis, M.I.T., Nov. 3, 1950.

Mickley, H. S., Ross, R. C., Squyres, A. L., and Stewart, W. E.: Heat, Mass, and Momentum Transfer for Flow Over a Flat Plate with Blowing or Suction. M.I.T., Sept. 1952, NACA Contract Naw 5960, NACA TN 3208, 1954.

Squyres, A. L.: Heat Transfer for Flow Over a Flat Plate with Blowing or Suction. Doctoral Thesis, M.I.T., Jan. 12, 1953.

Gessner, A.: Momentum Transfer for Flow Over a Flat Plate with Blowing and Mainstream Acceleration. Doctoral Thesis, M.I.T., 1954.

Curl, R. L.: Heat Transfer for Flow Over a Flat Plate with Blowing, Acceleration, and Nonuniform Wall Temperature. Doctoral Thesis, M.I.T., Jan. 1955.

Mickley, H. S., Curl, R., Gessner, A., and Ginwala, K.: Heat and Momentum Transfer for Flow Over a Flat Plate with Blowing and Main Stream Acceleration. M.I.T., Feb. 1955, NACA Contract Naw 6228.

Davis, R. S.: Interaction of Mass and Momentum Transfer in Turbulent Boundary Layers. Doctoral Thesis, M.I.T., Aug. 21, 1955.

Mickley, H. S. and Davis, R. S.: Momentum Transfer for Flow Over a Flat Plate with Blowing. NACA TN 4017, Nov. 1957.

Dutton, R. A.: The Effects of Distributed Suction on the Development of Turbulent Boundary Layers. Aeronautical Research Council, A.R.C. 20,036, F.M. 2671, Mar. 27, 1958.

17. Kendall, R. M.: Interaction of Mass and Momentum Transfer in the Turbulent Boundary Layer. Doctoral Thesis, M.I.T., 1959.

18. Goodwin, B. M.: The Transpired Turbulent Boundary Layer with Zero Pressure Gradient. Doctoral Thesis, M.I.T., 1961.

19. Butensky, M. S.: The Transpired Turbulent Boundary Layer on a Flat Plate. Doctoral Thesis, M.I.T., 1962.

20. Smith, K. A.: The Transpired Turbulent Boundary Layer. Doctoral Thesis, M.I.T., May 1962.

21. Dorrance, W. H. and Dore, F. J.: The Effect of Mass Transfer on the Compressible Turbulent Boundary-Layer Skin Friction and Heat Transfer. Jour. Aero. Sci., vol. 21, no. 6, 1954.

22. Rubesin, M. W.: An Analytical Estimation of the Effect of Transpiration Cooling on the Heat Transfer and Skin Friction Characteristics of a Compressible, Turbulent Boundary Layer. NACA TN 3341, 1954.

23. Van Driest, E. R.: Turbulent Boundary Layer in Compressible Fluids. J. Aero. Sci., vol. 18, Mar. 1951, pp. 145-161.

24. Clarke, J. H., Menkes, J., and Libby, P. A.: A Provisional Analysis of Turbulent Boundary Layers with Injection. Jour. Aero. Sci., vol. 22, no. 4, 1955.

25. Rubesin, M. W., Pappas, C. C., and Okuno, A. F.: The Effect of Fluid Injection on the Compressible Turbulent Boundary Layer - Preliminary Tests on Transpiration Cooling of a Flat Plate at $M = 2.7$ with Air as the Injected Gas. NACA RM A55I19, 1955.

26. Danberg, J. E.: Measurement of the Characteristics of the Compressible Turbulent Boundary Layer with Air Injection. NAVORD Rep. 6683, Sept. 3, 1959.

27. Rubesin, M. W. and Pappas, C. C.: A Study of Binary Gas Diffusion in a Turbulent Boundary Layer on a Flat Plate. Rand Symposium Rep., S-51, Paper No. 18, June 24, 1957.

28. Culick, F. E. C.: Turbulent Diffusion Boundary Layer. Technical Rep. 279, Apr. 1958, AFOSR-TN-58-336.

29. Pappas, C. C. and Okuno, A. F.: Measurements of Skin Friction of the Compressible Turbulent Boundary Layer on a Cone with Foreign Gas Injection. Jour. Aero. Sci., vol. 27, no. 5, 1960, p. 321.

30. Tendeland, T. and Okuno, A. F.: The Effect of Fluid Injection on the Compressible Turbulent Boundary Layer - The Effect on Skin Friction of Air Injected into the Boundary Layer on a Cone at $M = 2.7$. NACA RM A56D05, 1956.

31. Ness, N.: Foreign Gas Injection in a Compressible Turbulent Boundary Layer on a Flat Plate. Jour. Aero Sci., vol. 28, no. 8, Aug. 1961.

32. Ness, N.: On the Continuity of the Schmidt Number at the Interface Between the Laminar Sublayer and Outer Turbulent Region. Jour. Aero/Space Sci., fol. 26, no. 6, June 1959.

33. Hidalgo, H.: A Theory of Ablation of Glassy Materials for Laminar and Turbulent Heating. AVCO Research Rep. No. 62, June 1959.

34. Pappas, C. C. and Okuno, A. F.: Measurement of Heat Transfer and Recovery Factor of a Compressible Turbulent Boundary Layer on a Sharp Cone with Foreign Gas Injection. NASA TN D-2230, Apr. 1964.

35. Tewfik, O. E., Eckert, E. R. G., and Shirtliffe, C. J.: Thermal Diffusion Effects on Energy Transfer in a Turbulent Boundary Layer with Helium Injection. Proc. of the 1962 Heat Transfer and Fluid Mech. Inst., June 1962, pp. 42-61.

36. Leadon, B. M. and Bartle, E. R.: On Mass Transfer Effectiveness. AIAA Jour., vol. 1, no. 5, May 1963, pp. 1185-1186.

37. Black, T. J. and Sarneshi, A. J.: The Turbulent Boundary Layer with Suction or Injection. Aero. Res. Conc. (Great Britain), Rep. ARC 20, 501, F.M. 2745, 1958.

38. Dorrance, W. H.: Viscous Hypersonic Flow. McGraw-Hill, 1962, pp. 180-181.

39. Hirschfelder, J. O., Curtiss, C. F., and Bird, R. B.: Molecular Theory of Gases and Liquids. John Wiley, 1954.

40. Clauser, F. H.: Turbulent Boundary Layer in Adverse Pressure Gradients. Jour. Aero Sci., vol. 21, no. 2, Feb. 1954.

41. Reichardt, H.: Complete Representation of the Turbulent Velocity Distribution in Smooth Pipe. Z. Angew. Math. u. Mech., vol. 31, no. 7, July 1951.

42. Rannie, W. D.: Heat Transfer in Turbulent Shear Flow. Jour. Aero. Sci., vol. 23, no. 5, May 1956.

43. Deissler, R. G.: Analysis of Turbulent Heat Transfer, Mass Transfer, and Friction in Smooth Tubes at High Prandtl and Schmidt Numbers. NACA NT 3145, May 1954.

44. Rotta, J.: Velocity Law of Turbulent Flow Valid in the Neighborhood of a Wall. Ingr. Arch., vol. 18, 1956, p. 277.

45. von Kármán, T.: The Analogy between Fluid Friction and Heat Transfer. Trans. ASME, vol. 61, 1939, pp. 705-710.

46. van Driest, E. R.: On Turbulent Flow Near a Wall. Jour. Aero. Sci., vol. 23, no. 11, Nov. 1956.

47. Elrod, H. G., Jr.: Note on the Turbulent Shear Stress Near a Wall. Jour. Aero. Sci., Readers Forum, vol. 24, no. 6, June 1957 (Erratum JAS, vol. 27, no. 2, p. 145).

4 Laufer, J.: The Structure of Turbulence in Fully Developed Pipe Flow. NACA TR 1174, 1954.

49. Klebanoff, R. S.: Characteristics of Turbulence in a Boundary Layer with Zero Pressure Gradient. NACA TR 1247, Apr. 1953.

50. Smith, D. W. and Walker, J. H.: Skin-Friction Measurements in Incompressible Flow. NASA TN 4231, March 1958.

51. Schubauer, G. B.: Turbulent Processes as Observed in Boundary Layer and Pipe. Jour. Appl. Physics, vol. 25, no. 2, Feb. 1954.

52. van Driest, E. R.: On Mass Transfer Near the Stagnation Point. AFOSR No. TN 57-458, June 1, 1957.

53. Spalding, D. B.: A Single Formula for the Law of the Wall. Jour. Appl. Mech., Trans. ASME, Series E, Sept. 1961, pp. 455-458.

54. Leadon, B. M.: Comments on "A Theory for Fluid Injection" and Turcotte, Turcotte, D. L.: Author's Reply. Reader's Forum, Jour. Aero/Space Sci., Oct. 1961.

55. Danberg, J. E.: Characteristics of the Turbulent Boundary Layer with Heat and Mass Transfer at M = 6.7. Aero. Res. Rep. No. 228, NOL TR 64-99, Oct. 19, 1964.

56. Pappas, C. C.: Ames Research Center, private communication.

57. Coles, D. E.: The Turbulent Boundary Layer in a Compressible Fluid. Rand Rep. R-403-PR, Sept. 1962.

58. Schultz-Grunow: New Friction Resistance Law for Smooth Flat Plates (Translation). NACA TM 986, 1941.

TABLE I

ANALYTICAL REPRESENTATION OF THE LAW OF THE WALL

Model	Original Representation	Range of y^+	Equivalent Mixing Length Representation in Equation (2-60)	Constant when $\kappa = 0.44$	Continuous Variation of		Monotonic dl^+/dy^+	Mixing Length as $y^+ \to 0$
					l^+	$\frac{d^n l^+}{dy^{+n}}$, $n < 2$		
Prandtl-Taylor Reference 2	$u^+ = y^+$	$0 - y_a^+$	$l^+ = 0$	$y_a^+ = 11.27$	no	no	yes	$l^+ = 0$
	$u^+ = \kappa y^+$, ϵ_M	$y_a^+ \to$	$l^+ = \kappa y^+ \left(1 - \frac{1}{\kappa y^+}\right)^{1/2}$	---				
van Kármán Reference 46	$u^+ = y^+$	$0 - y_a^+$	$l^+ = 0$	$y_a^+ = \frac{2}{\kappa} = 4.5$	no	no	yes	$l^+ = 0$
	$u^+ = \frac{2}{\kappa}\left(\log_e y^+ + 1 - \log_e \frac{2}{\kappa}\right)$	$y_a^+ - y_b^+$	$l^+ = \frac{\kappa}{2} y^+ \left(1 - \frac{2}{\kappa y^+}\right)^{1/2}$	$y_b^+ = 35.5$				
	$u^+ = \frac{1}{\kappa}\left(\log_e y^+ + \log_e y_b^+ + 2 - 2\log_e \frac{2}{\kappa}\right)$	$y_b^+ \to$	$l^+ = \kappa y^+ \left(1 - \frac{1}{\kappa y^+}\right)^{1/2}$	---				
Rotta Reference 45	$l^+ = 0$	$0 - y_a^+$	---	$y_a^+ = 6.91$	yes	no	yes	$l^+ = 0$
	$l^+ = \kappa\left(y^+ - y_a^+\right)$	$y_a^+ \to$	---	---				
Reichardt Reference 41	$\frac{\epsilon_M}{\nu} = \kappa\left(y^+ - y_a^+ \tanh \frac{y^+}{y_a^+}\right)$	$0 \to$	$l^+ = \frac{\epsilon_M}{\nu}\left(1 + \frac{\nu}{\epsilon_M}\right)^{1/2}$	$y_a^+ = 11.04$	yes	yes	yes	$l^+ \propto y^{+3/2}$
van Driest Reference 47	$l^+ = \kappa y^+\left[1 - \exp\left(-\frac{y^+}{y_a^+}\right)\right]$	$0 \to$	---	$y_a^+ = 27.8$	yes	yes	no	$l^+ \propto y^{+3}$
Present Analysis	$l^+ = \kappa\left\{y^+ - y_a^+\left[1 - \exp\left(-\frac{y^+}{y_a^+}\right)\right]\right\}^*$	$0 \to$	---	$y_a^+ = 11.83$	yes	yes	yes	$l^+ \propto y^{+2}$

*Constant shear, no surface mass transfer.

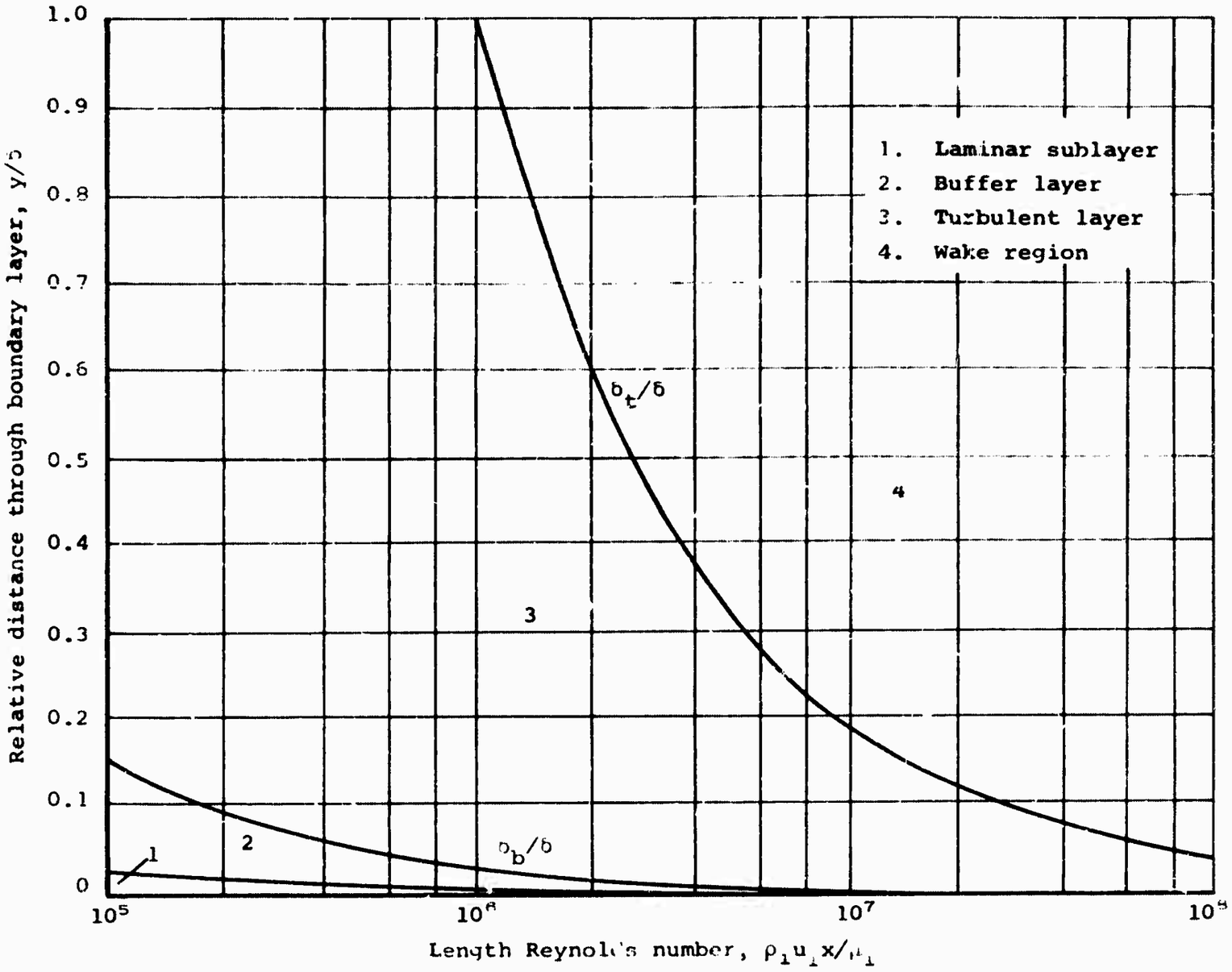

Figure 1.- Relative thickness of the four structurally different zones within the turbulent boundary layer, zero surface mass transfer, and constant fluid properties.

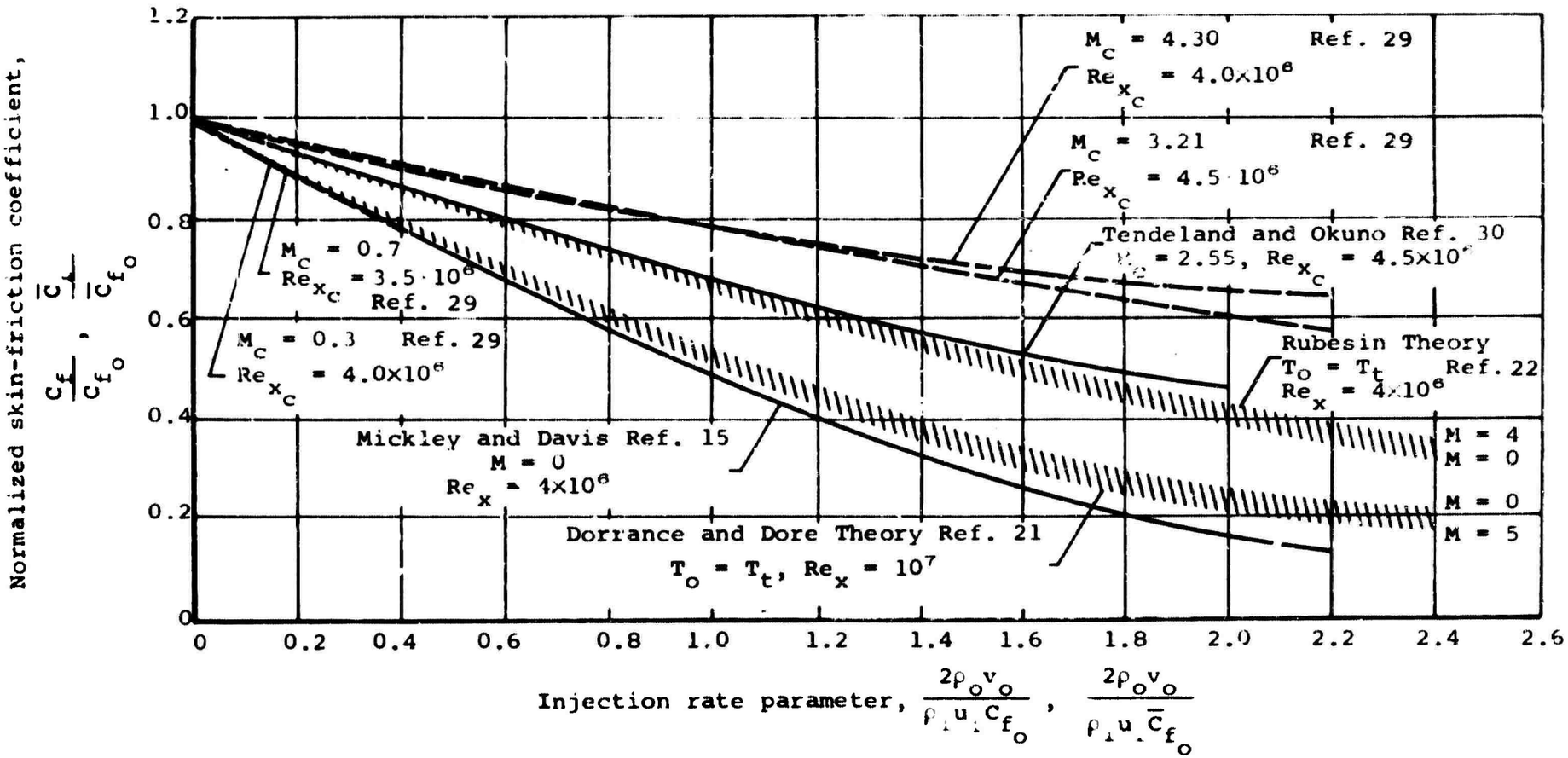

Figure 2.- Comparison of early skin-friction theories and experiment with air injection.

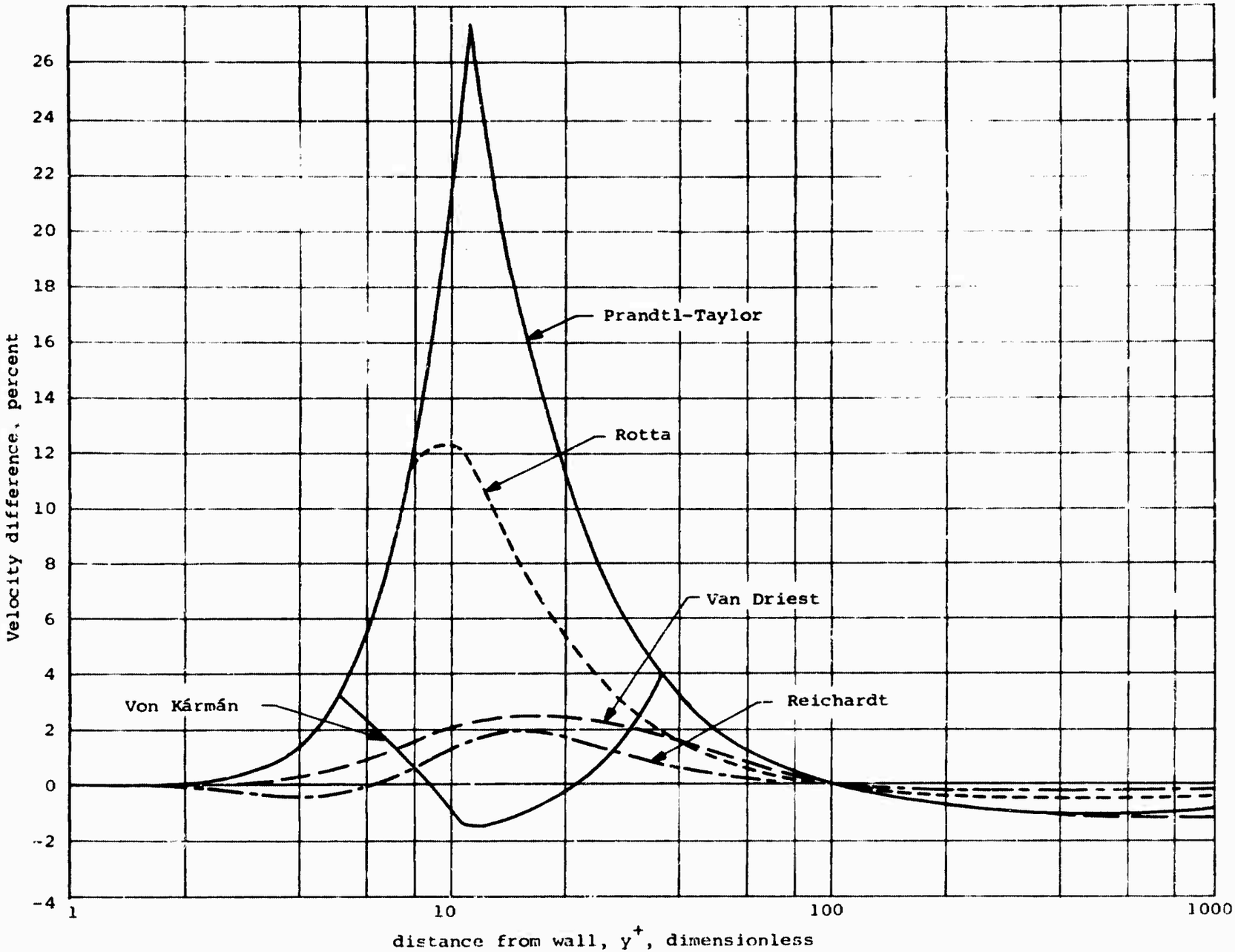

Figure 3.- Comparison of the various techniques of Table I with the adopted technique for the law of the wall, $v_o^+ = 0$.

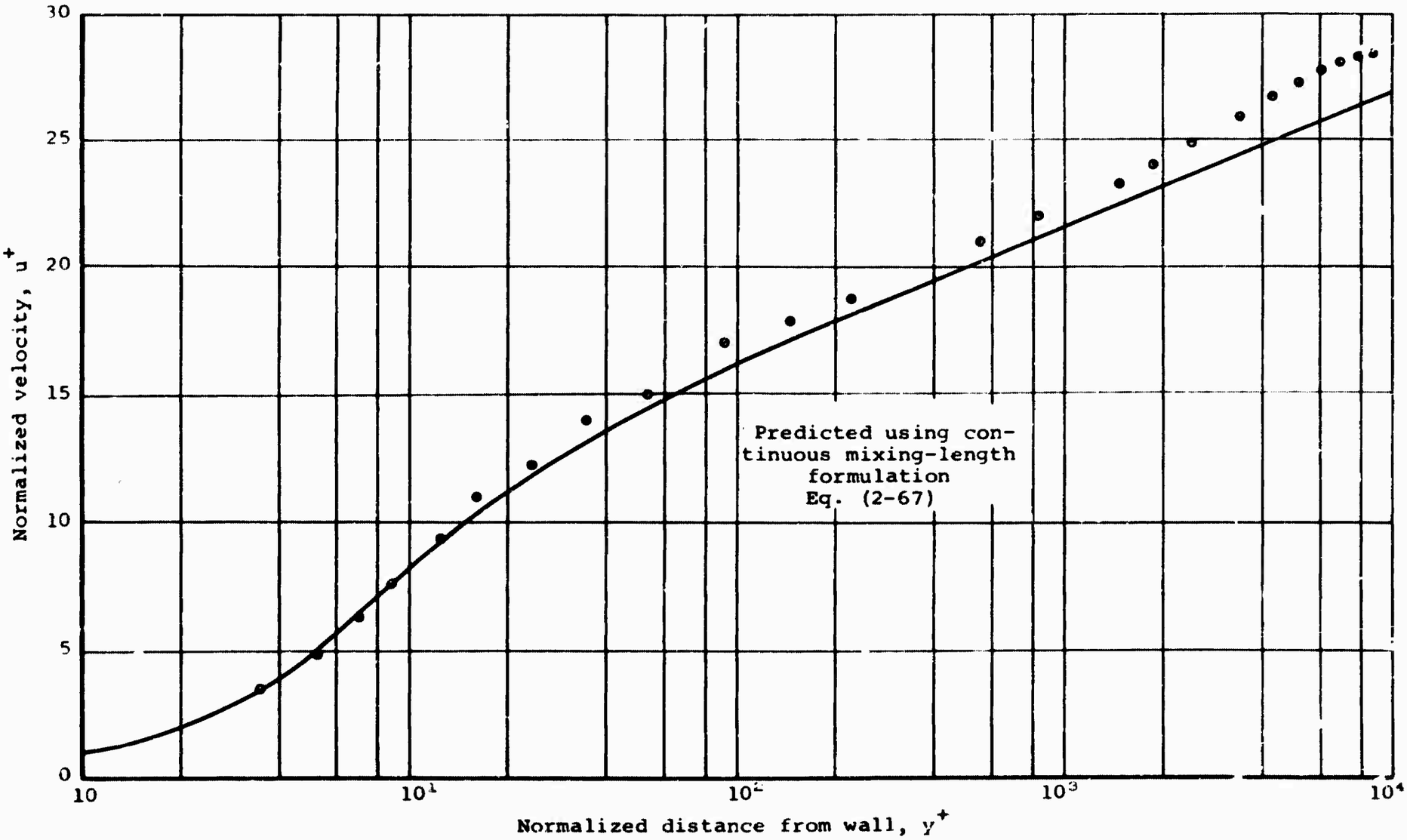

(a) Velocity distribution in a pipe, Reference 48, Reynolds number based on diameter = 5.0×10^5.

Figure 4.- Comparison of mixing length formulations with data.

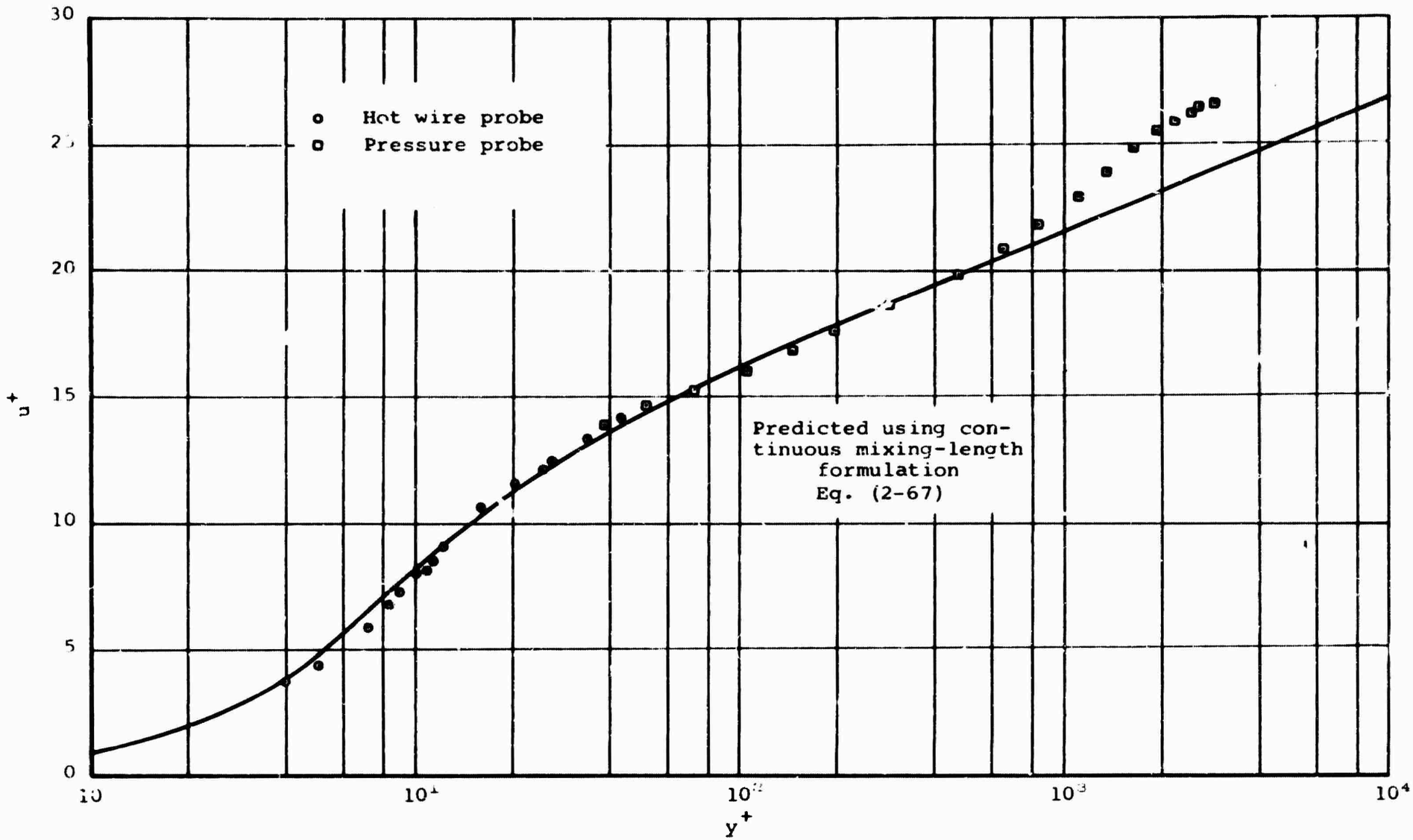

(b) Velocity distribution over a flat plate, Reference 49.

Figure 4.- Continued.

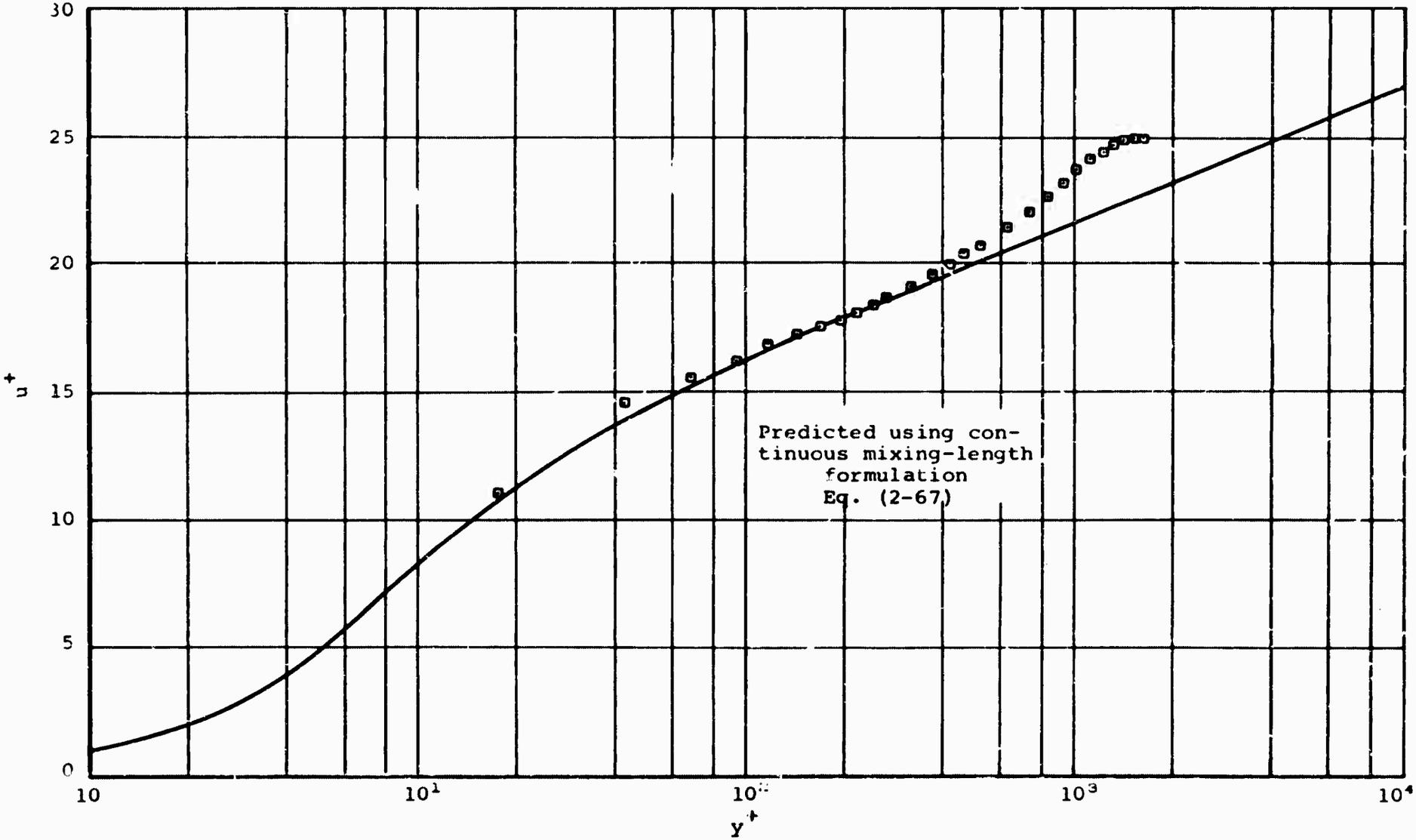

(c) Velocity distribution over a flat plate, Reference 50.

Figure 4.- Concluded.

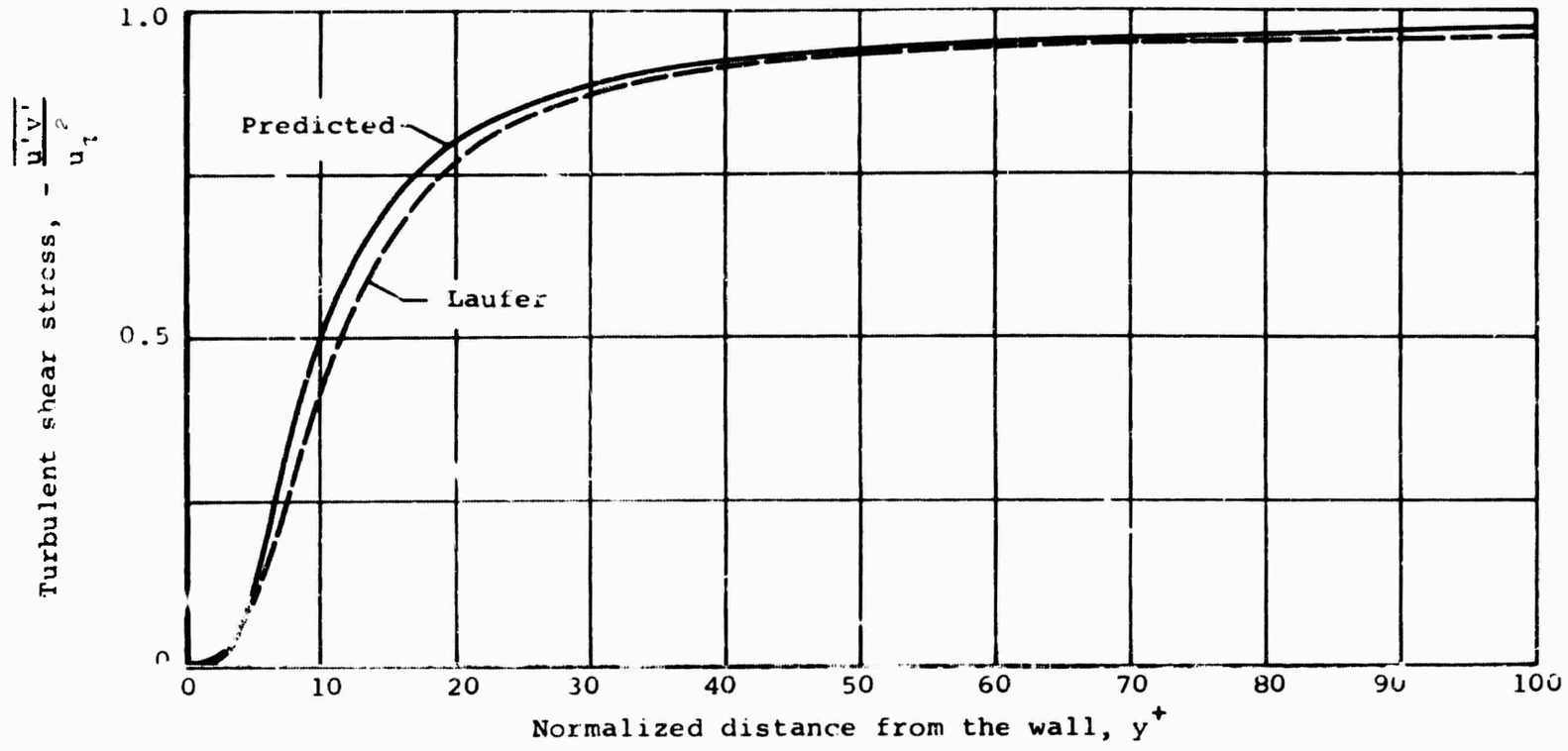

Figure 5.- Comparison of predicted turbulent shear distribution with data, Laufer, Reference 48, $v_o^+ = 0$.

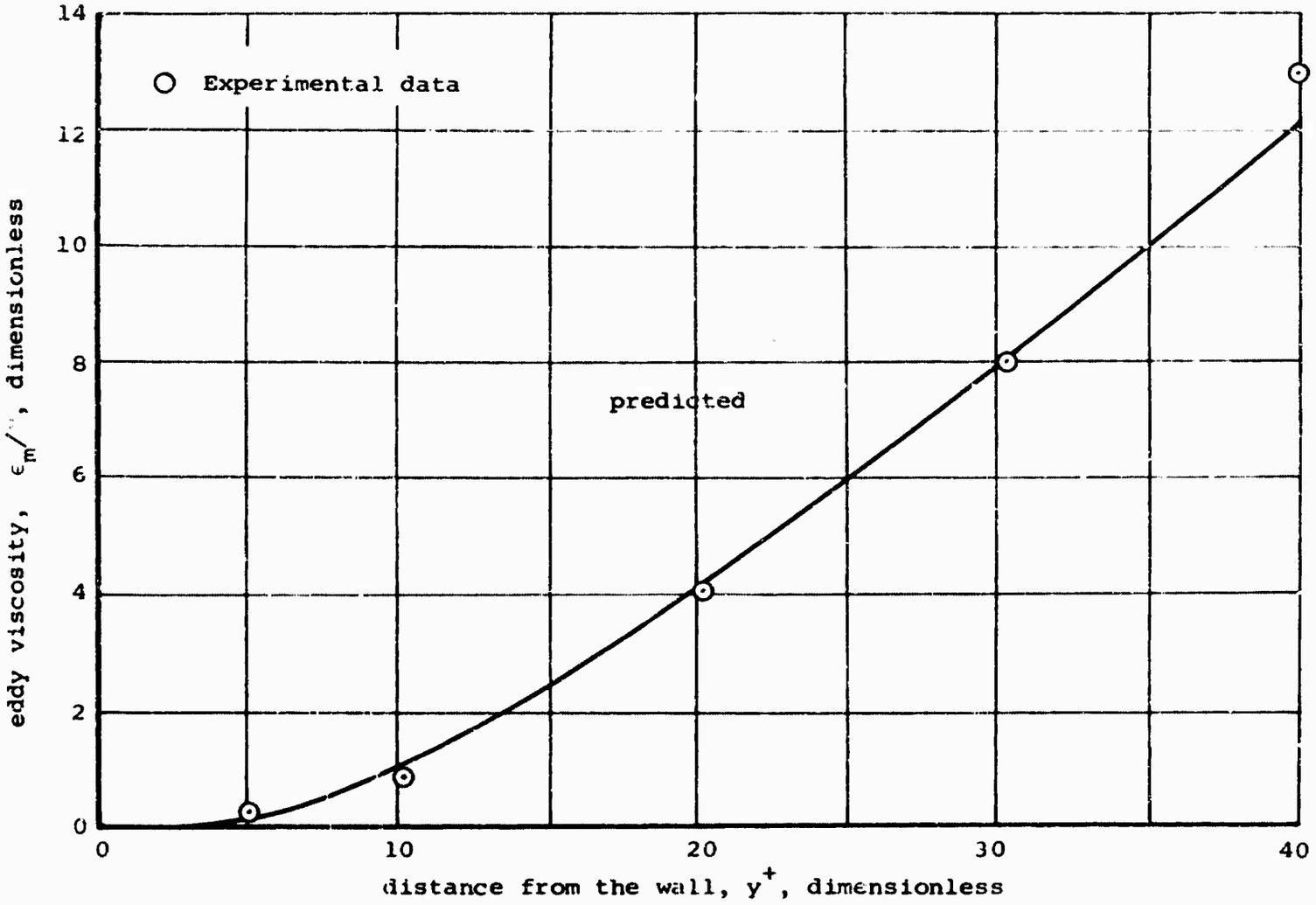

Figure 6.- Comparison of predicted eddy viscosity with data, zero mass transfer, Schubauer, Reference 53.

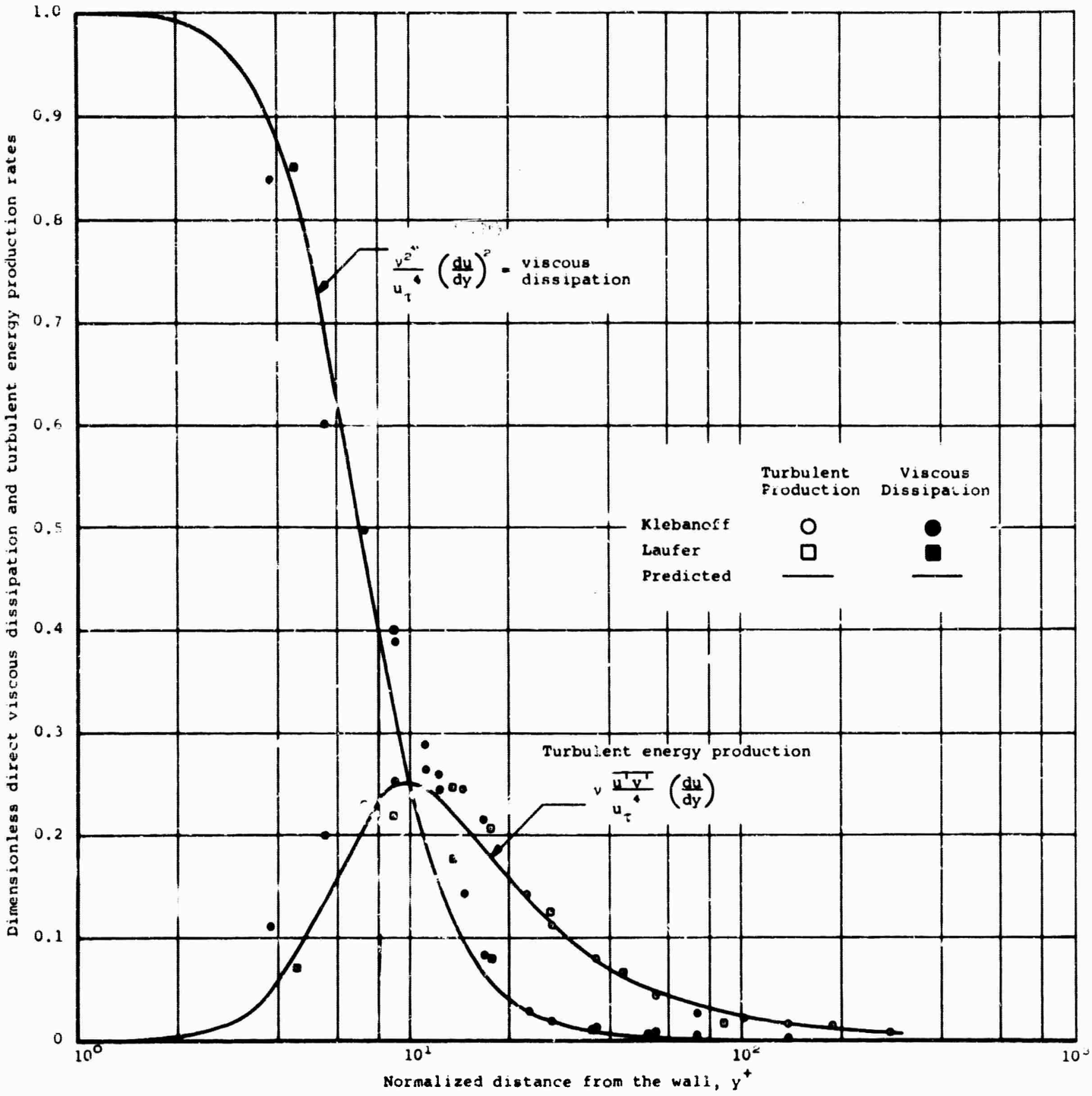

Figure 7.- Comparison of predicted direct viscous dissipation and turbulent energy production rates with the data of Klebanoff and Laufer.

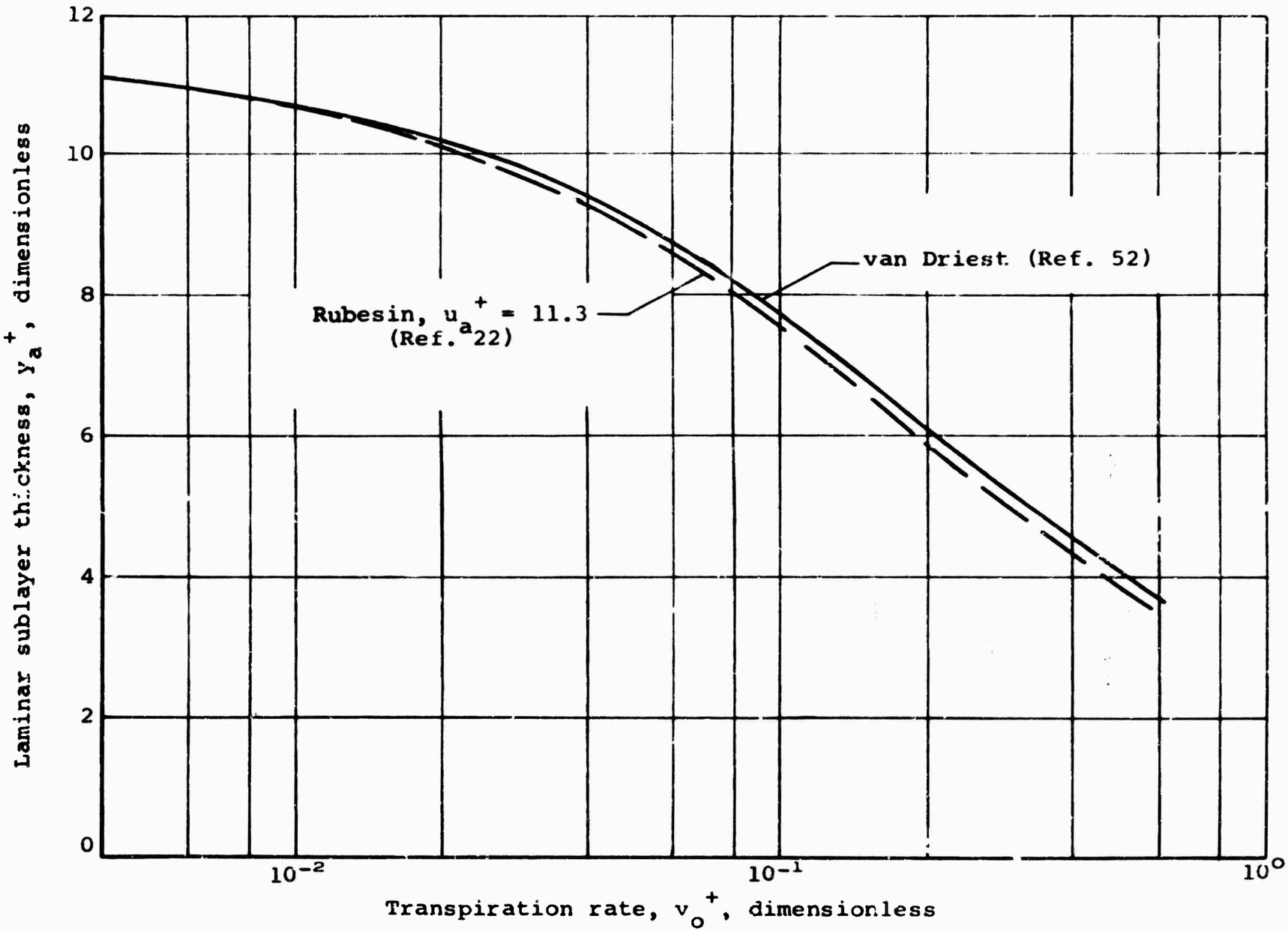

Figure 8.- Variation of sublayer thickness with transpiration rate for two hypotheses in the two-layer boundary-layer model.

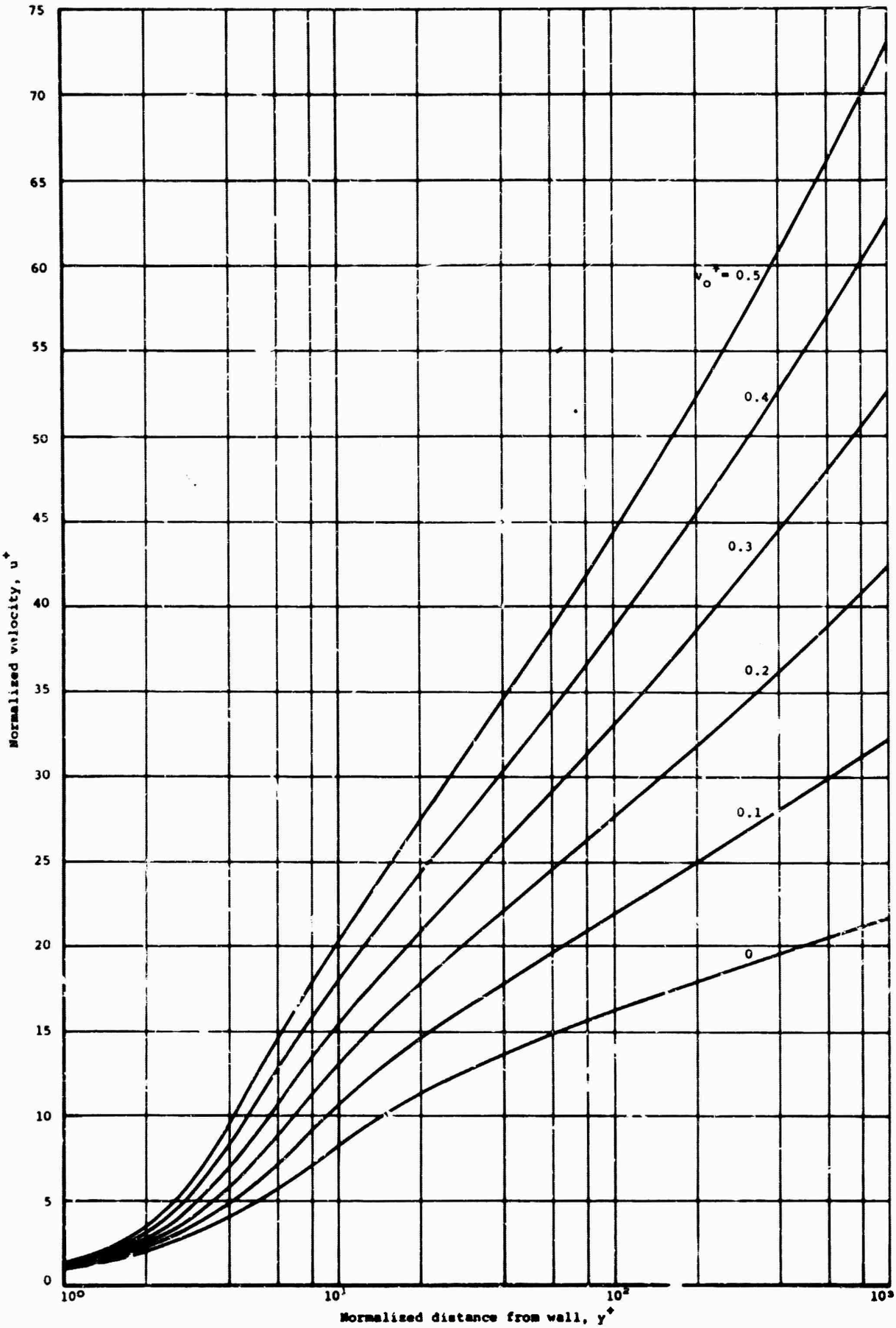

Figure 9.- Predicted variation of dimensionless velocity with and without transpiration.

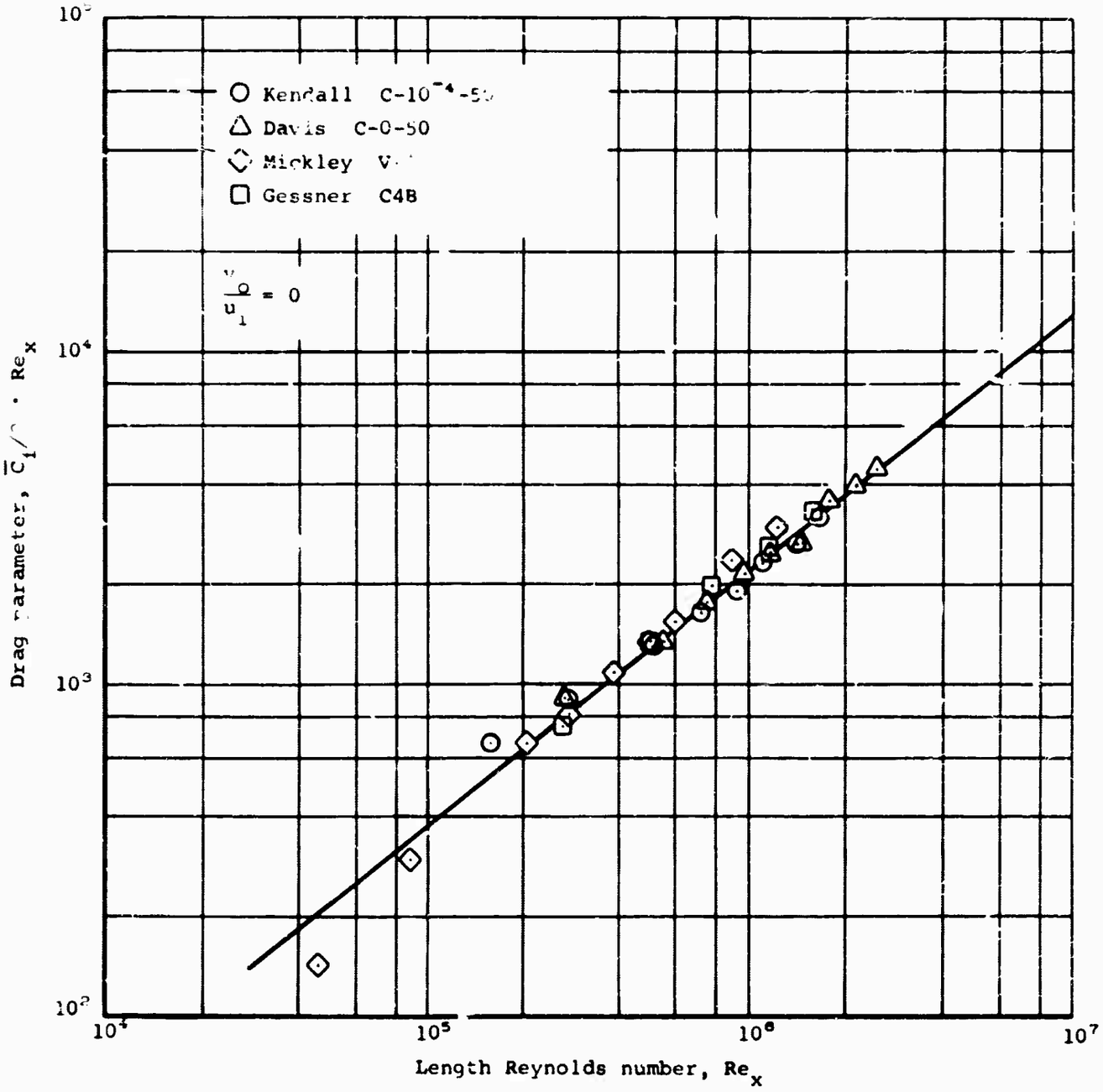

(a) $v_o/u_1 \approx 0$.

Figure 10.- Composite plot of integral momentum equation results for MIT data.

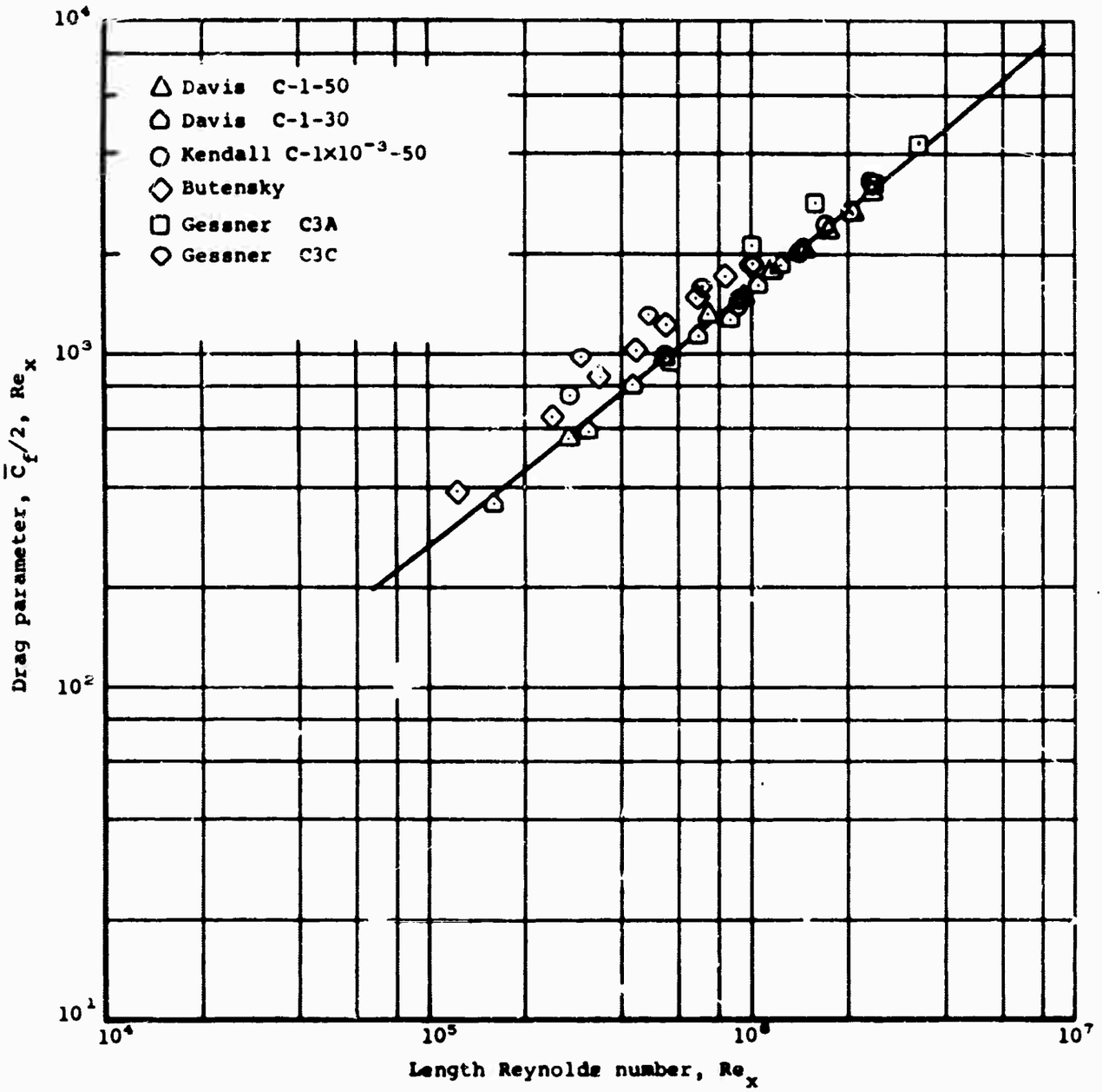

(b) $v_o/u_1 \approx 0.001$.

Figure 10.- Continued.

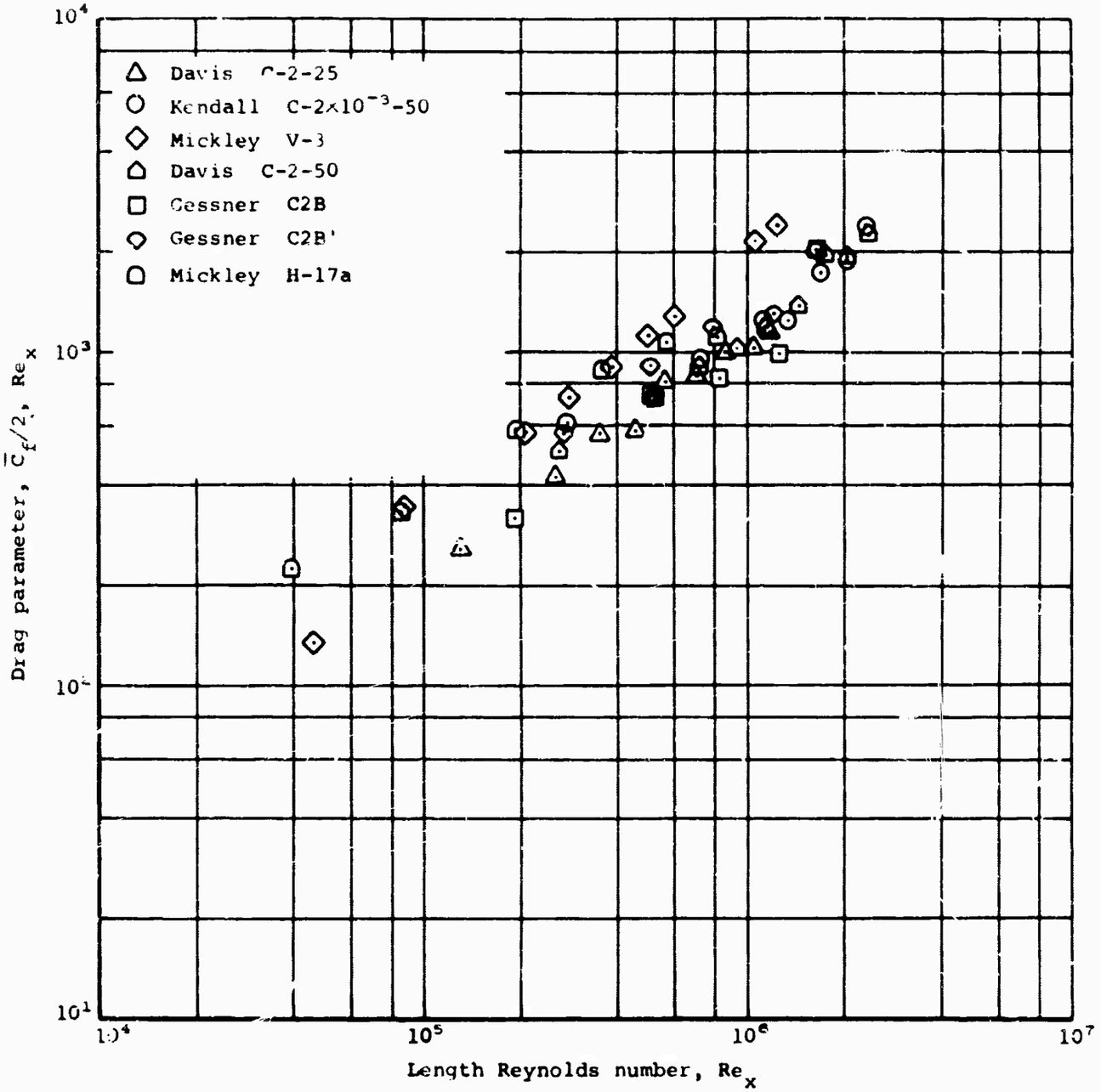

(c) $v_o/u_1 \approx 0.002$.

Figure 10.- Continued.

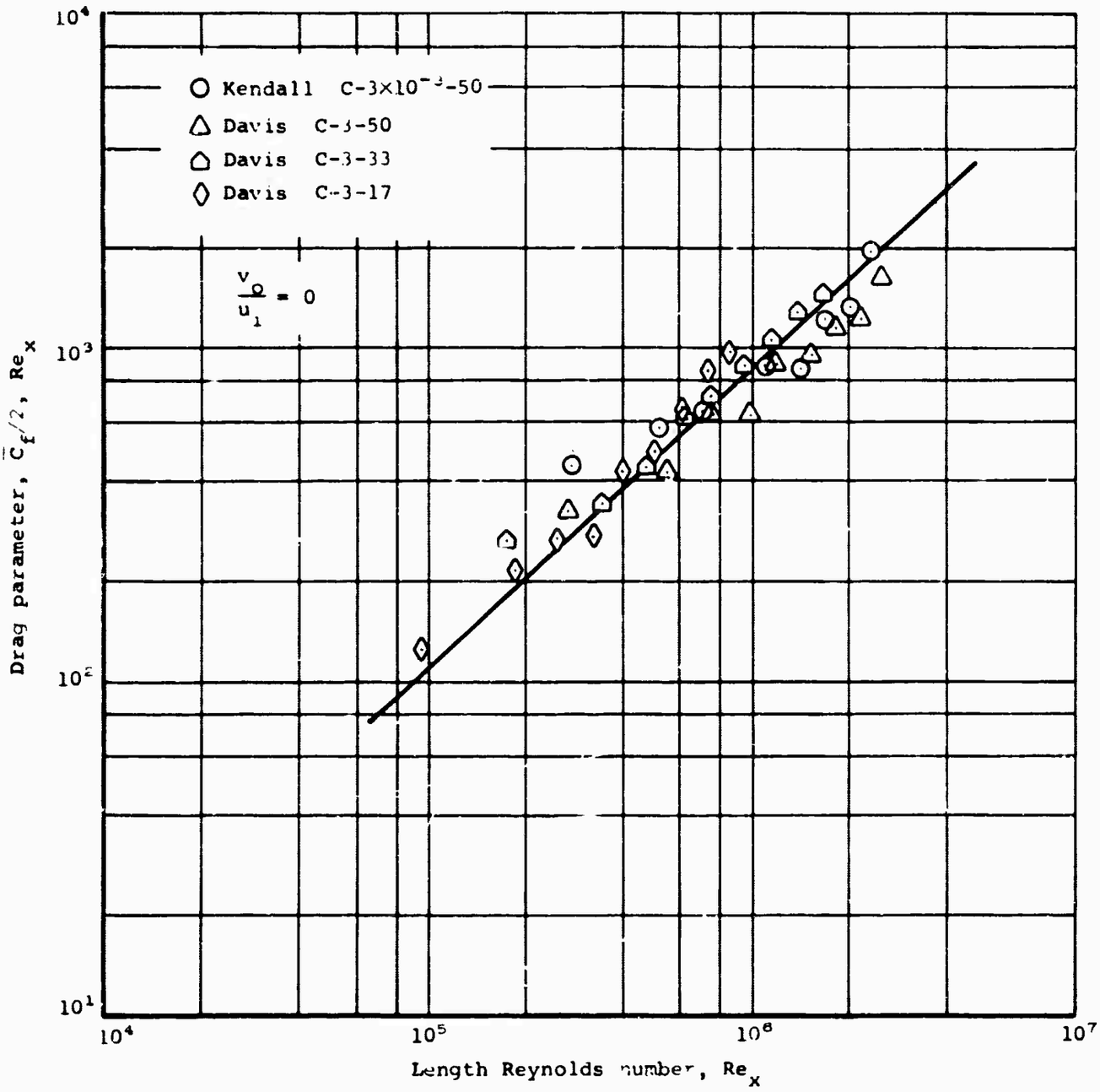

(d) $v_o/u_1 \approx 0.003$.

Figure 10.- Continued.

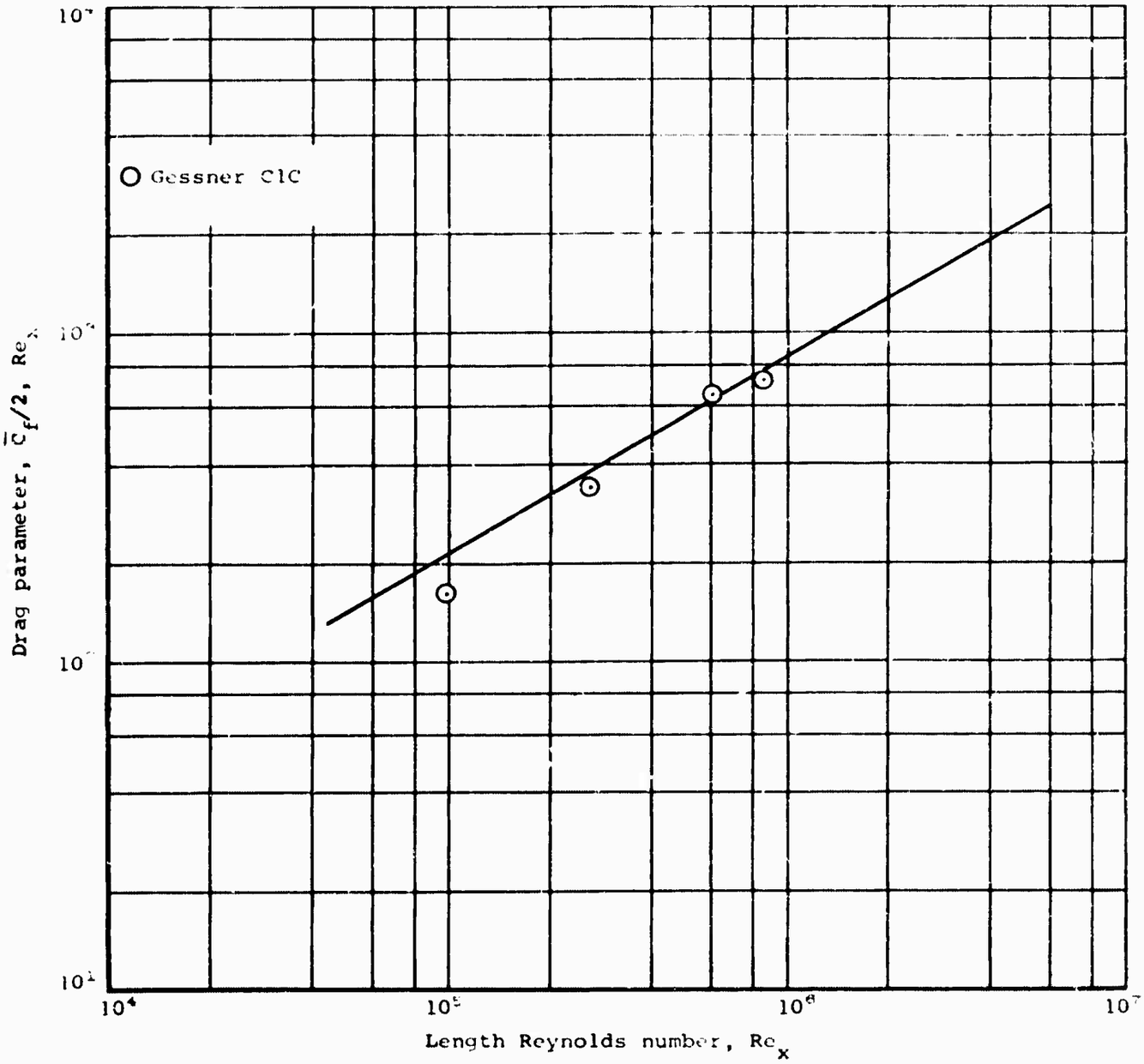

(c) $v_o/U_\infty = 0.004$.

Figure 10.- Concluded.

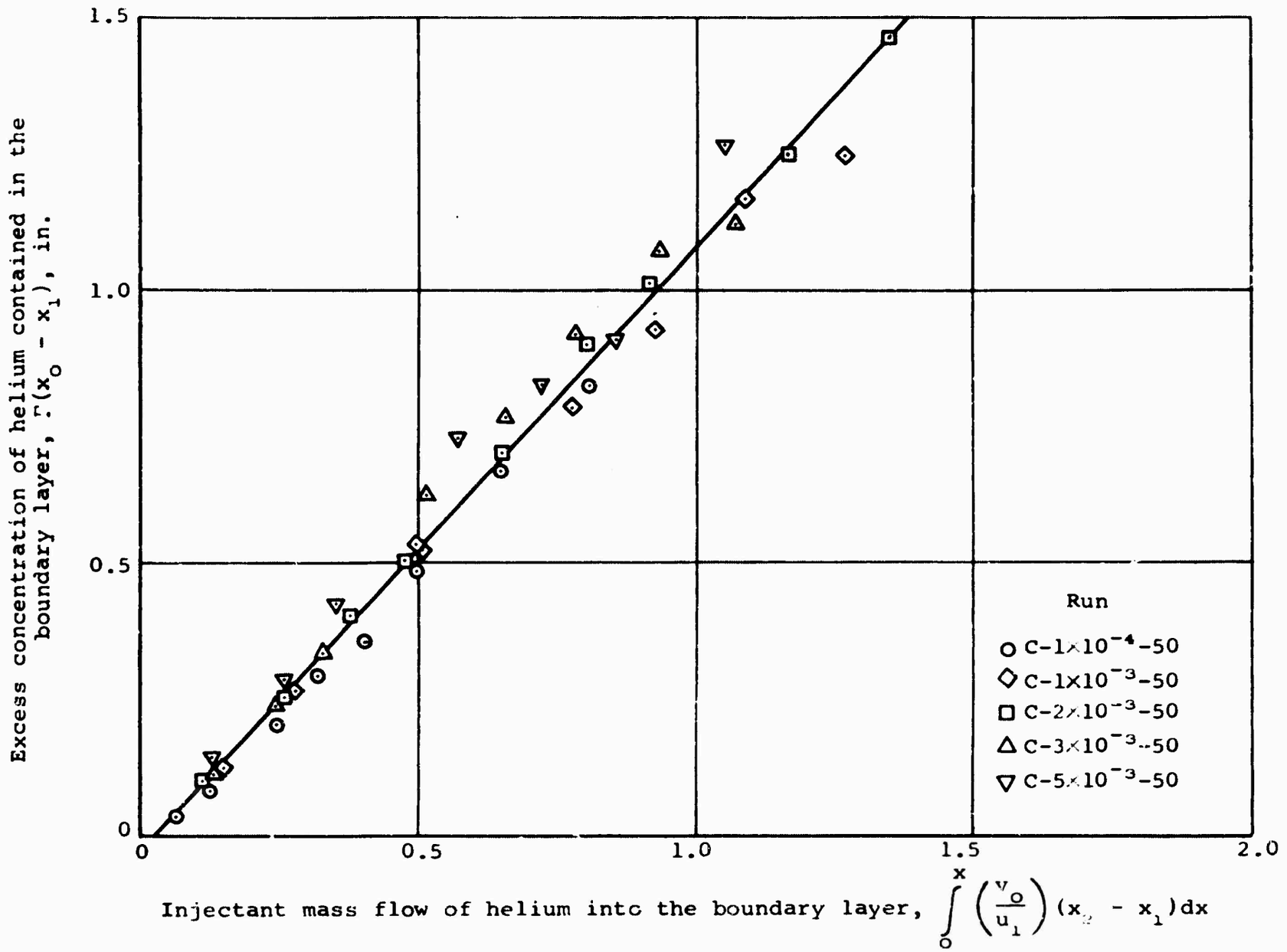

Figure 11.- Mass balance in the boundary layer, Reference 17.

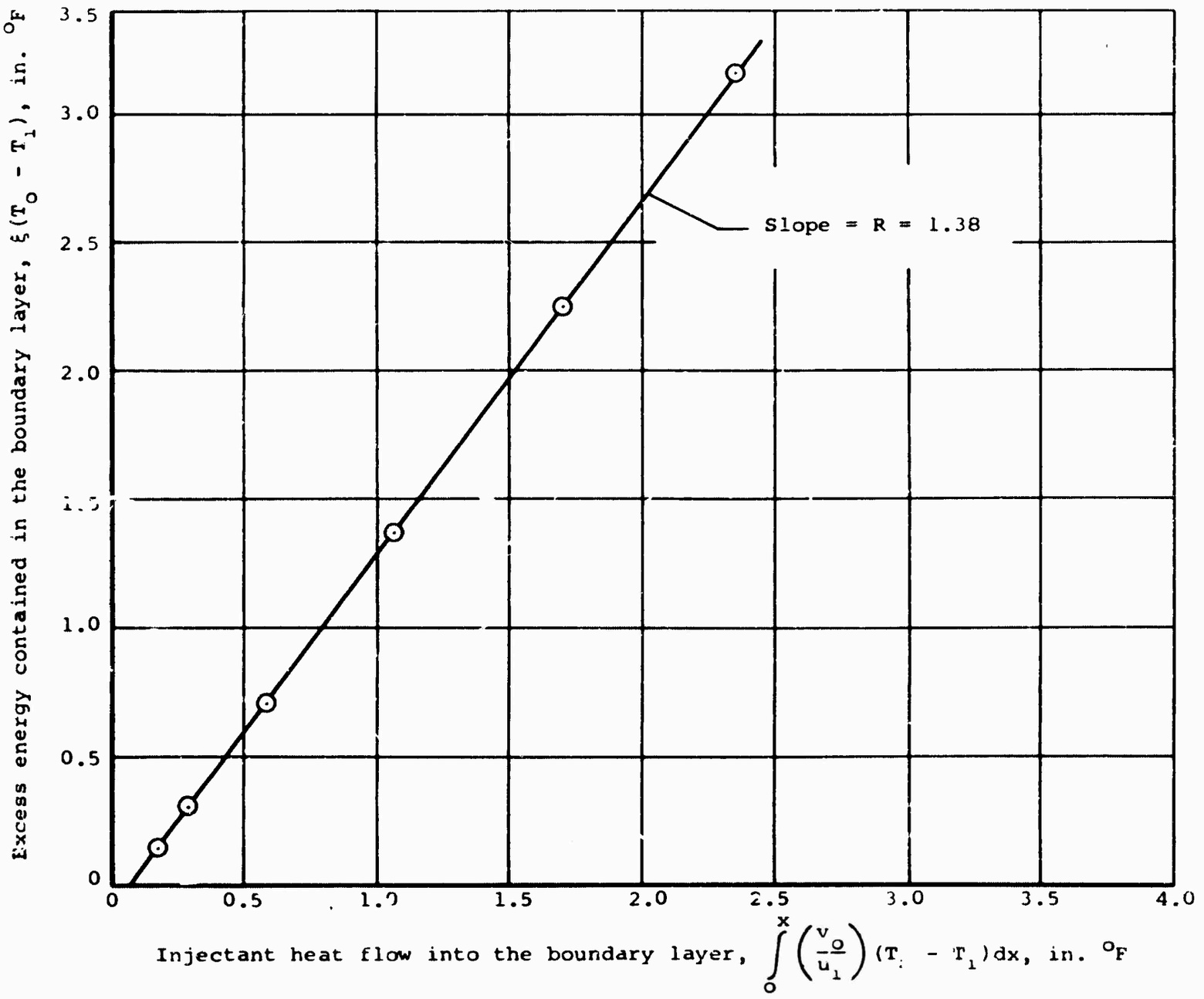

(a) Run H-17a of Reference 9.

Figure 12.- Energy balance in the boundary layer.

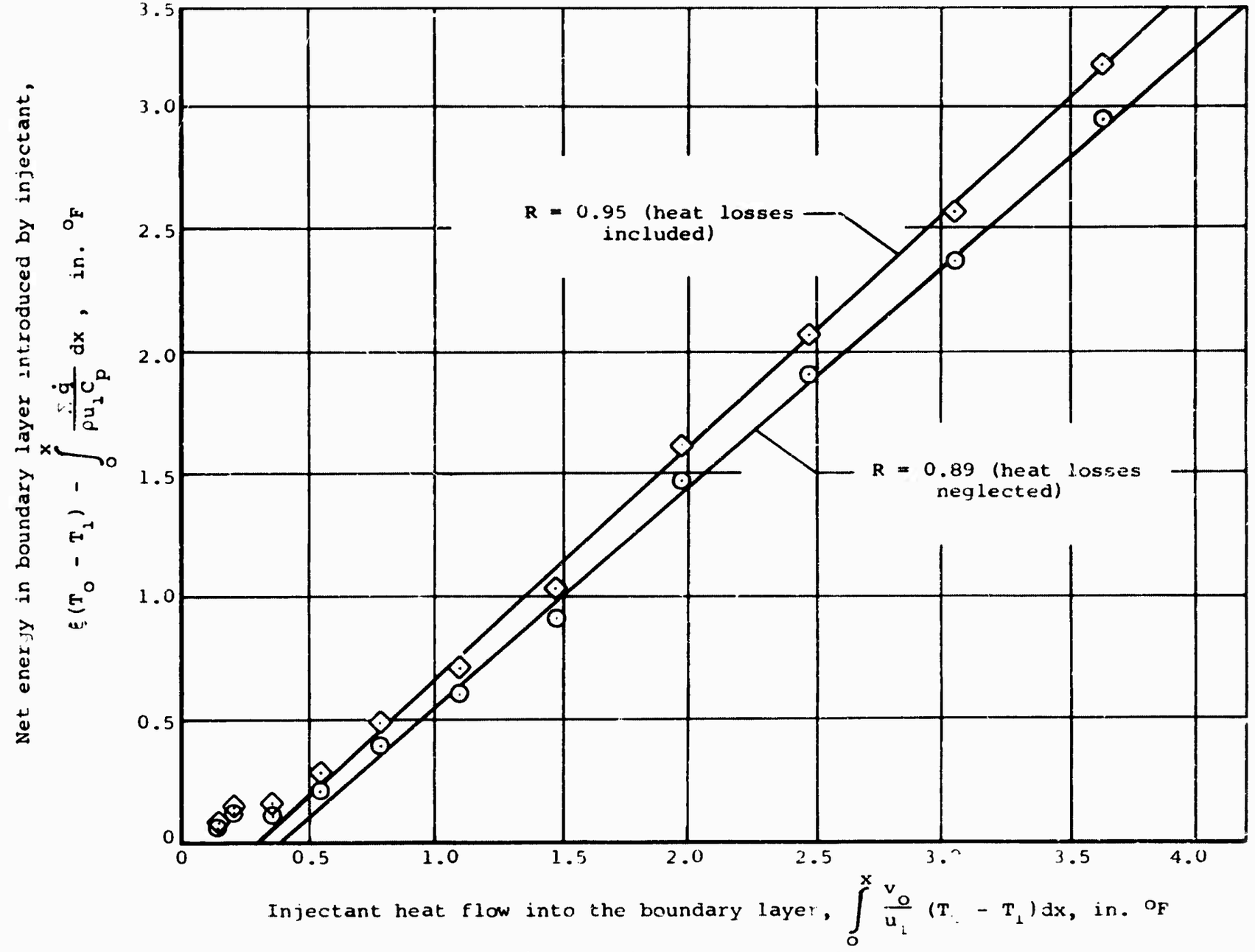

(b) Run C1C of Reference 12.

Figure 12.- Concluded.

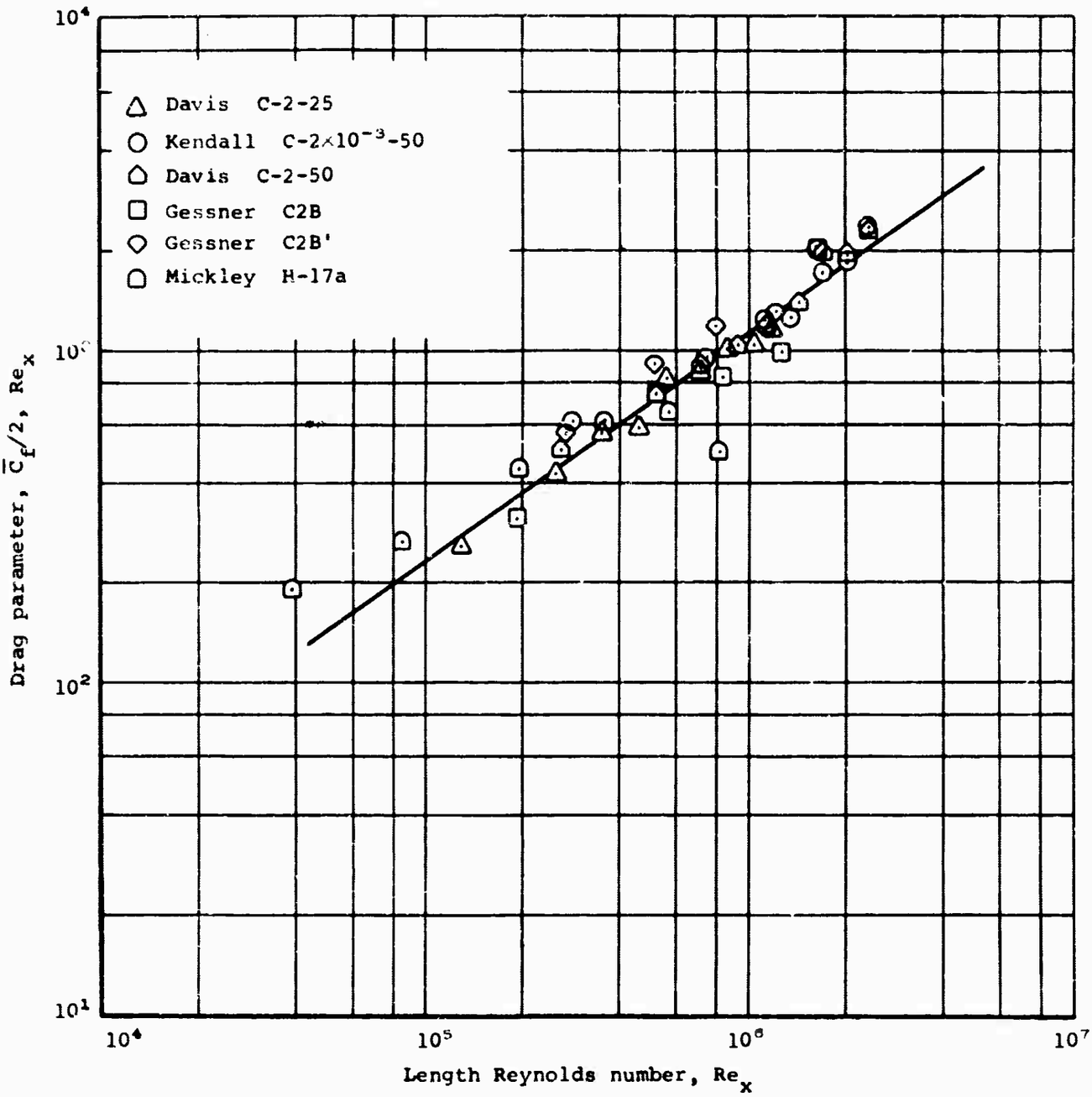

Figure 13.- Composite plot of integral momentum equations results for MIT data after correction of blowing rates for energy balance results, $v_o/u_i \approx 0.002$.

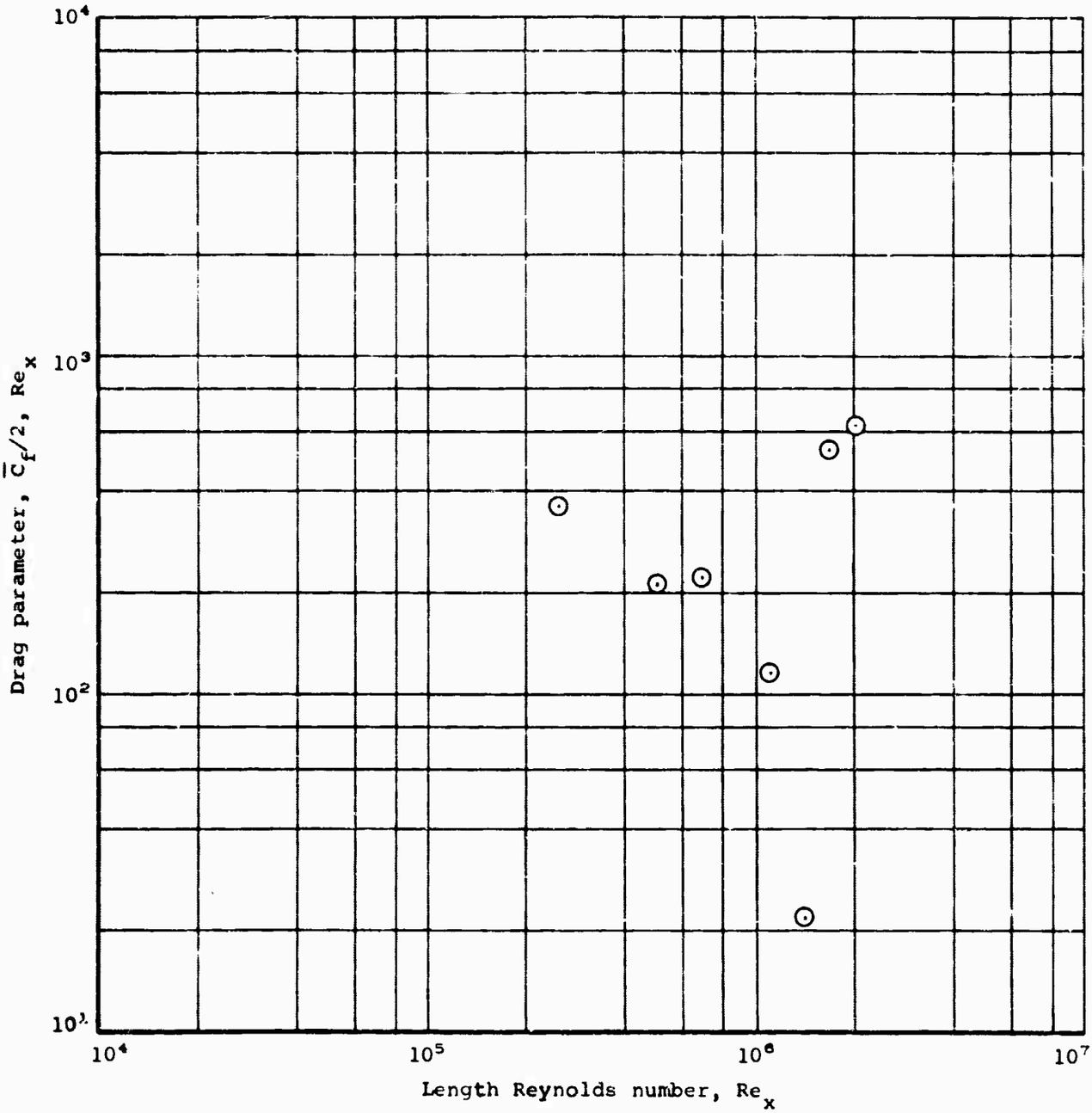

Figure 14.- Integral momentum equation results for MIT data of Reference 17, Run C-5×10^{-3}-50, $v_o/u_1 \approx 5\times10^{-3}$.

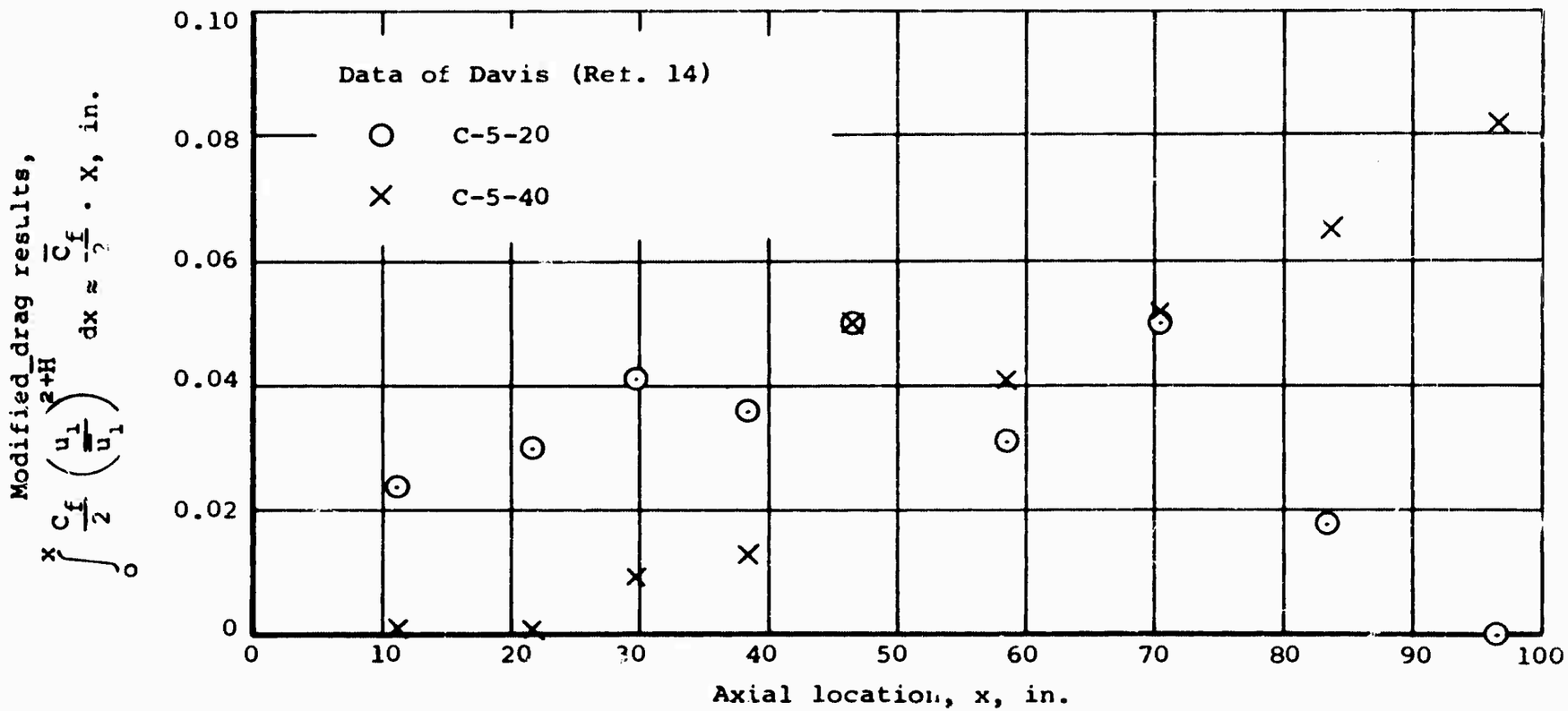

Figure 15.- Evaluation of high-blowing data of Davis in terms of a modified drag parameter, including the effects of free-stream acceler tion.

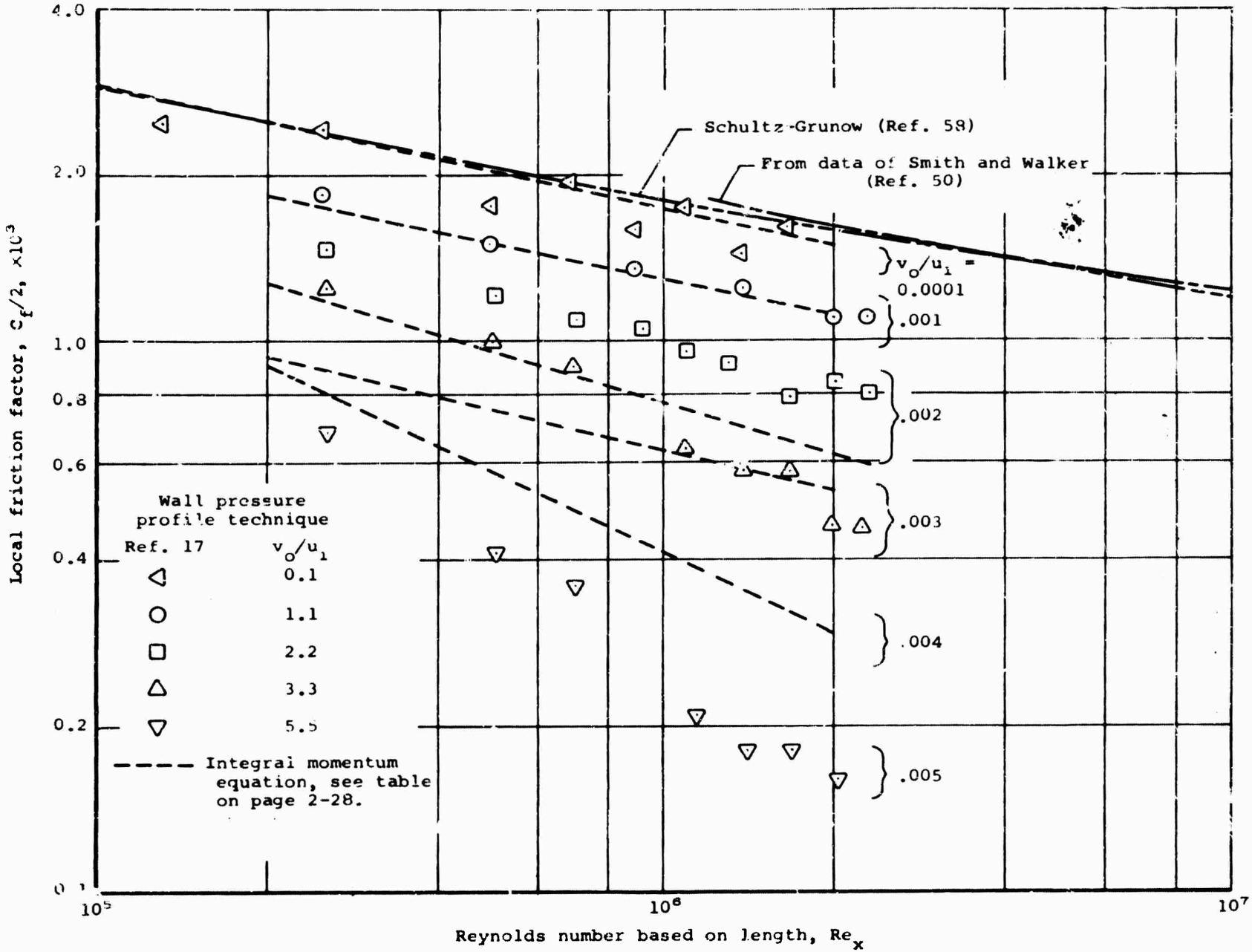

Figure 16.- Comparison of experimental determinations of friction factors with surface mass addition.

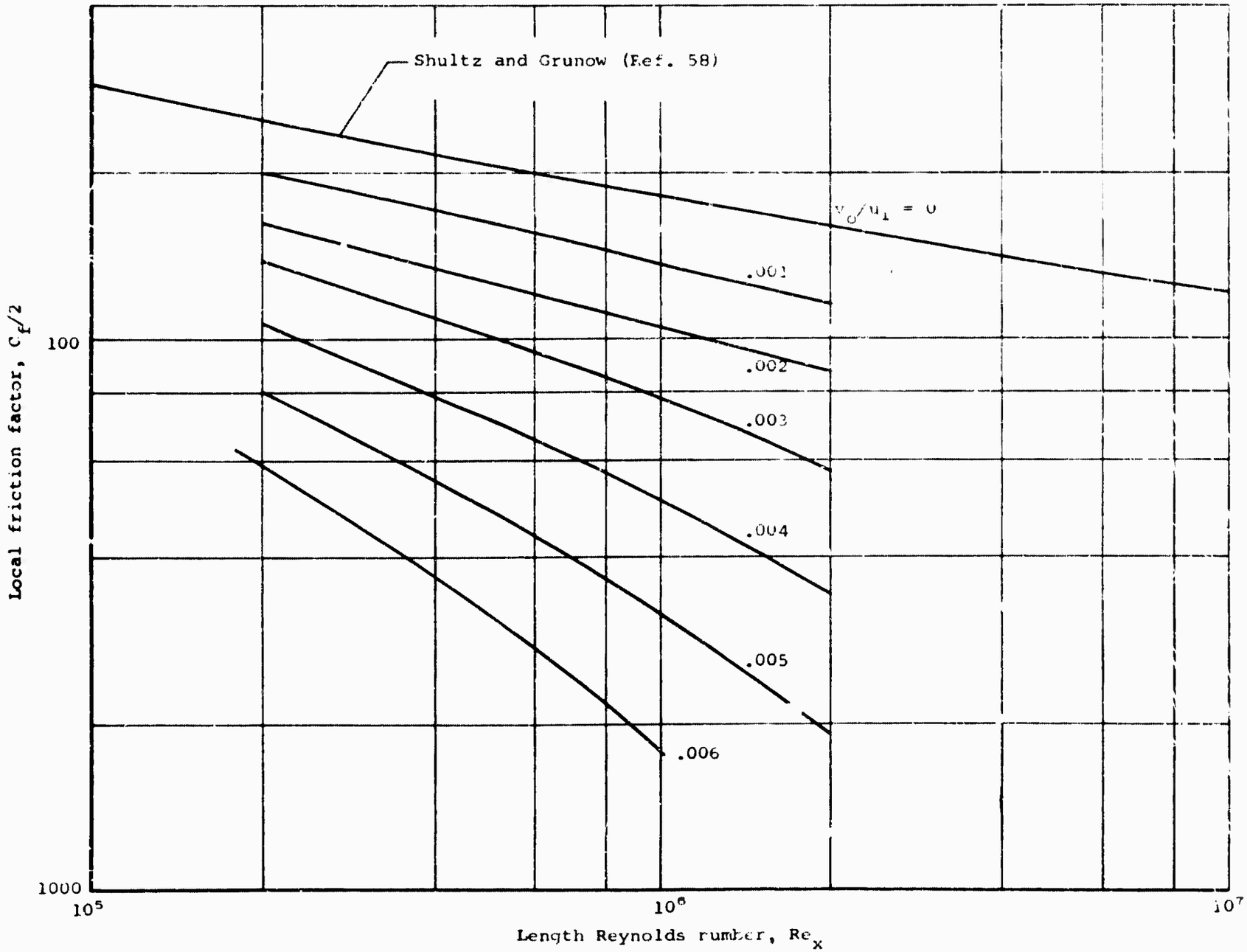

Figure 17.- Interpreted friction factors with surface mass addition based on data of Figure 16.

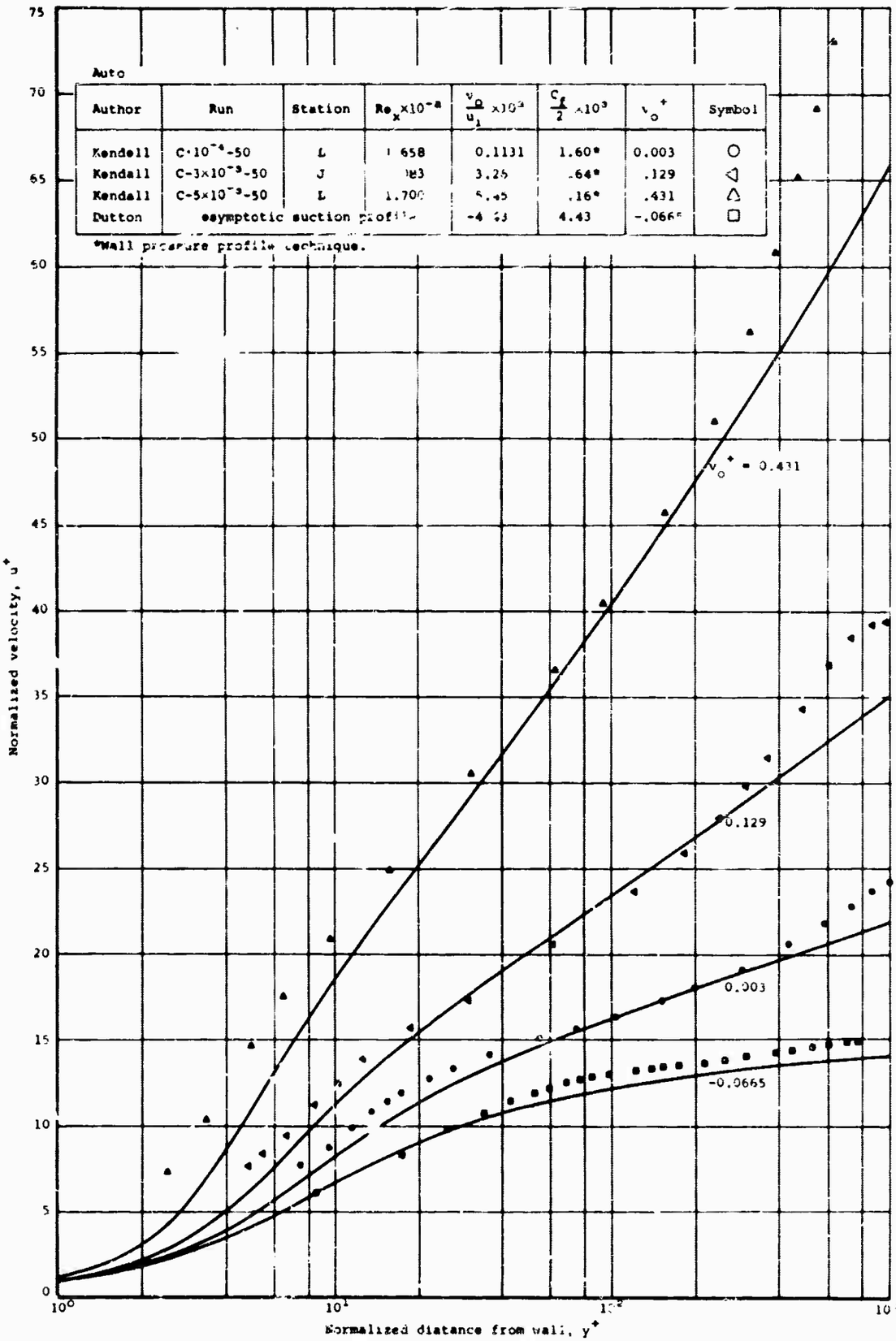

(a) Data of Kendall (blowing) and Dutton (suction).

Figure 18.- Comparison of the "law of the wall" with experimental velocity distribution data.

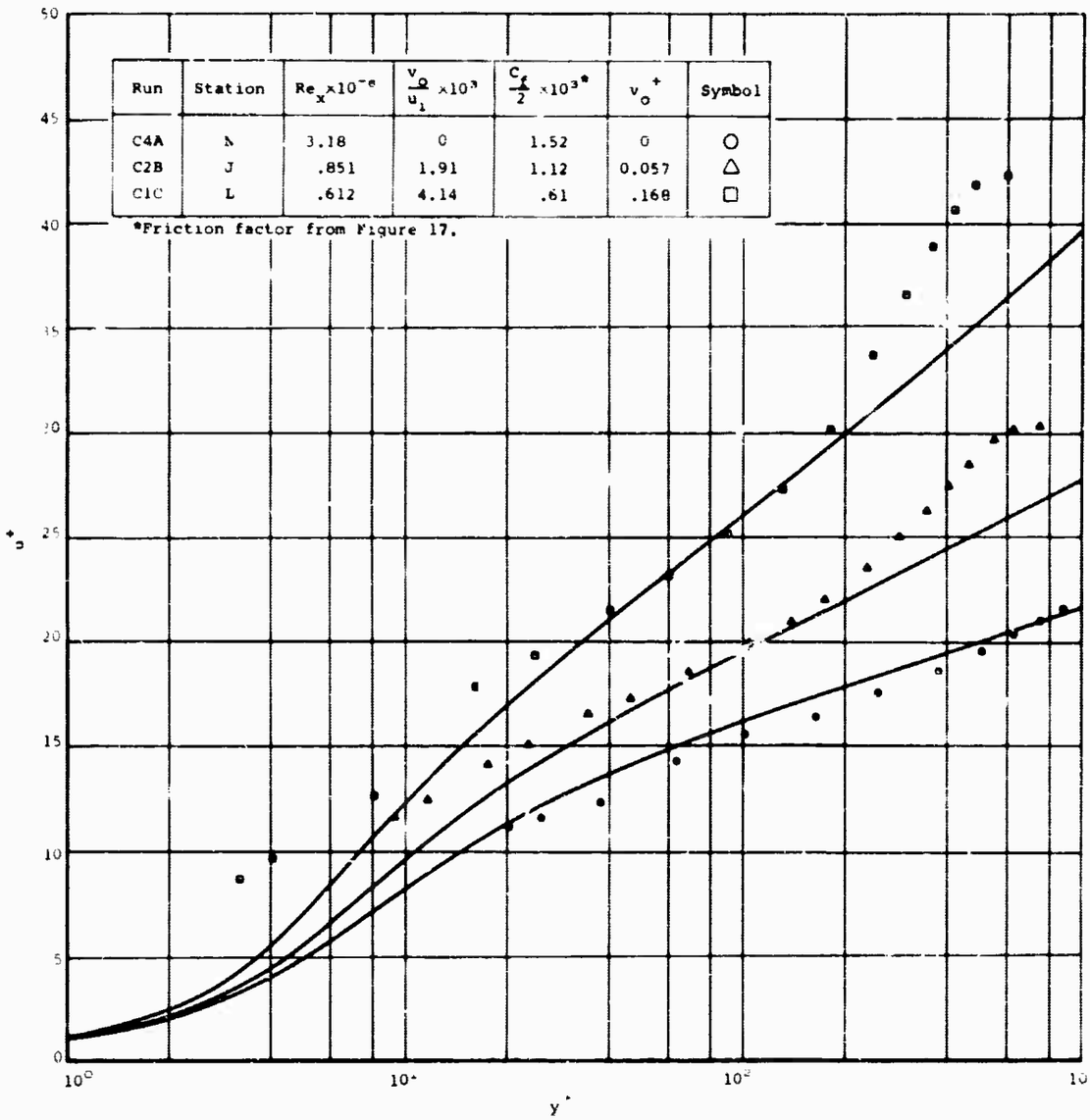

(b) Data of Gessner (blowing).

Figure 18.- Concluded.

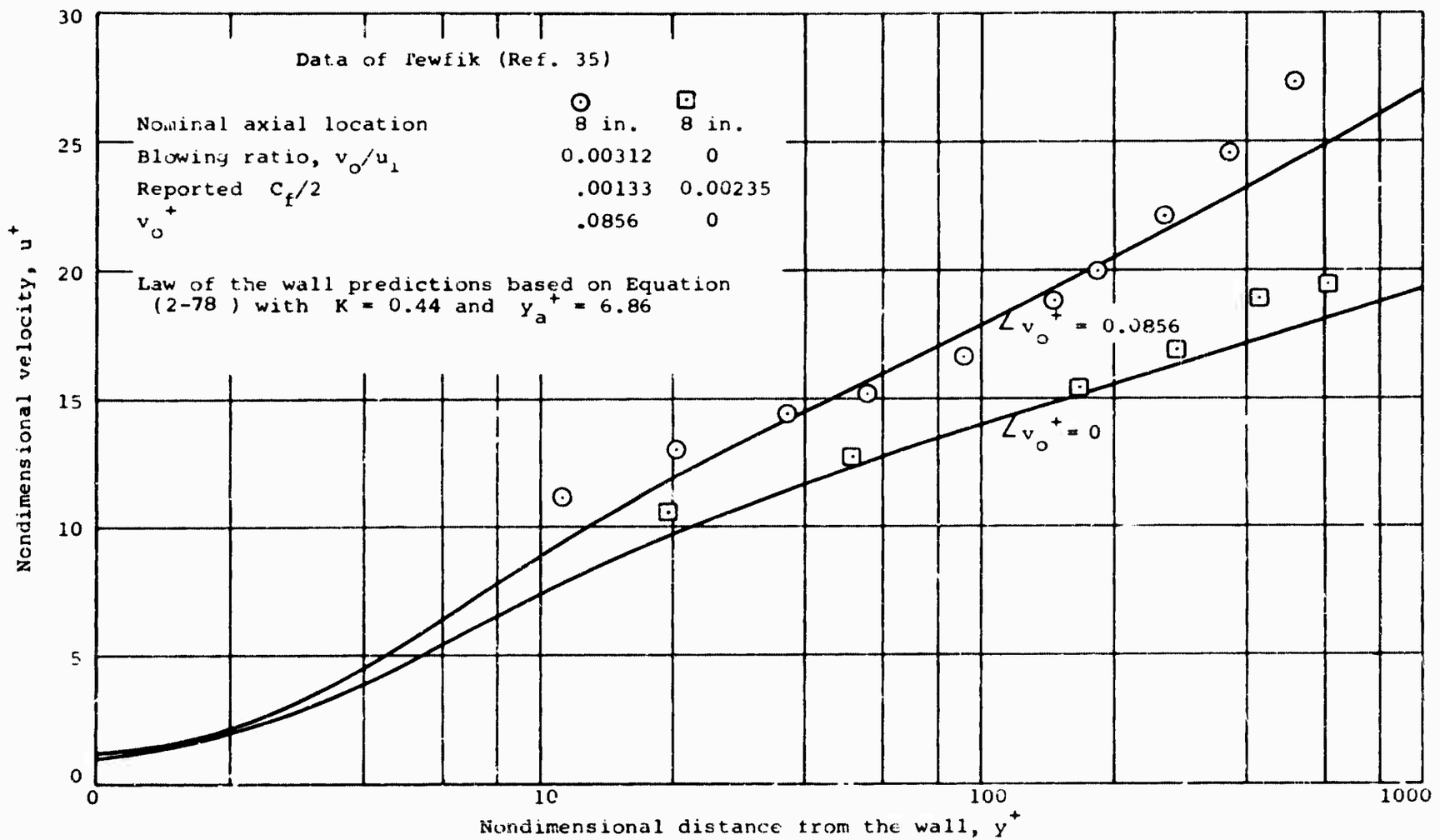

Figure 19.- Comparison of law-of-the-wall prediction with data of Tewfik (Ref. 35).

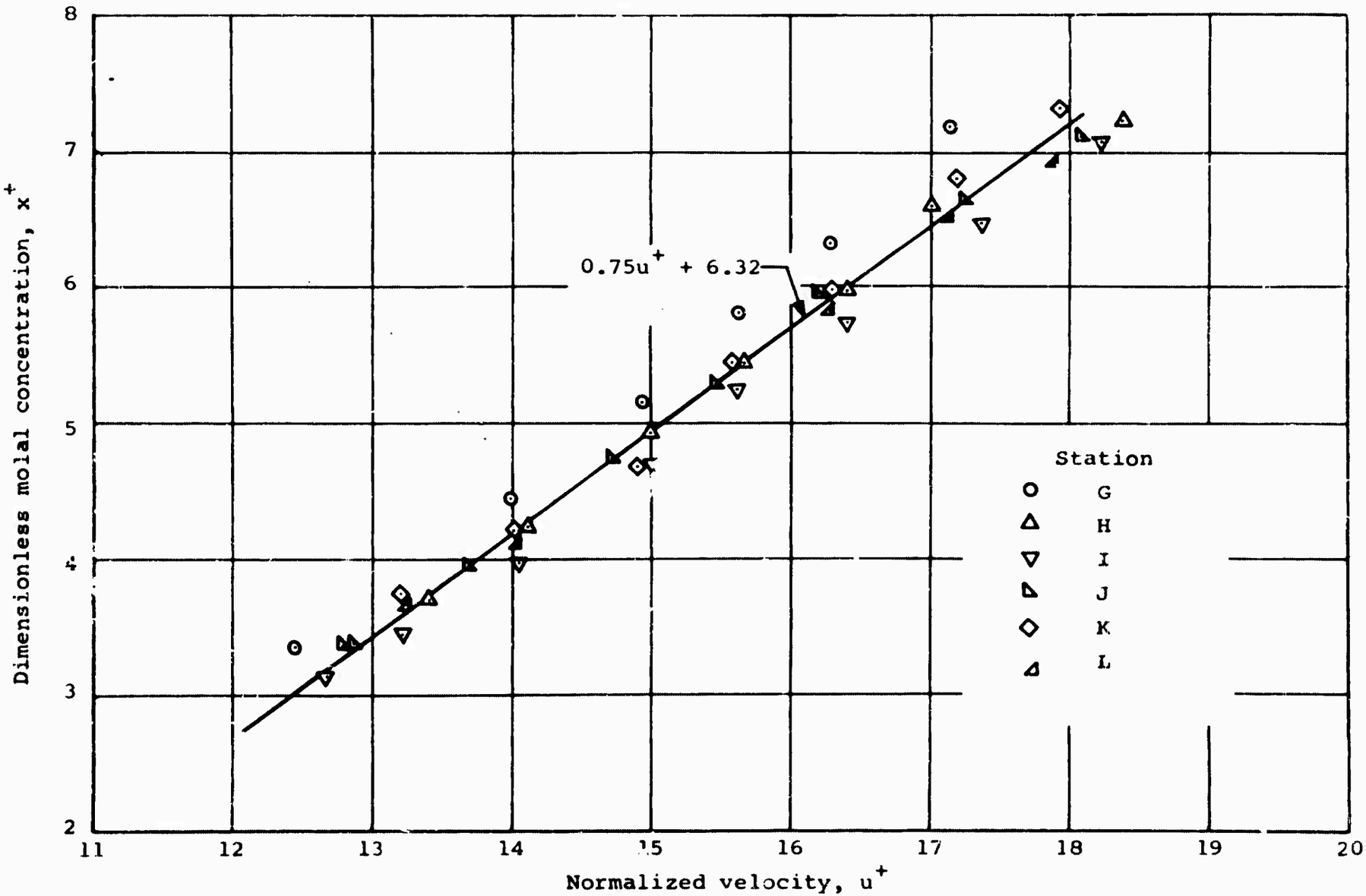

Figure 20.- Determination of the turbulent Schmidt number in the vicinity of the wall from the helium injection data of Reference 17.

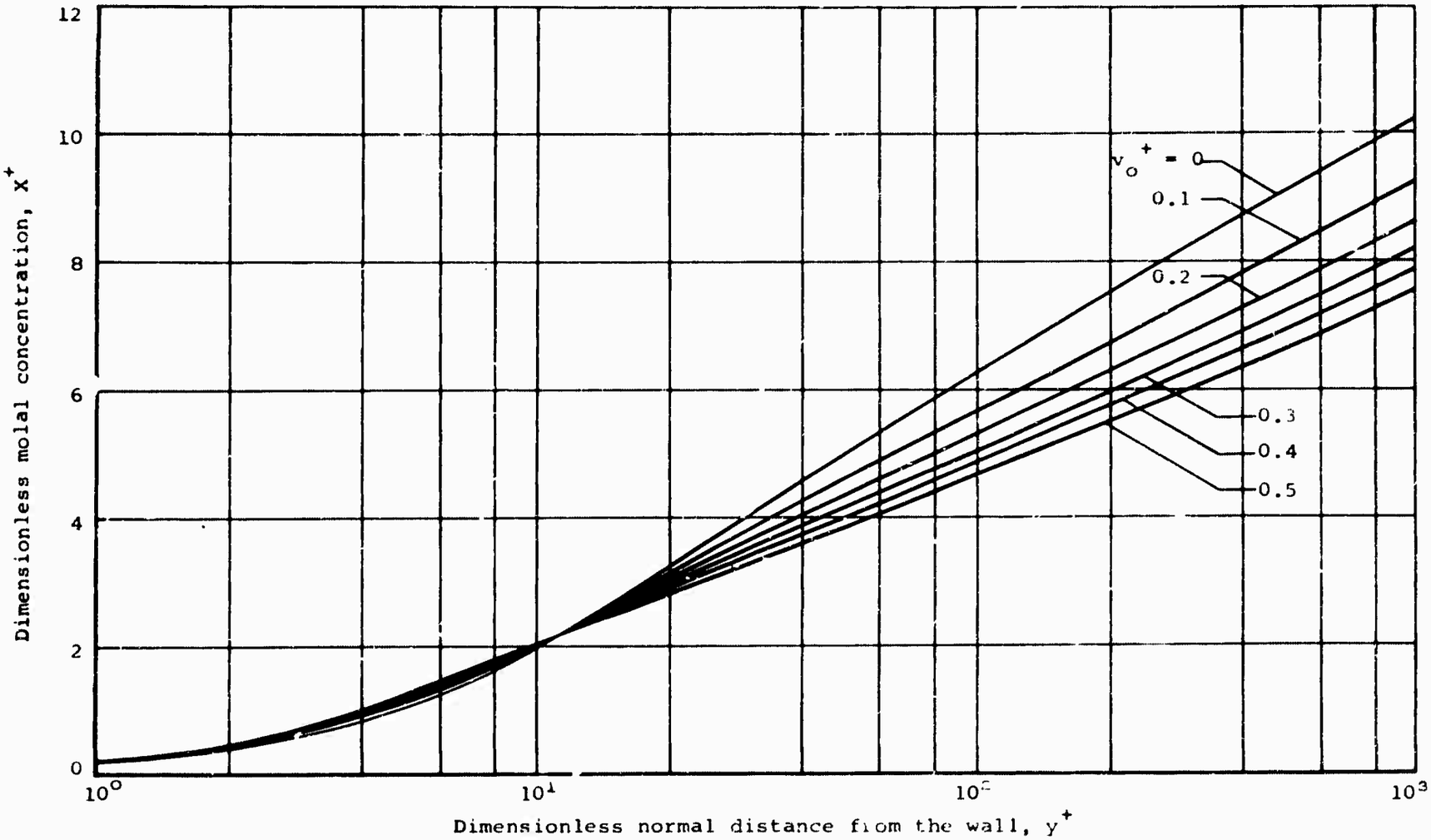

Figure 21.- Predicted variation of dimensionless concentration with and without transpiration (Sc = 0.21, Sc' = 0.75).

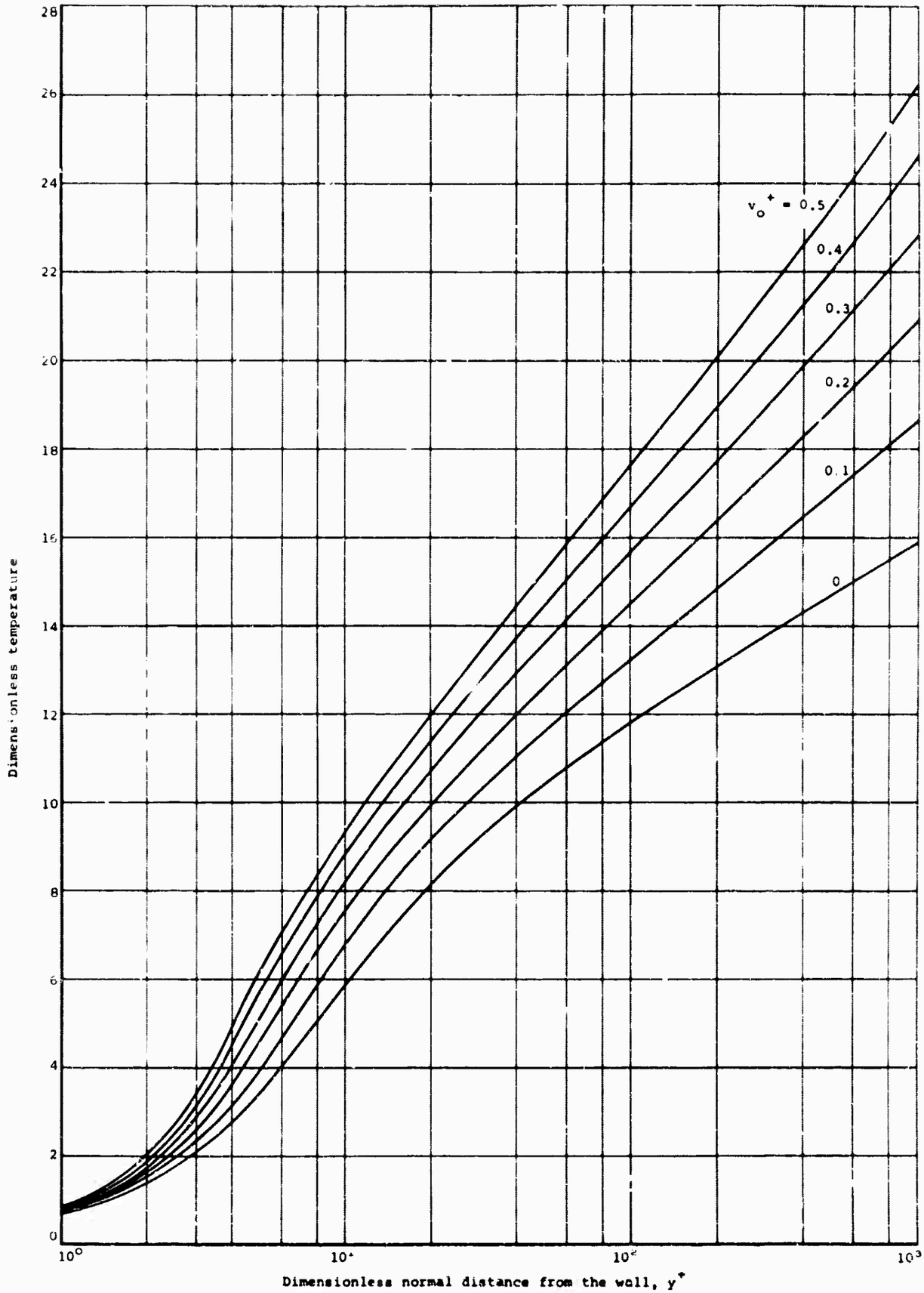

Figure 22.- Predicted variation of dimensionless temperature with and without transpiration (Pr = 0.7, Pr' = 0.75).

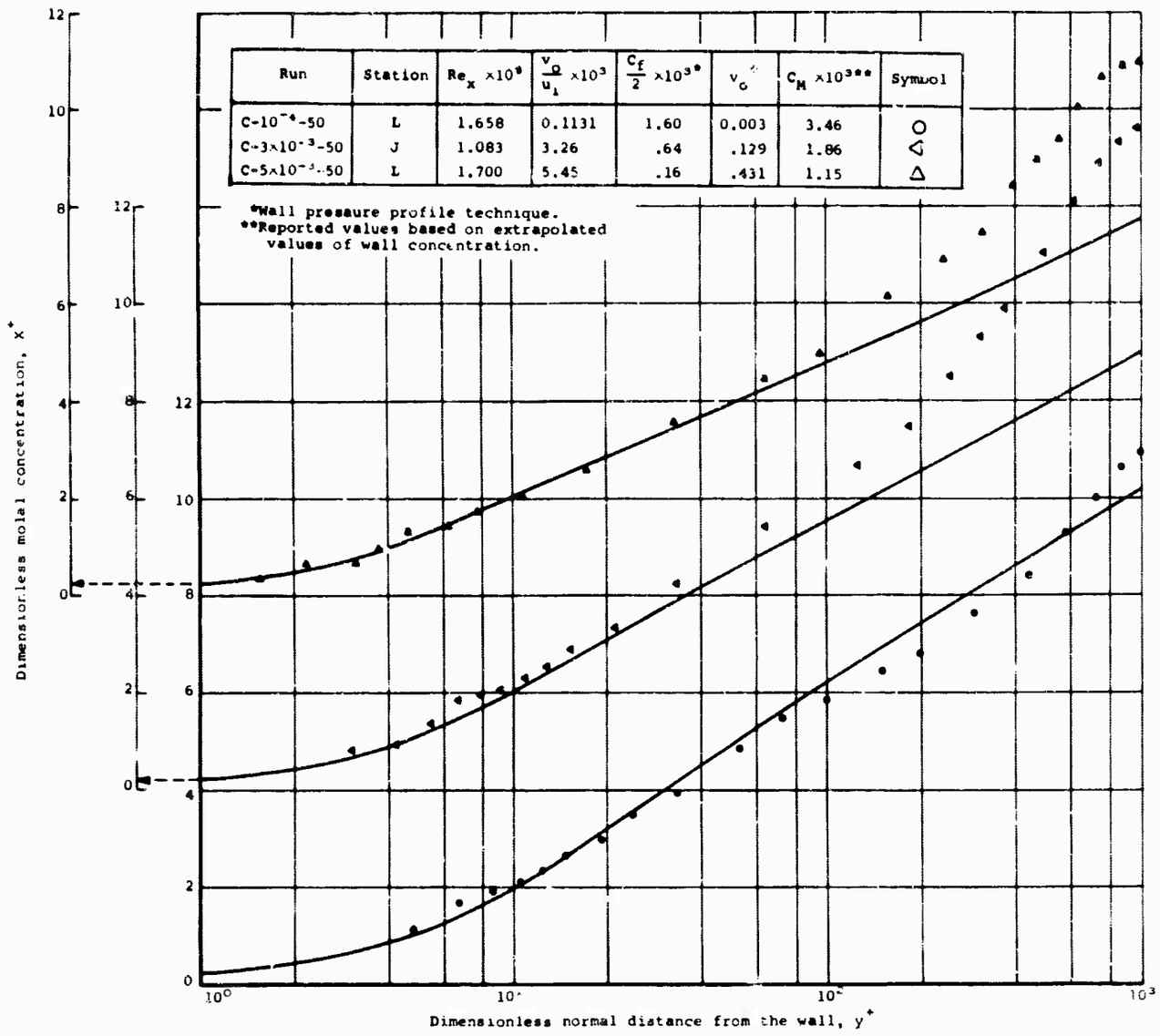

Figure 23.- Comparison of the predicted dimensionless concentration profiles with the data of Kendall (Sc = 0.21, Sc' = 0.75).

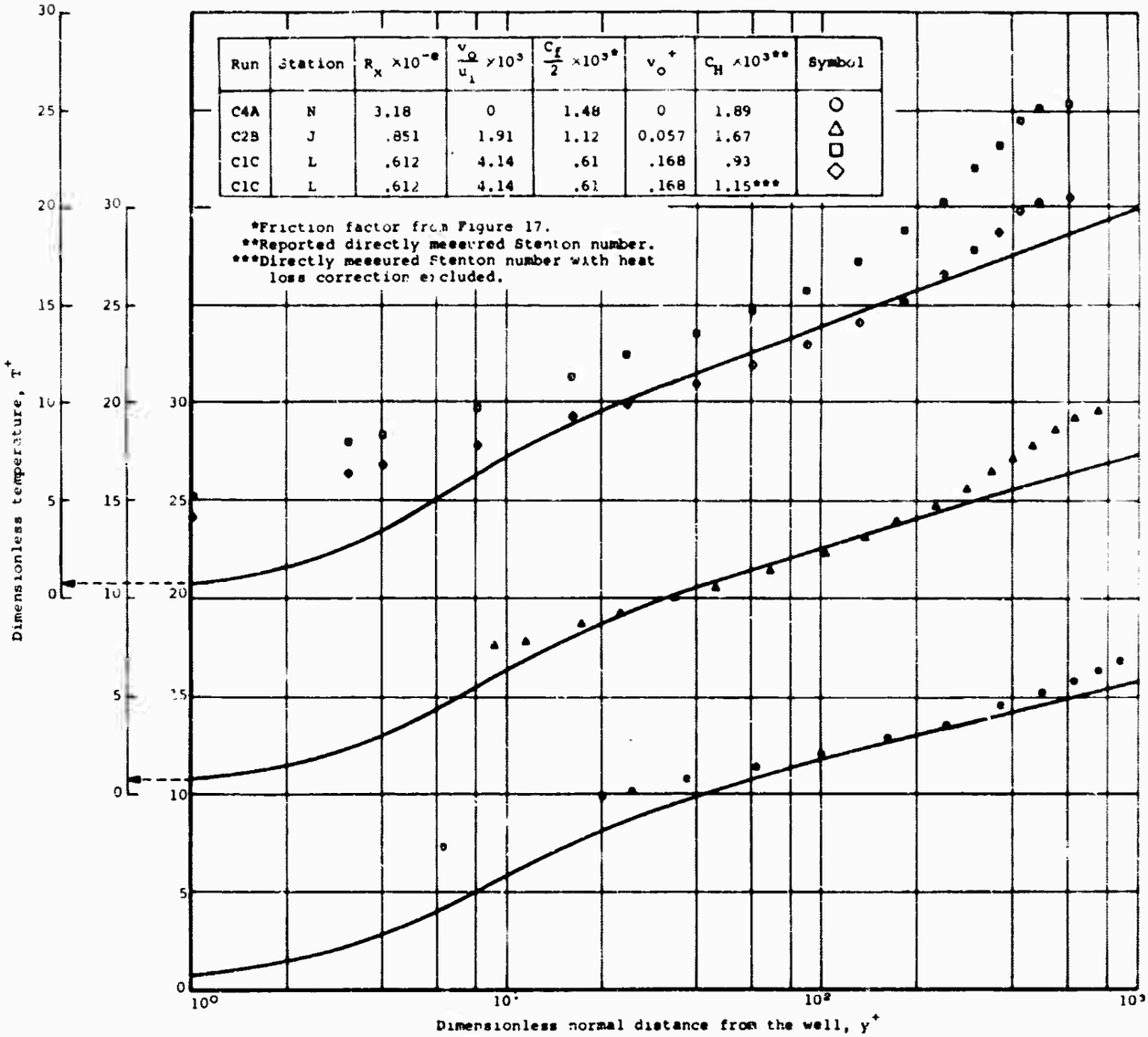

Figure 24.- Comparison of the predicted dimensionless temperature profiles with the data of Curl (Pr = 0.7, Pr' = 0.75).

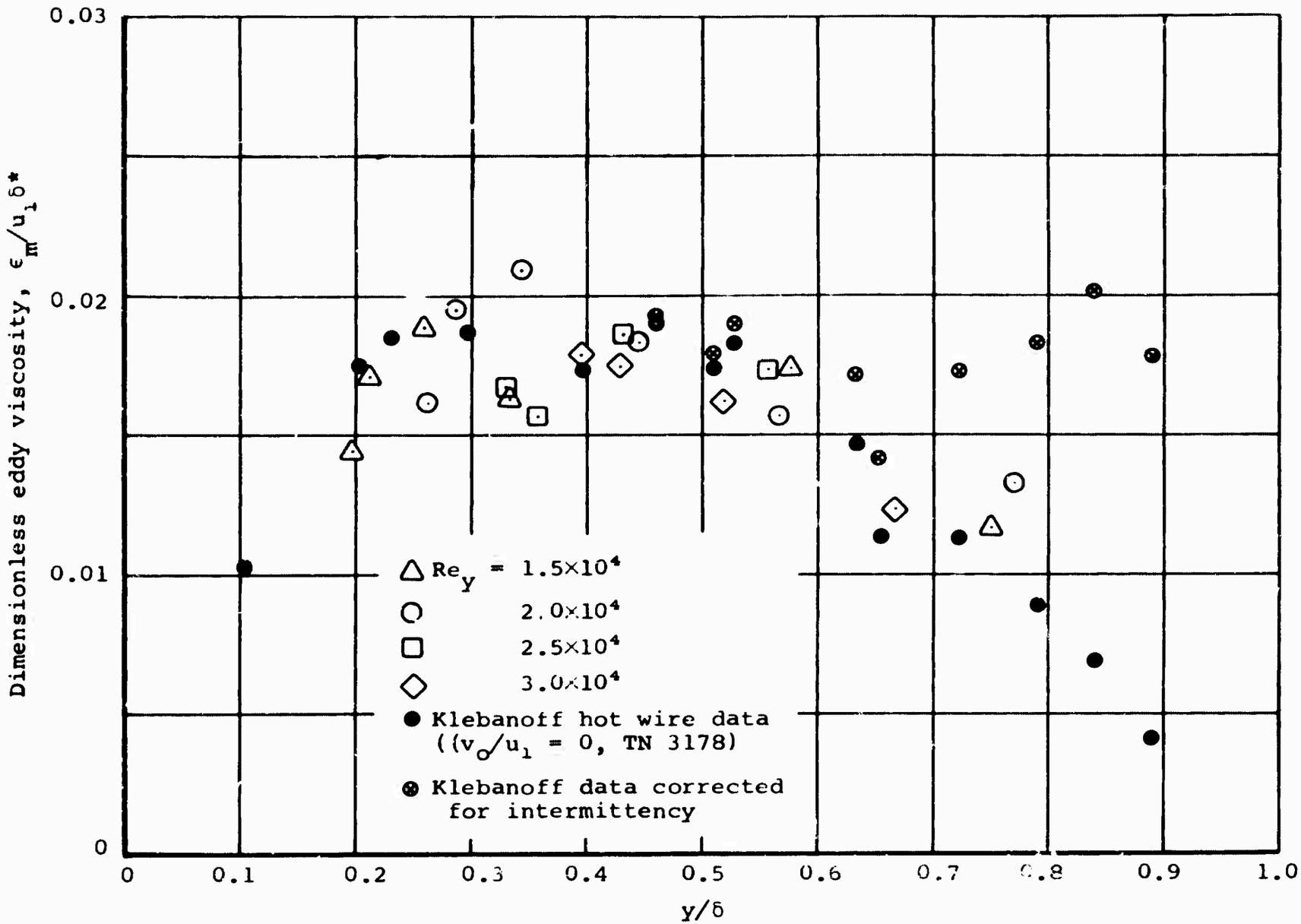

Figure 25.- Dimensionless eddy viscosity calculated from the data of Kendall ($v_o/u_1 \approx 0.0055$).

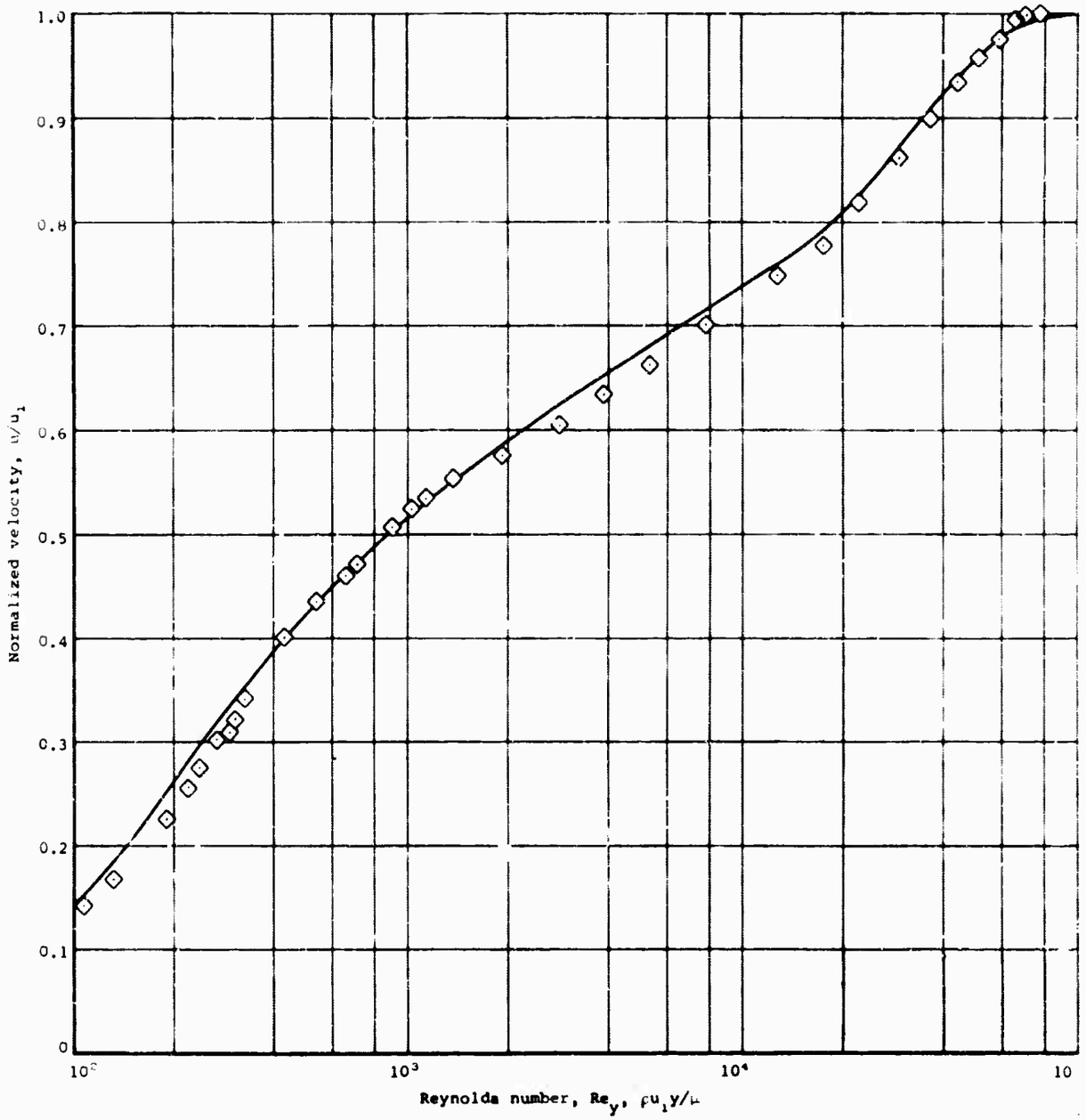

(a) Data of Klebanoff, Reference 51.

Figure 26.- Comparison of the prediction of the entire turbulent boundary-layer velocity profiles with flat-plate data, without transpiration.

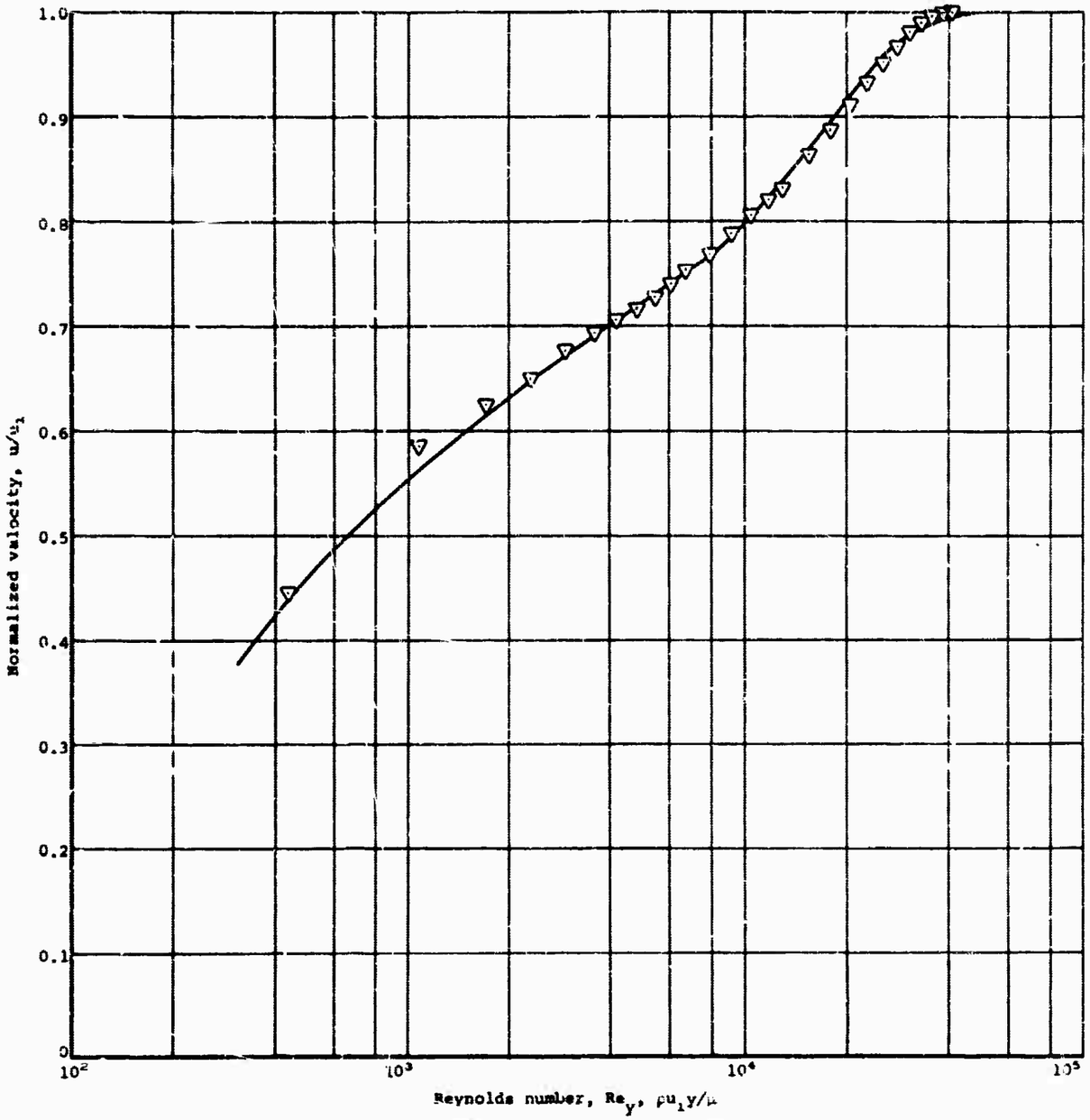

(b) Data of Smith and Walker, Reference 52.

Figure 26.- Continued.

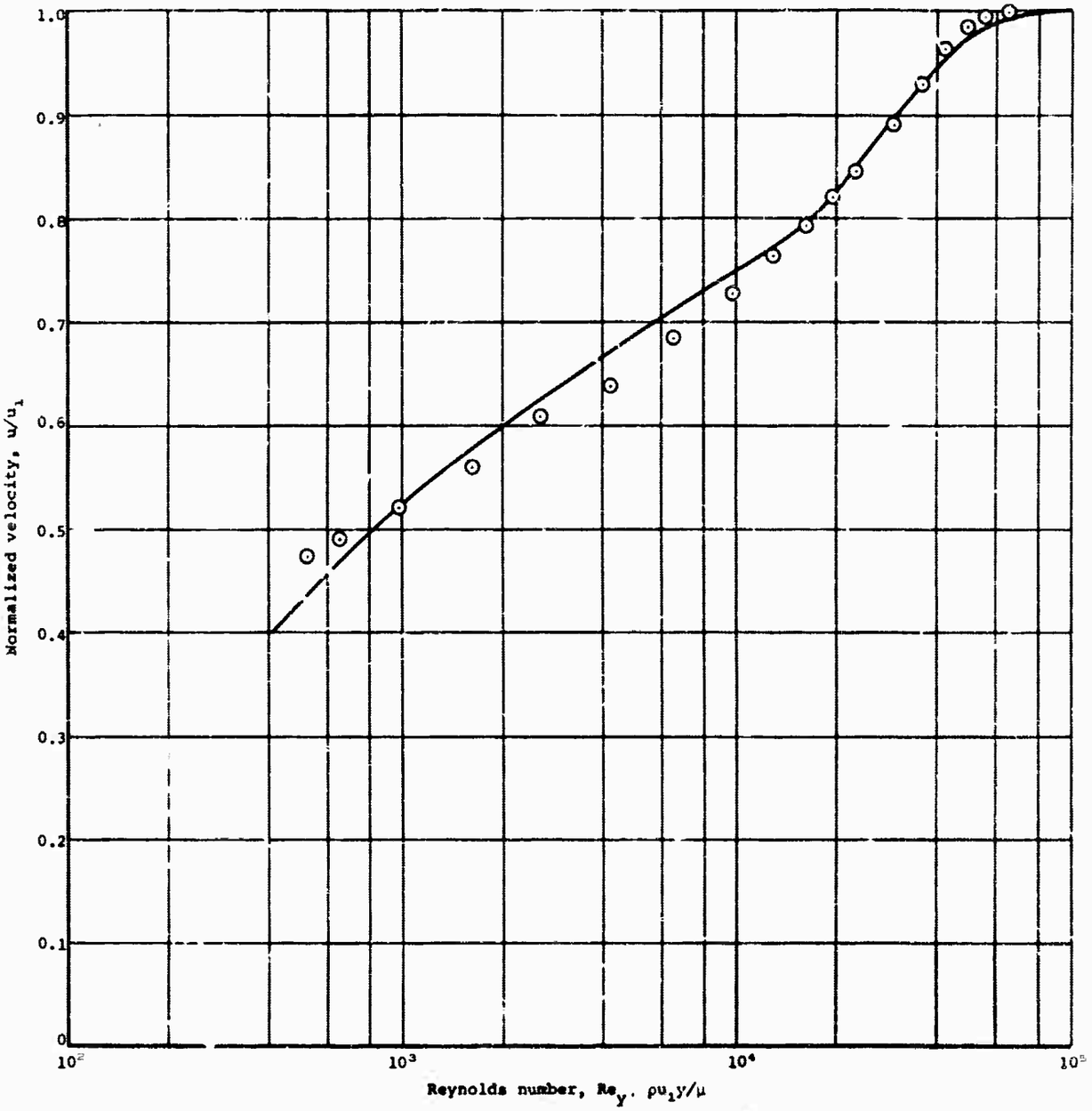

(c) Data of Gessner, Reference 11, Station N.

Figure 26.- Concluded.

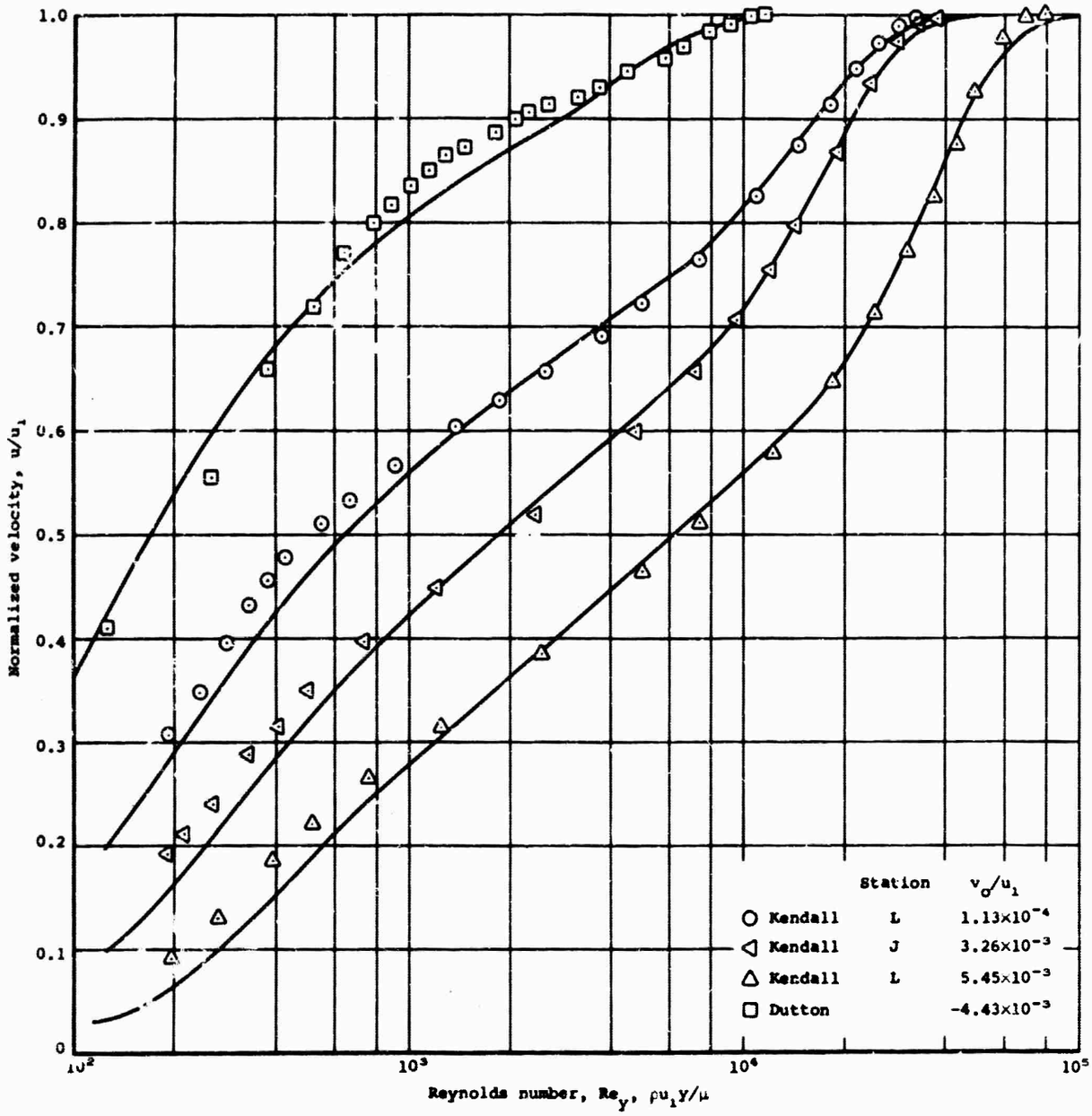

(a) Data of Kendall and Dutton, References 17 and 16.

Figure 27.- Comparison of the prediction of the entire turbulent boundary-layer velocity profiles with flat-plate data.

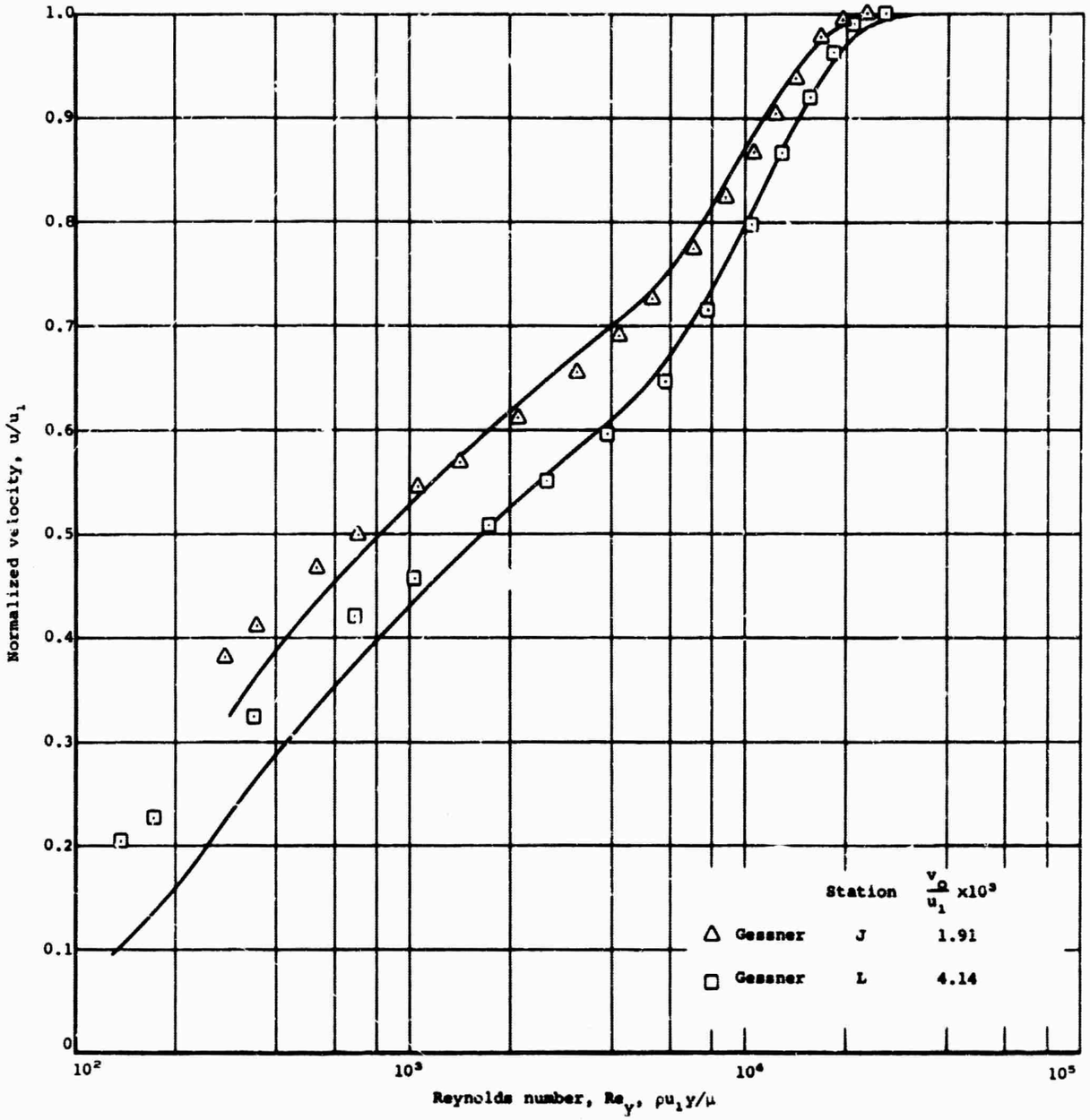

(b) Data of Gessner, Reference 11.

Figure 27.- Concluded.

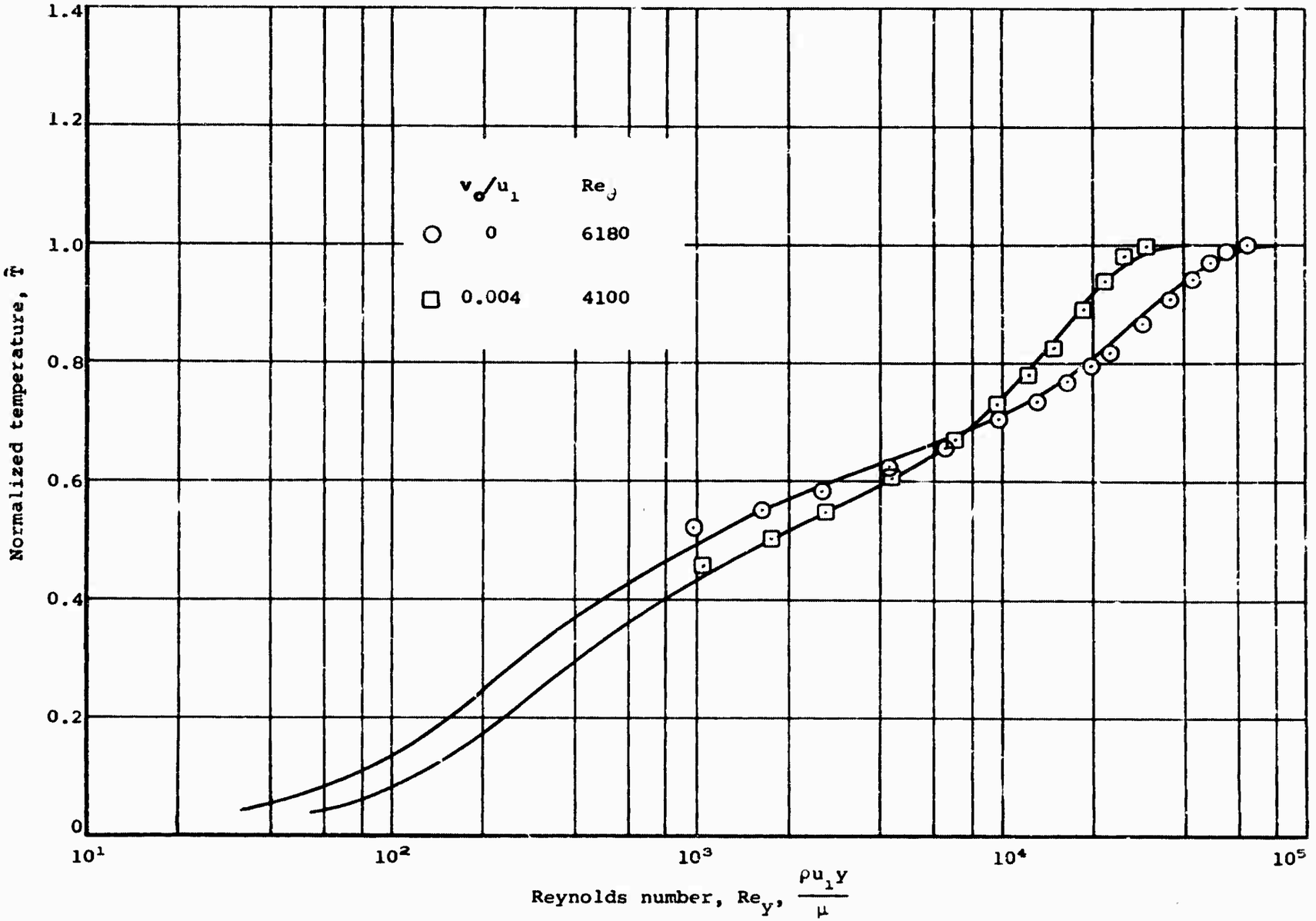

Figure 28.- Comparison of the prediction of the entire turbulent boundary-layer temperature profiles with the data of Curl, Reference 12.

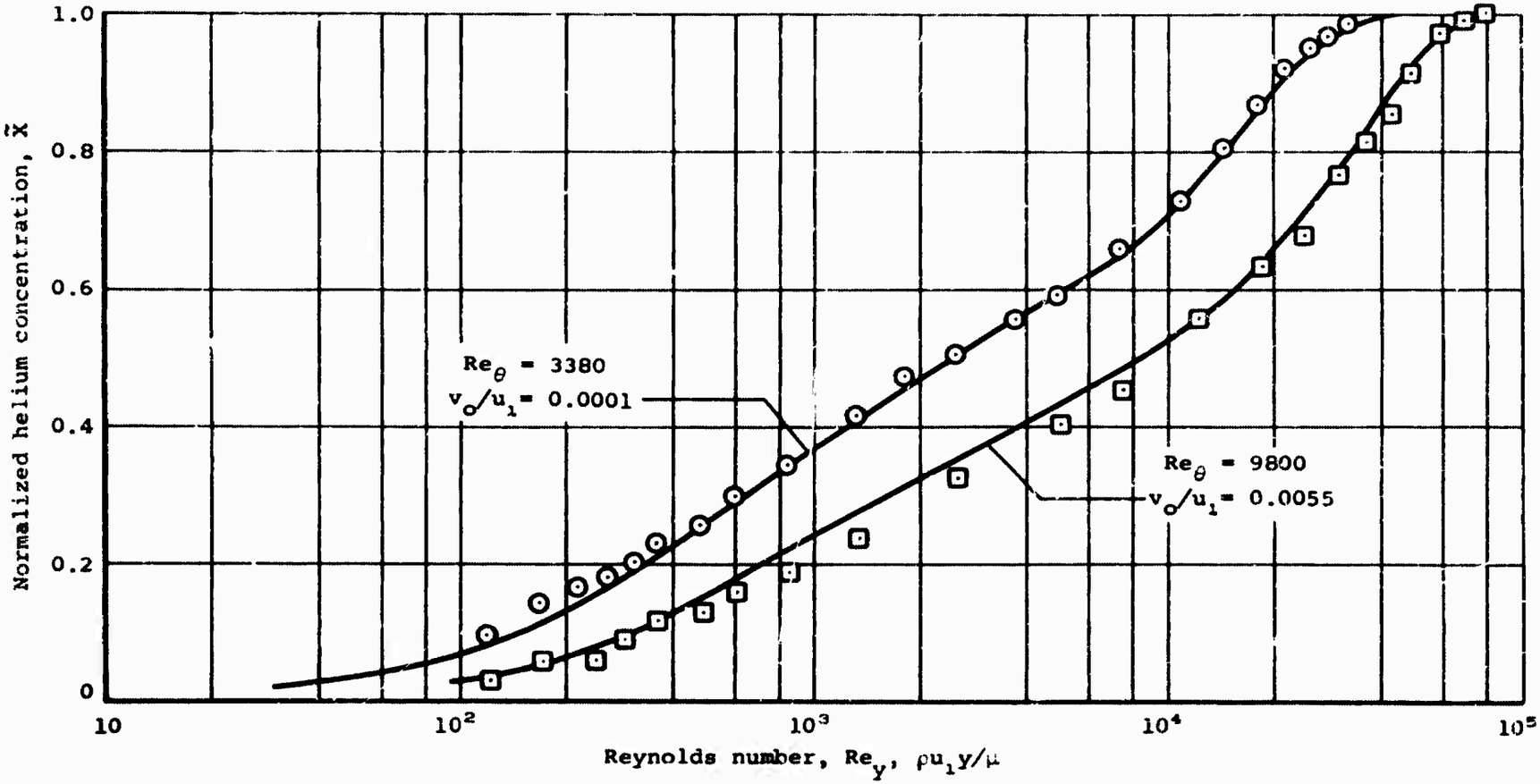

Figure 29.- Comparison of the prediction of the entire turbulent boundary-layer concentration profiles with the data of Kendall (Ref. 17).

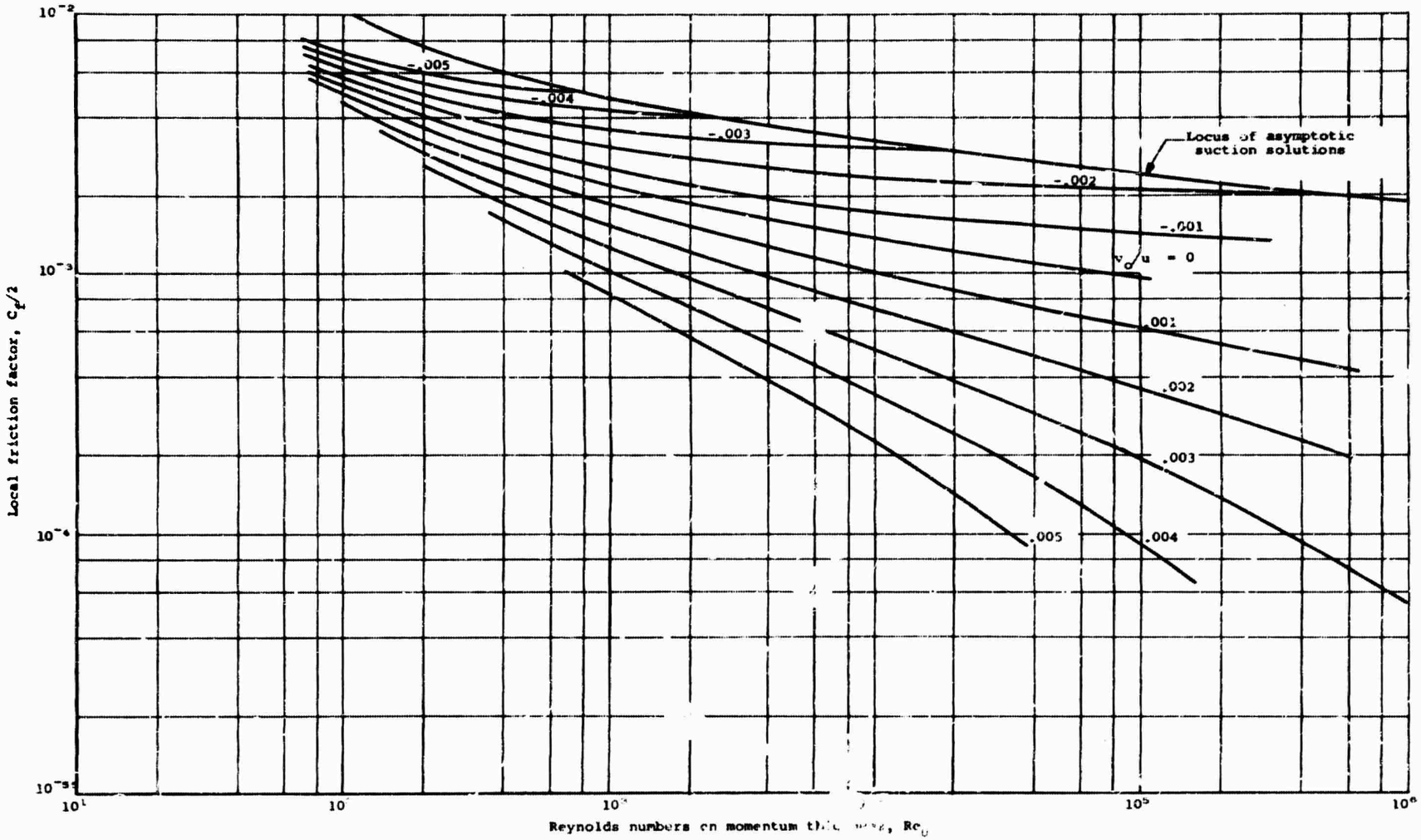

(a) Predicted skin-friction coefficient with and without transpiration.

Figure 30.- Skin-friction coefficient in terms of momentum thickness Reynolds numbers.

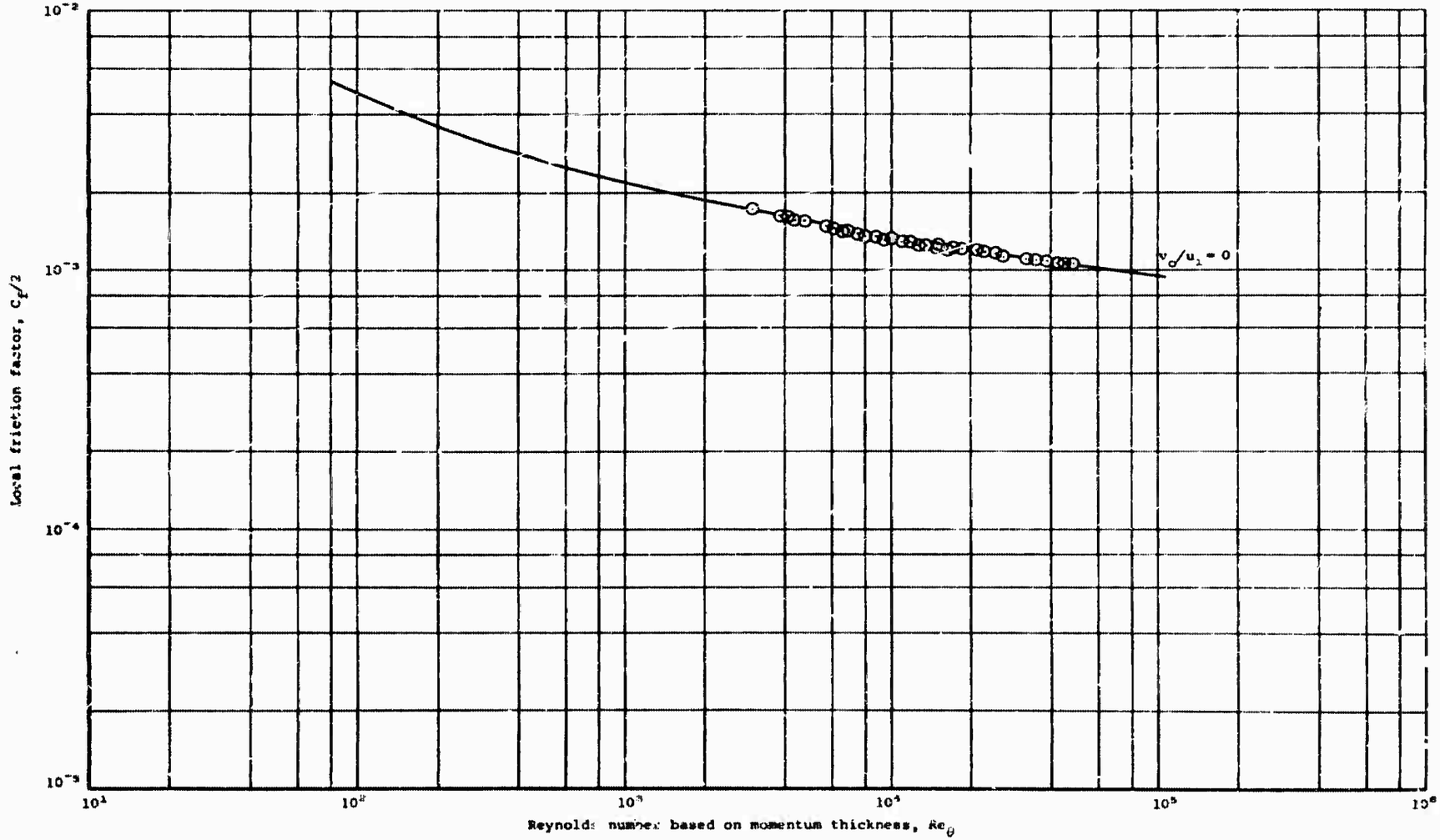

(b) Comparison with data of Reference 50 at $v_o/u_1 = 0$.

Figure 30.- Concluded.

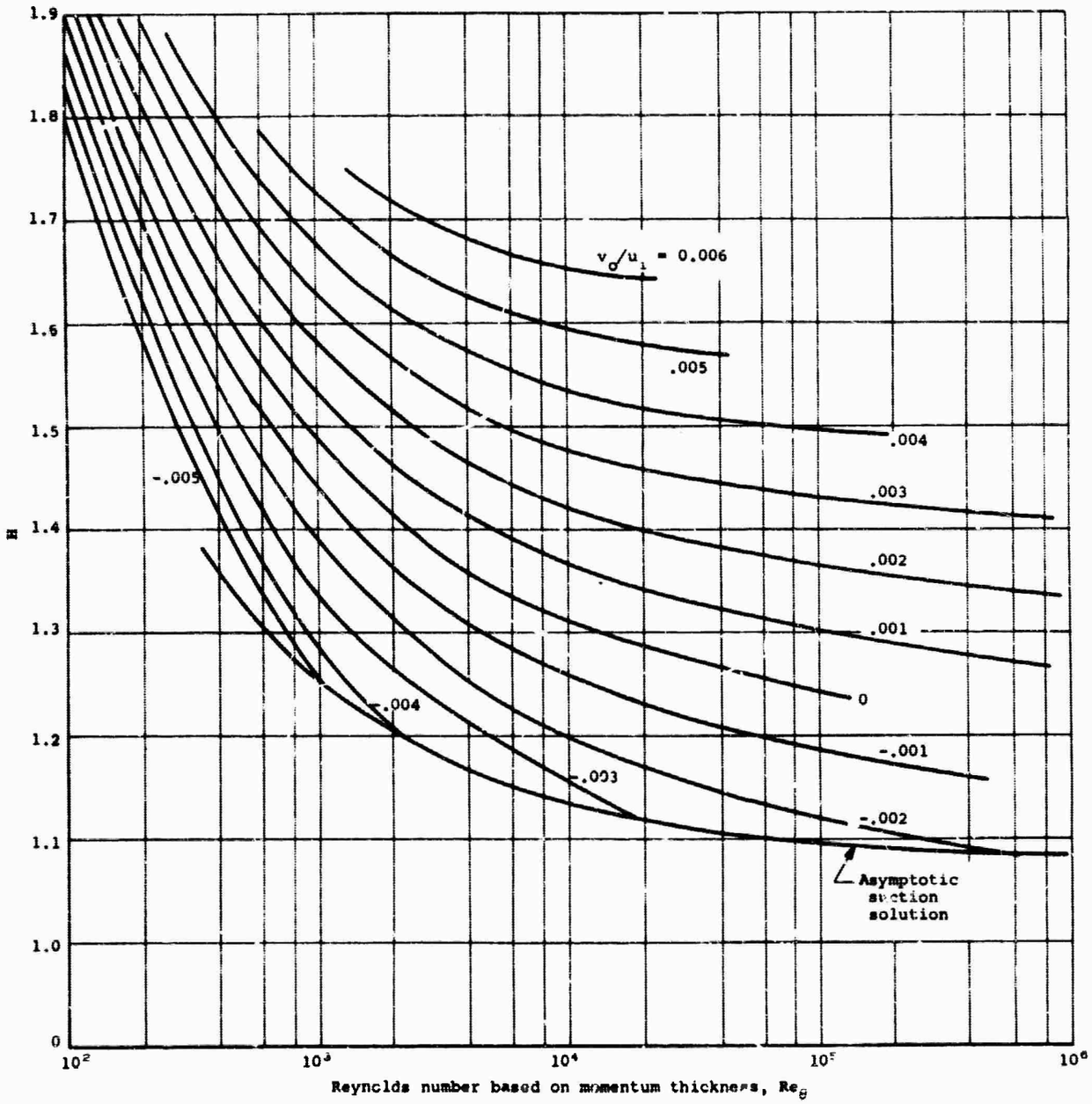

(a) Effect of mass transfer.

Figure 31.- Boundary-layer shape factor, $H = \delta^*/\theta$.

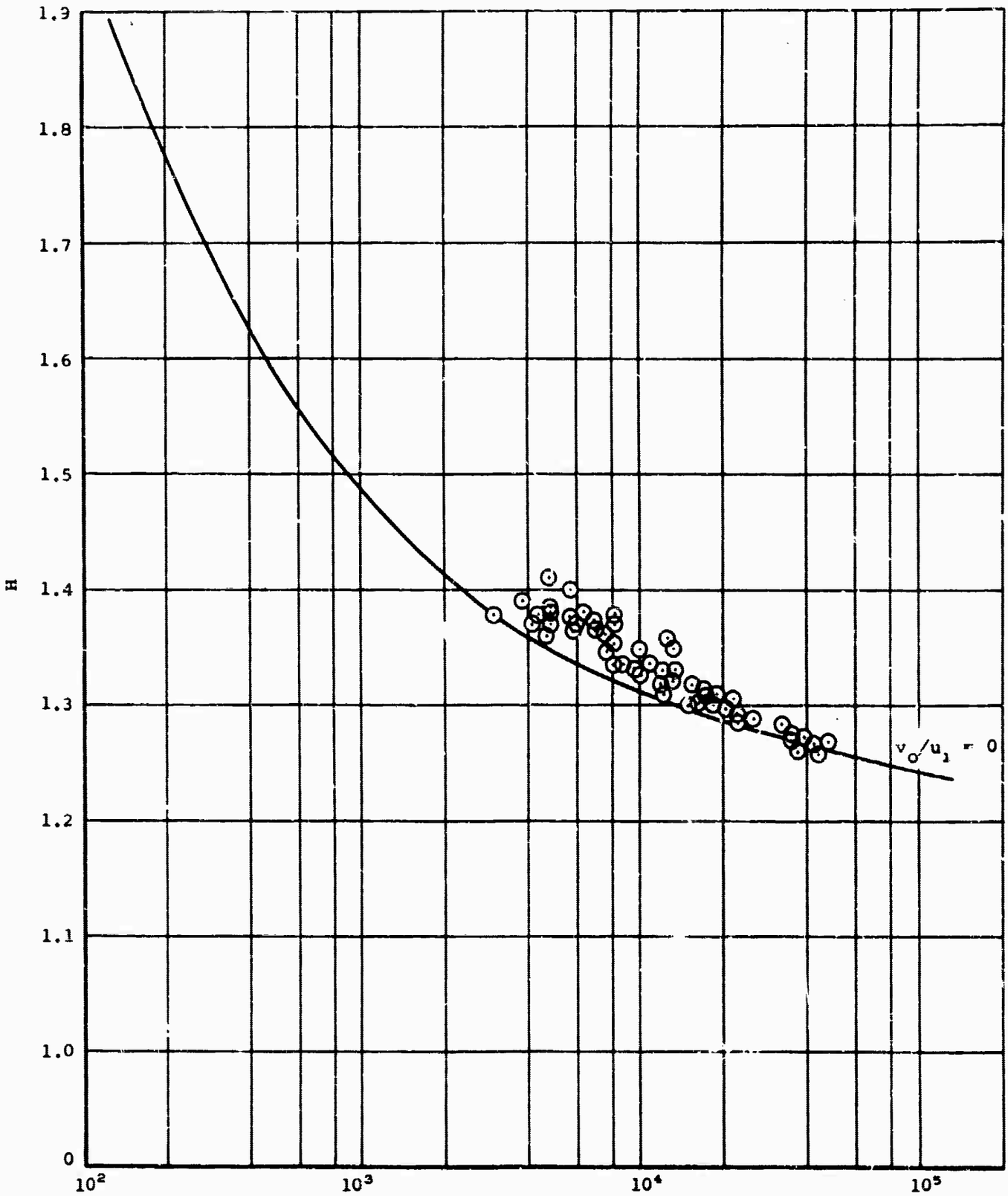

(b) Comparison with data of Reference 50 at $v_o/u_1 = 0$.

Figure 31.- Concluded.

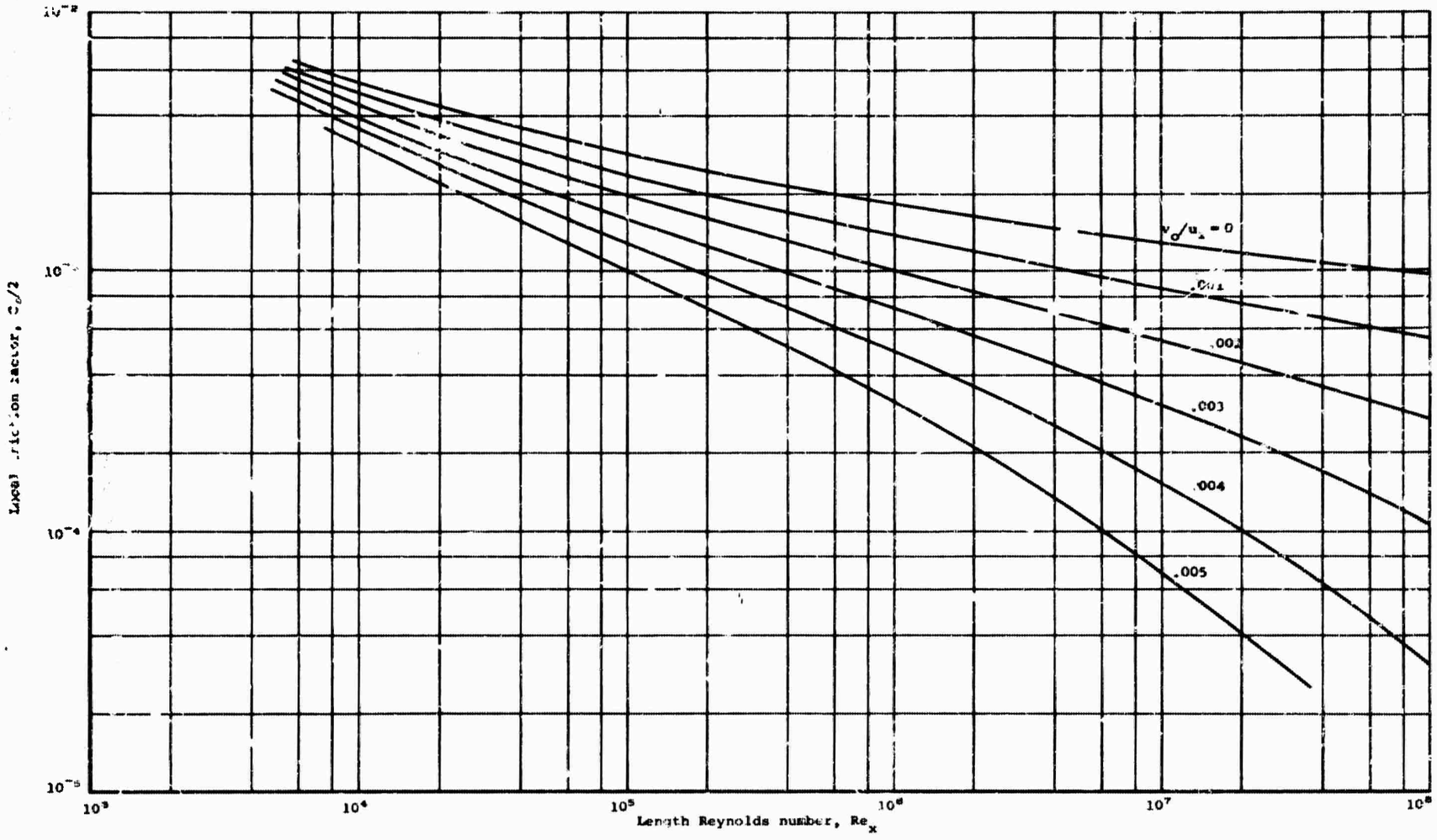

Figure 32.- Predicted friction factor with and without transpiration.

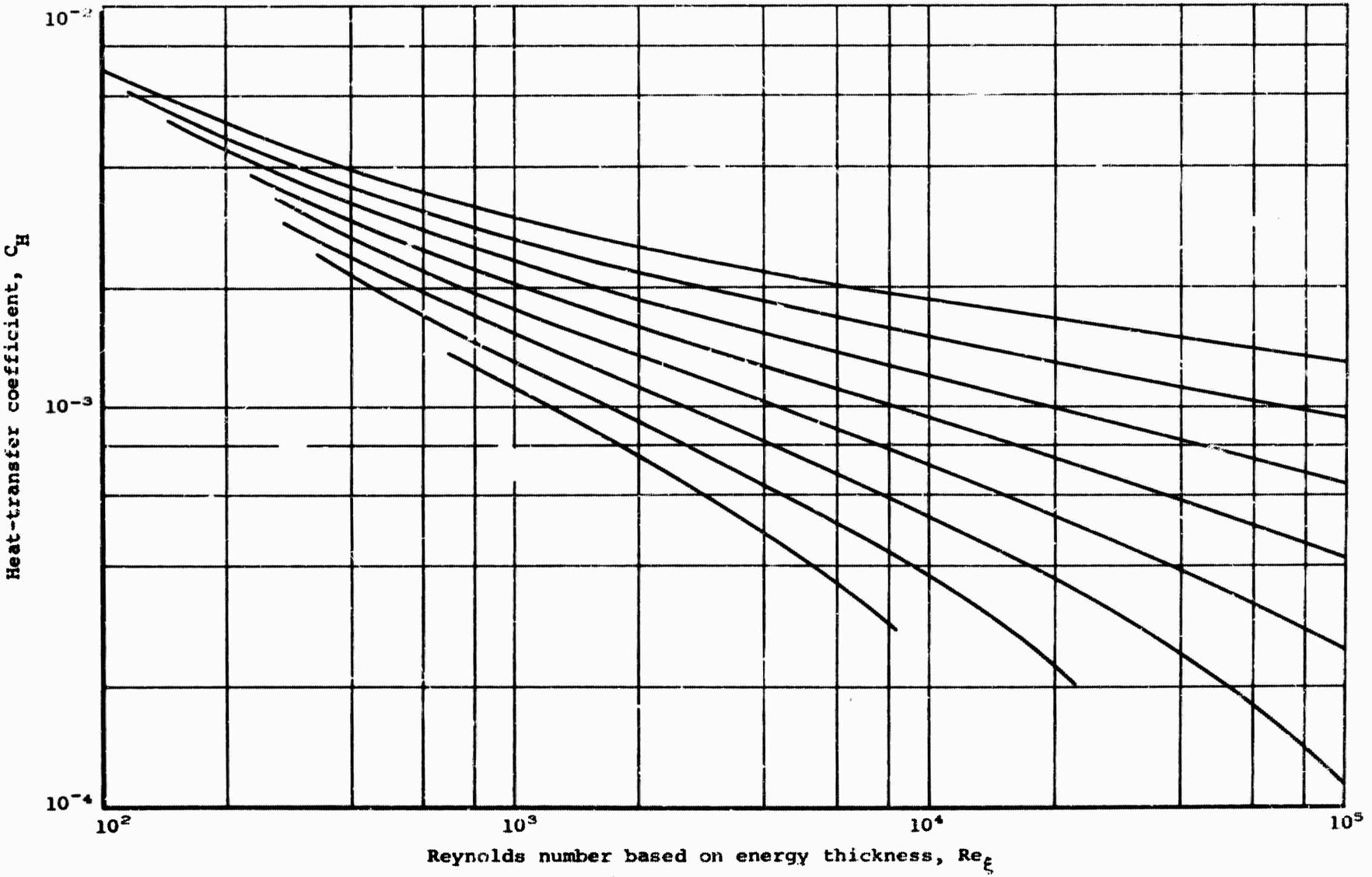

(a) Prediction.

Figure 33.- Heat-transfer coefficient with and without transpiration (Pr = 0.71, Pr' = 0.75).

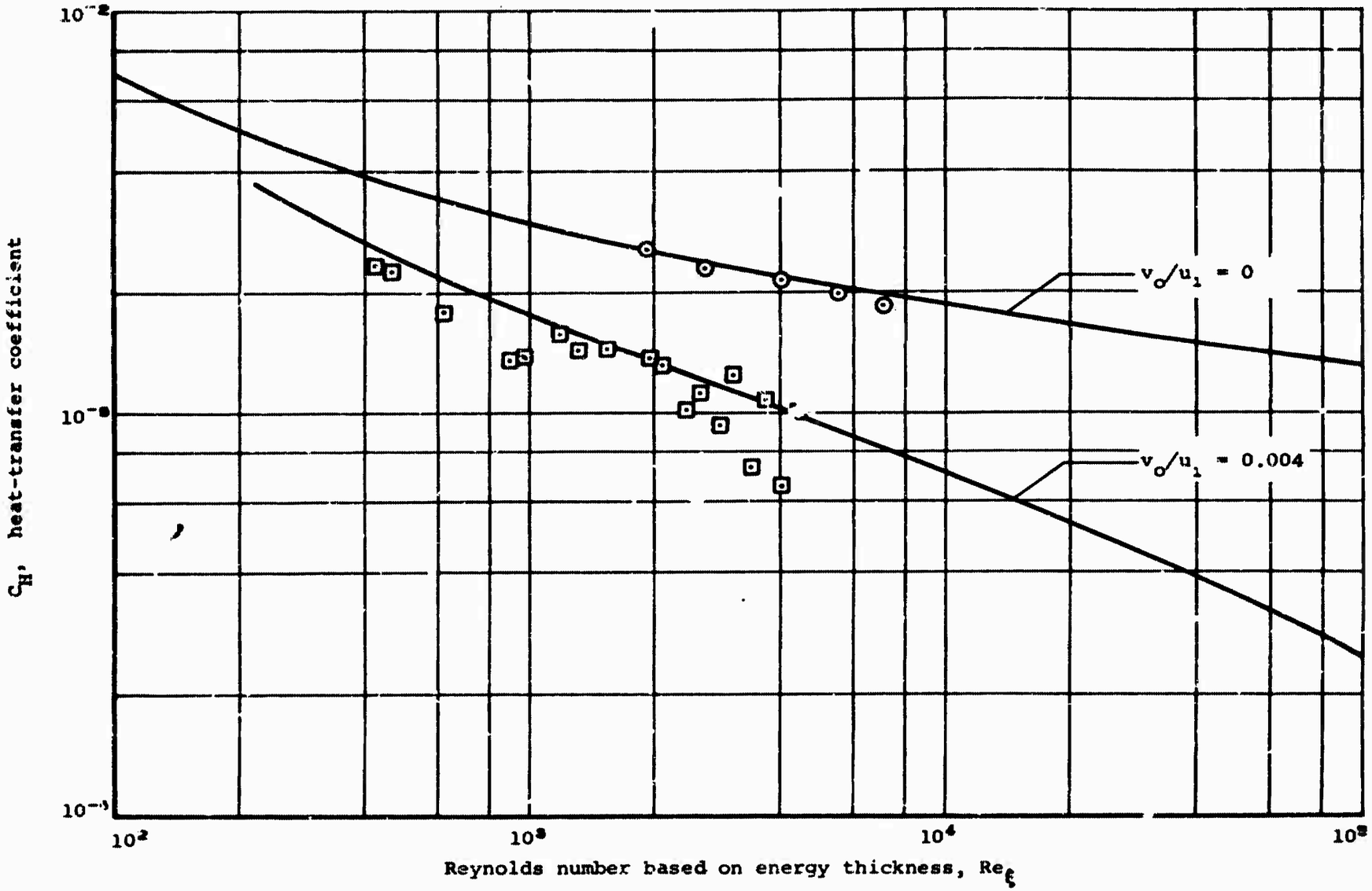

(b) Comparison with data of Reference 12.

Figure 33.- Concluded.

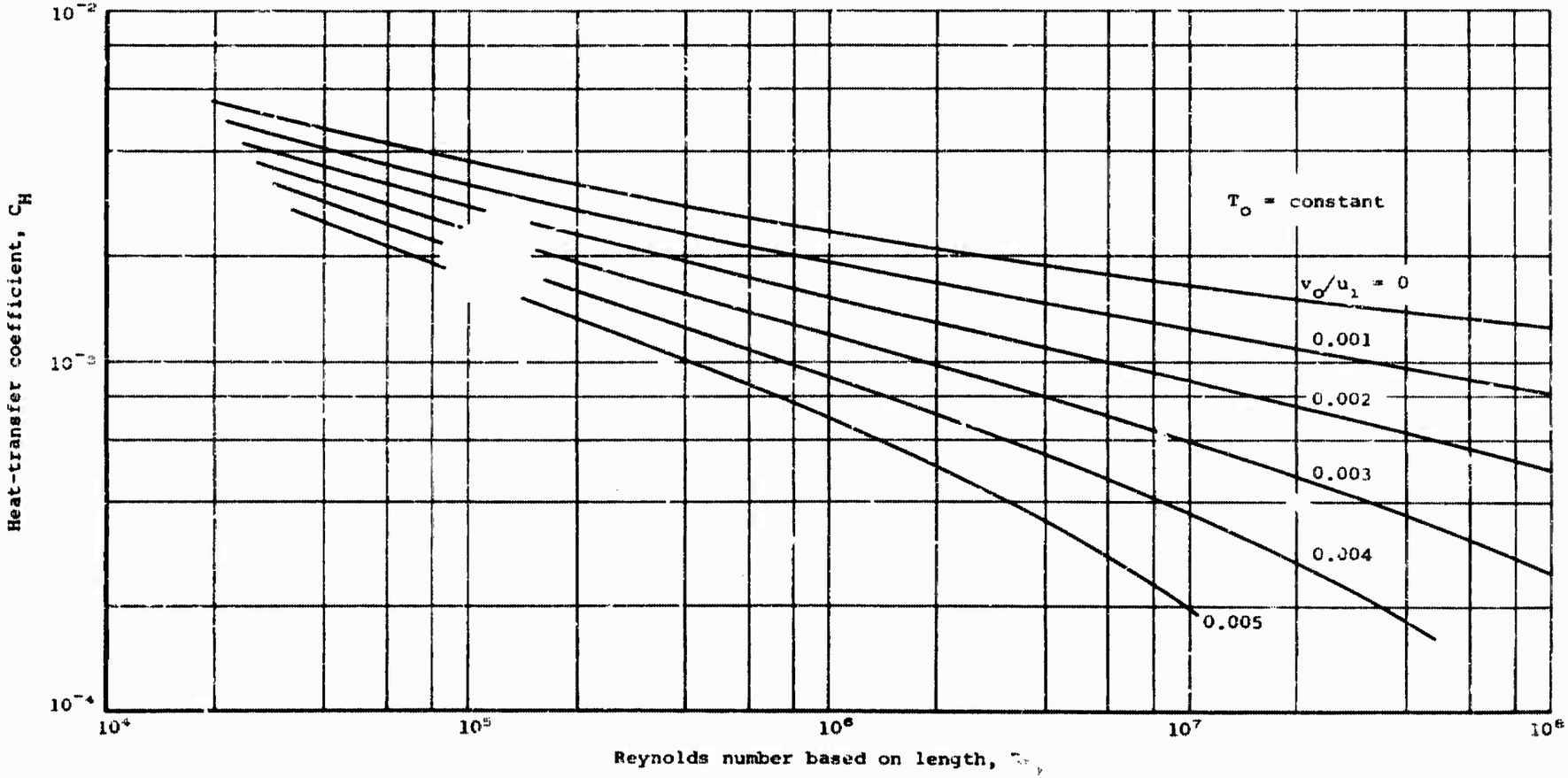

Figure 34.- Predicted heat-transfer coefficient with and without transpiration (Pr = 0.71, Pr' = 0.75).

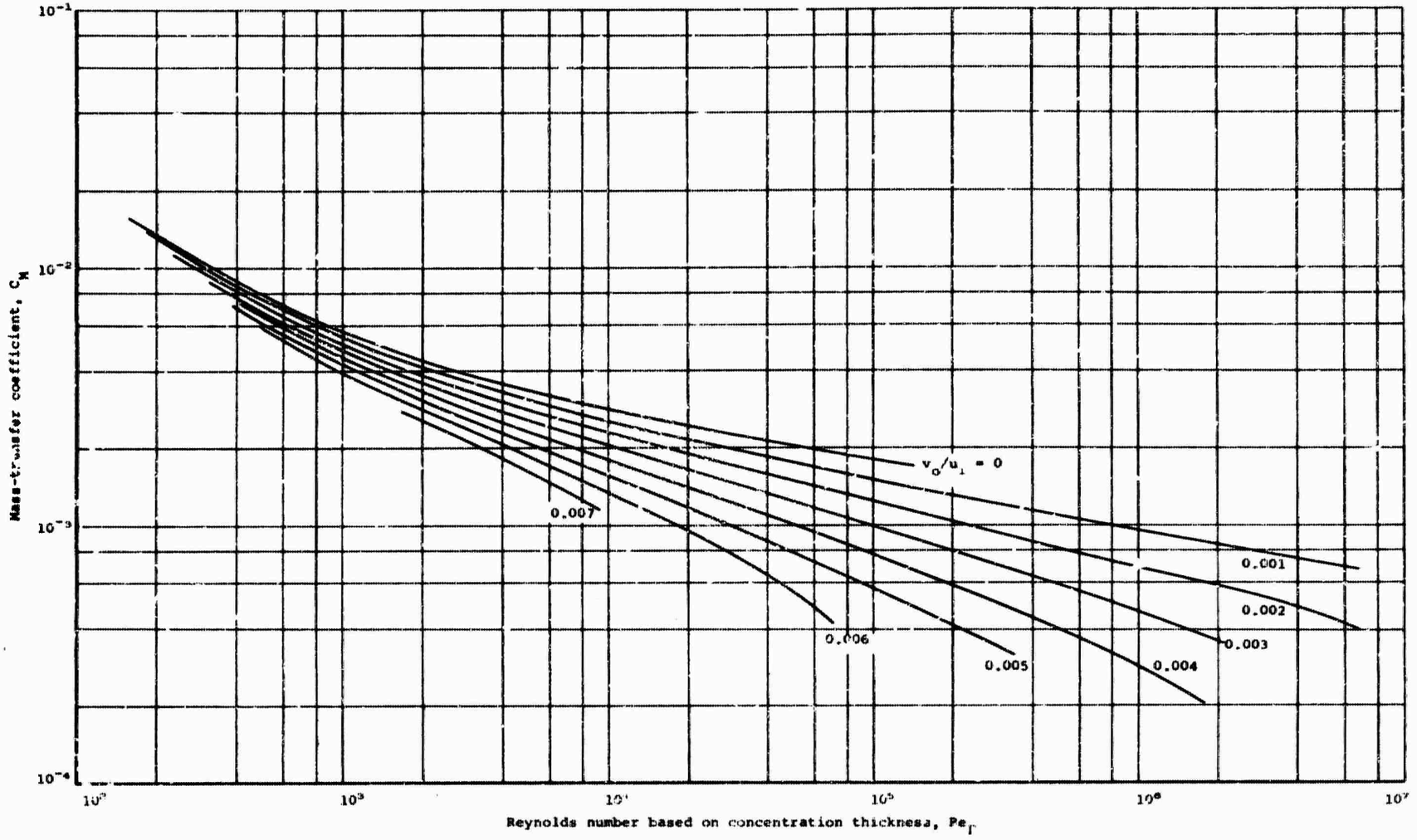

(a) Prediction.

Figure 35.- Mass-transfer coefficient (uniform transpiration, Sc = 0.2, Sc' = 0.75).

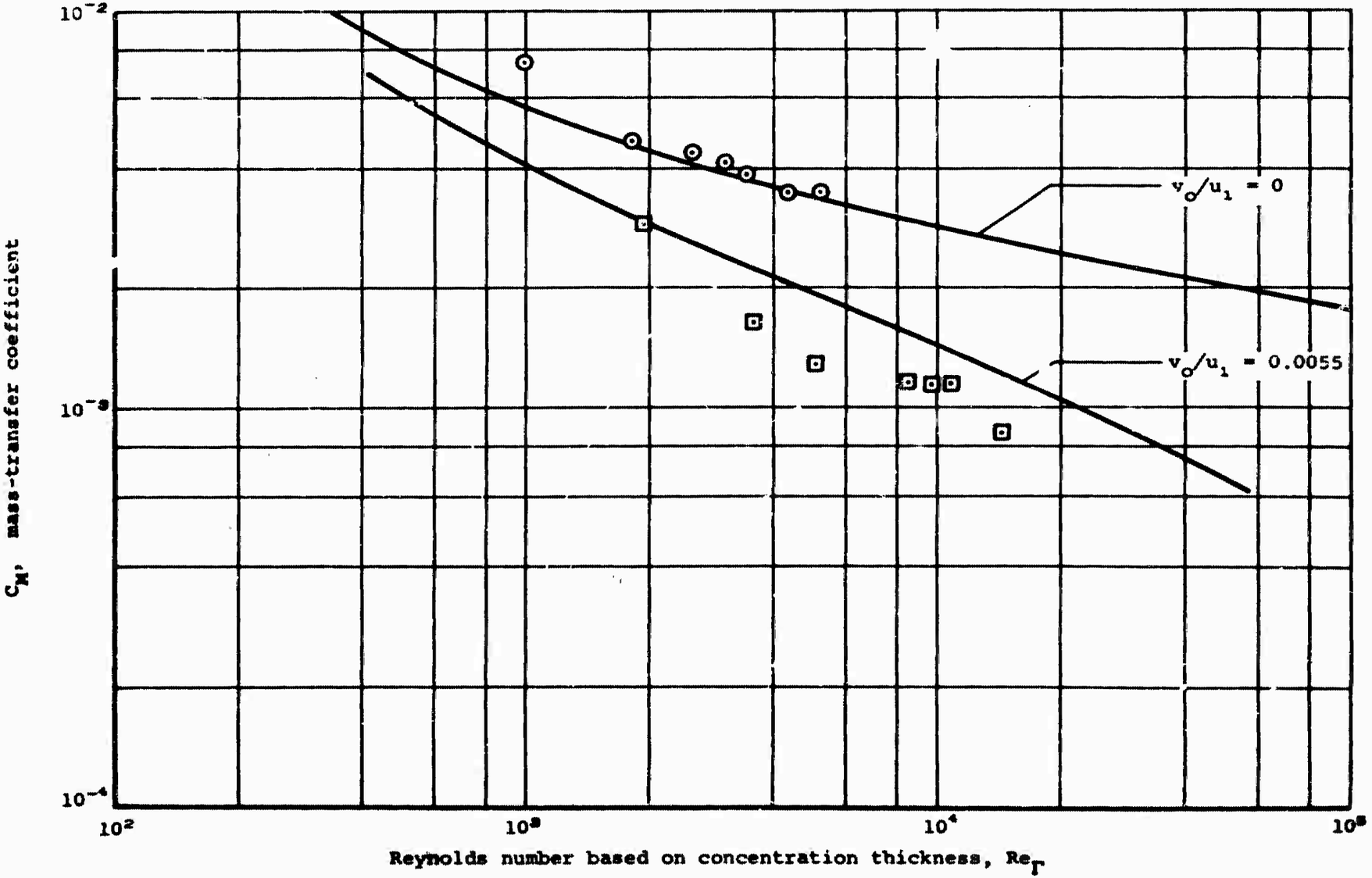

(b) Comparison with air-helium data of Reference 17.

Figure 35.- Concluded.

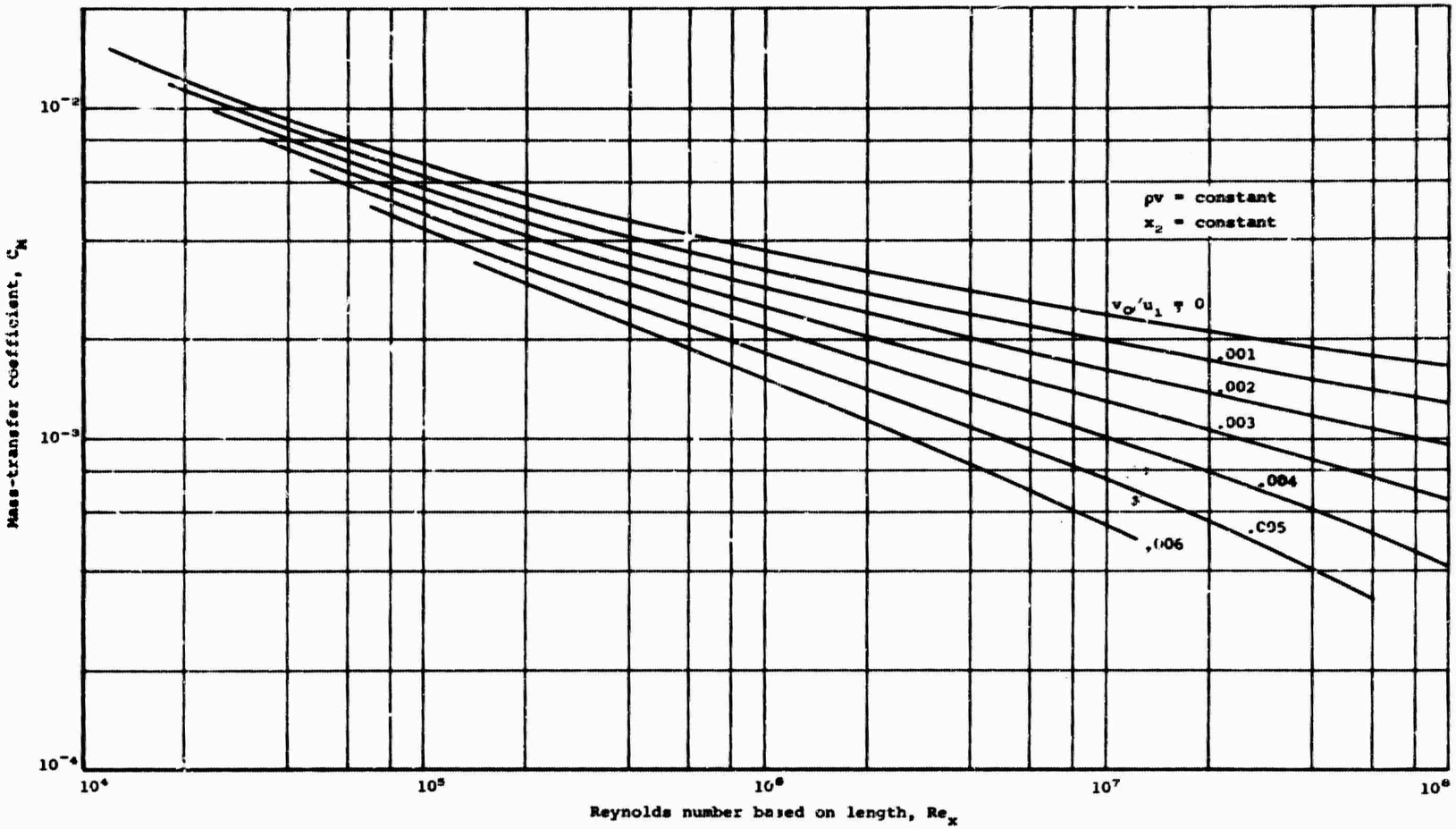

Figure 36.- Predicted mass-transfer coefficient with and without transpiration (Sc = 0.2, Sc' = 0.75).

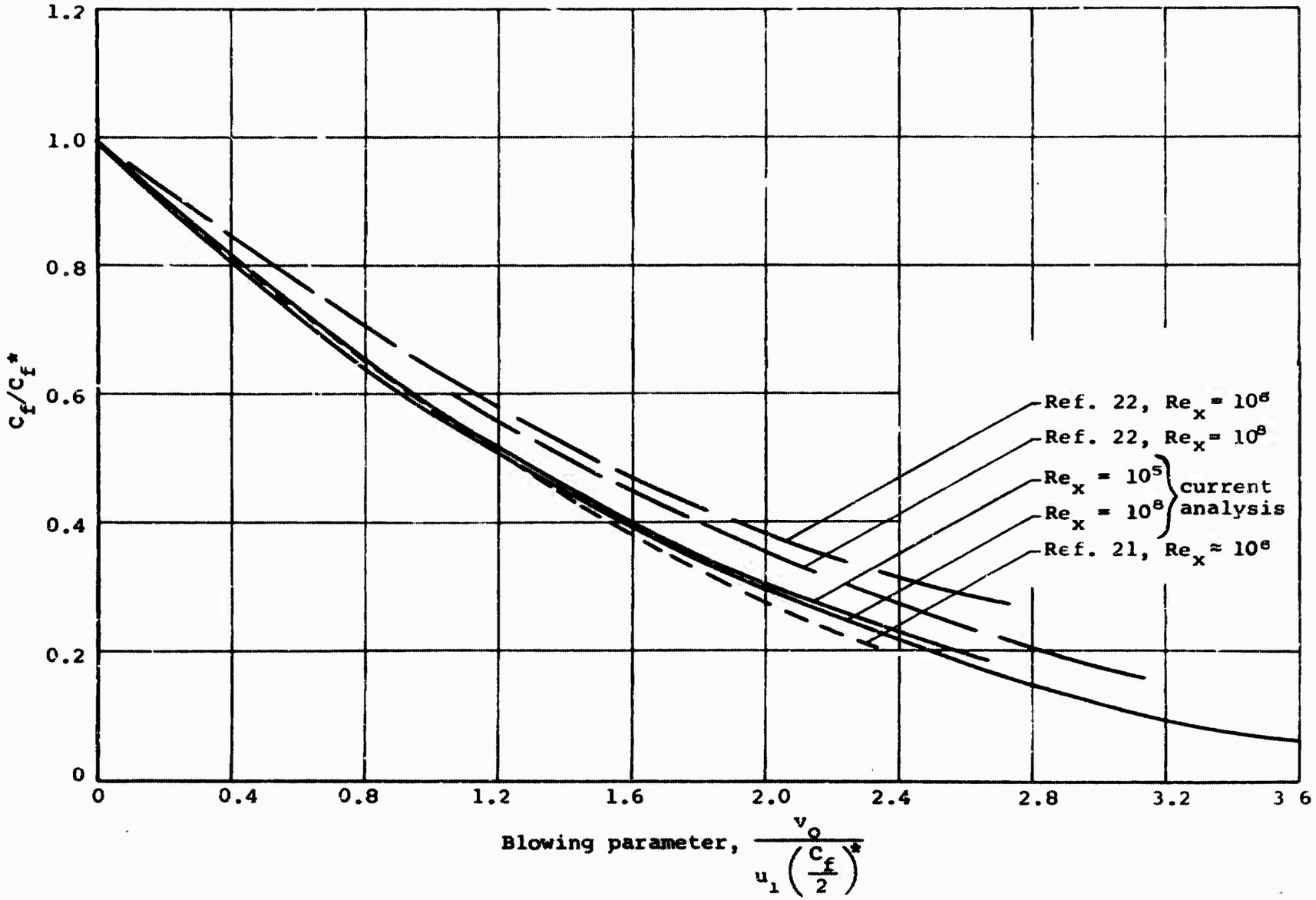

Figure 37.- Effect of surface mass transfer on the local skin friction at a constant length Reynolds number.

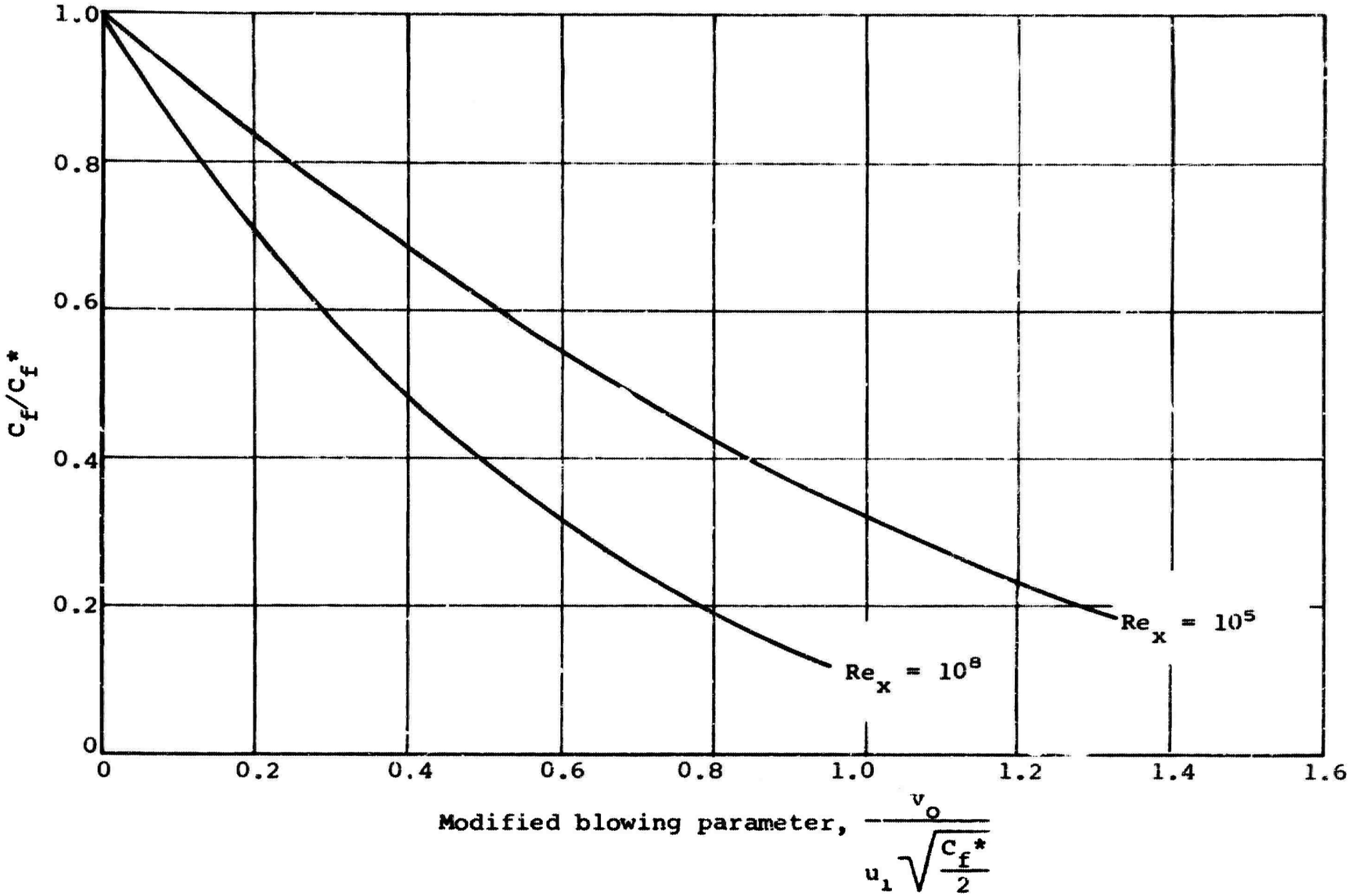

Figure 38.- Effect of surface mass transfer on the local skin friction at a constant length Reynolds number using modified blowing parameter.

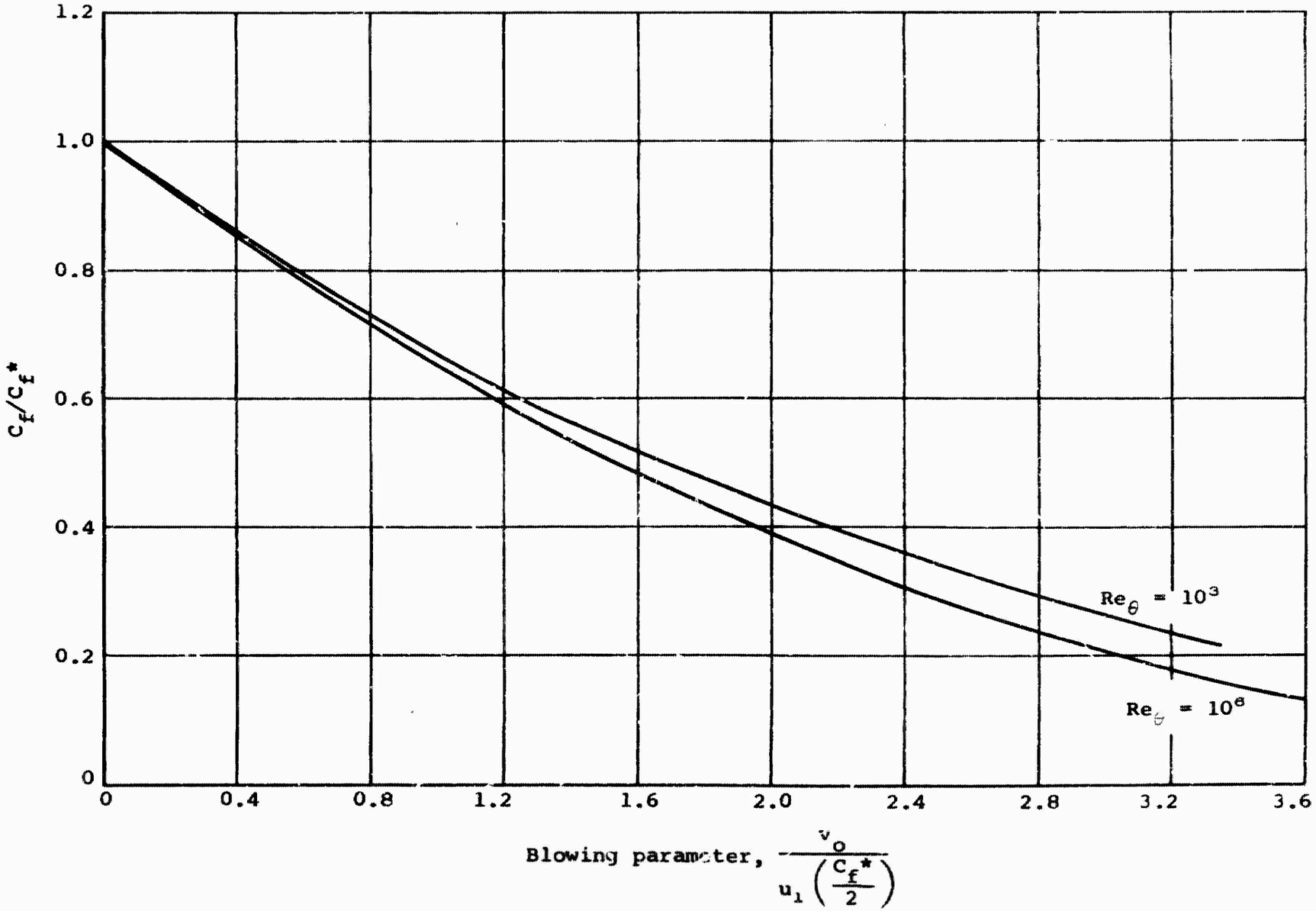

Figure 39.- Effect of surface mass transfer on the local skin friction at constant momentum thickness Reynolds numbers.

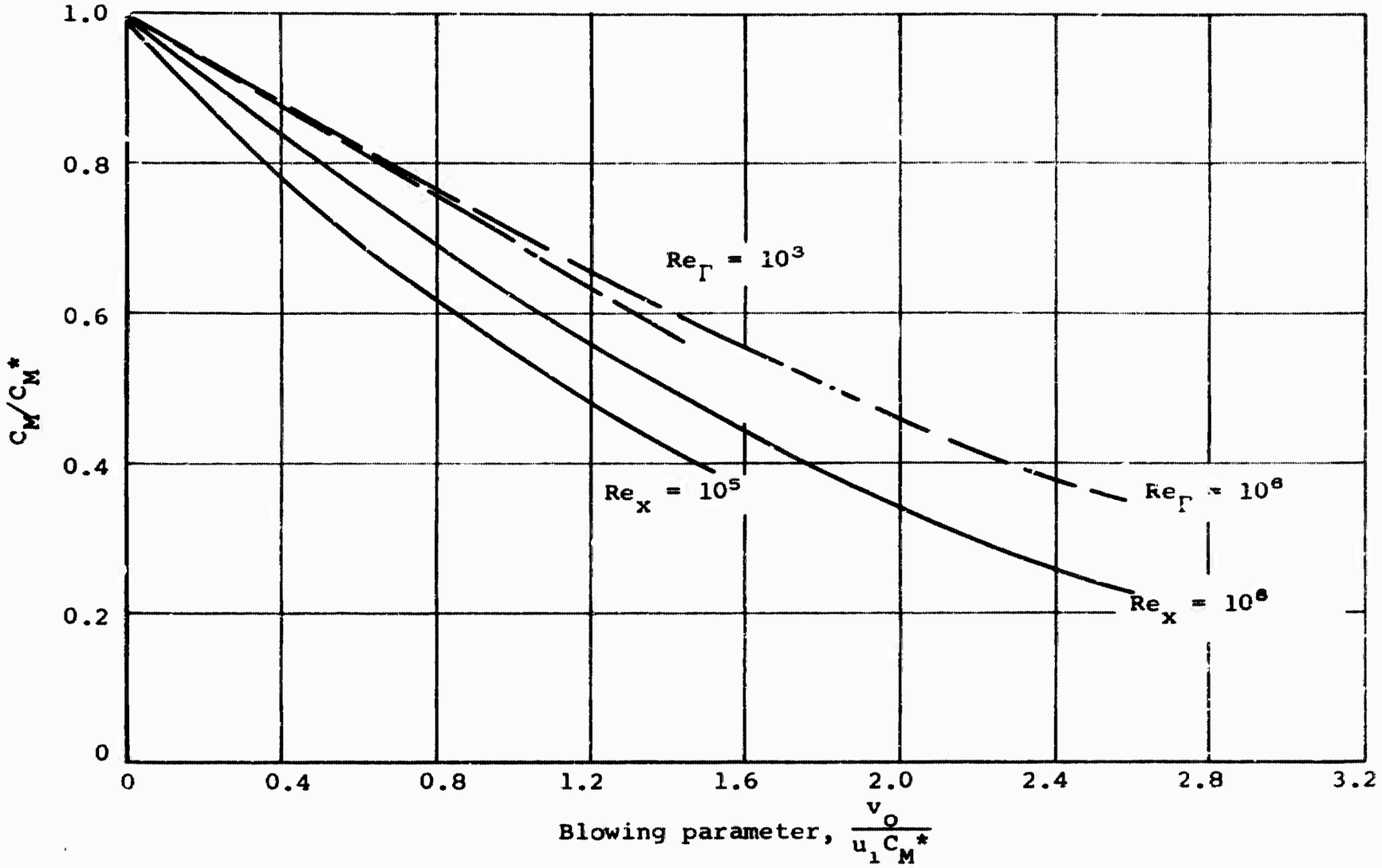

Figure 40.- Effect of surface mass transfer on the local mass-transfer coefficient.

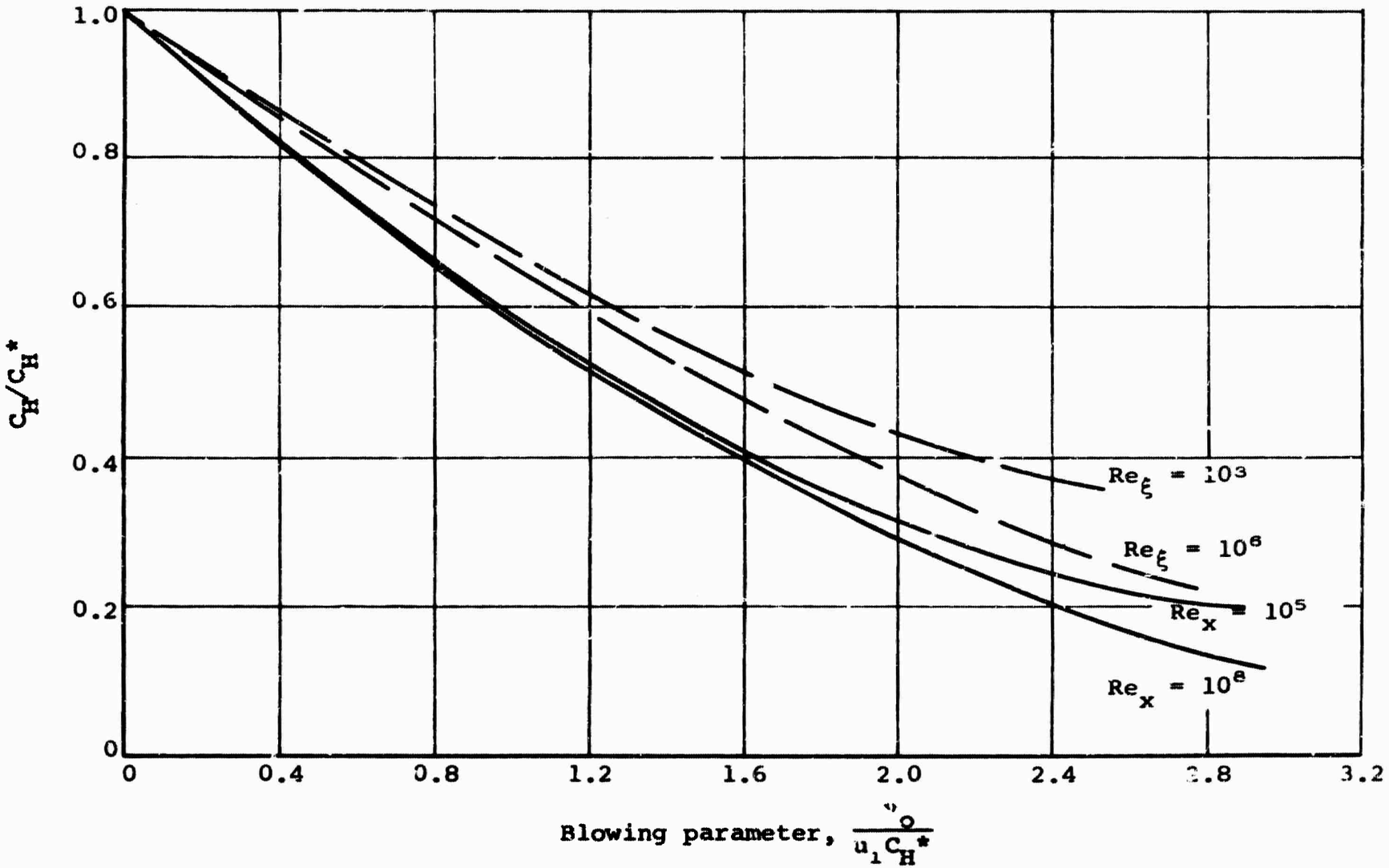

Figure 41.- Effect of surface mass transfer on the local heat-transfer coefficient.

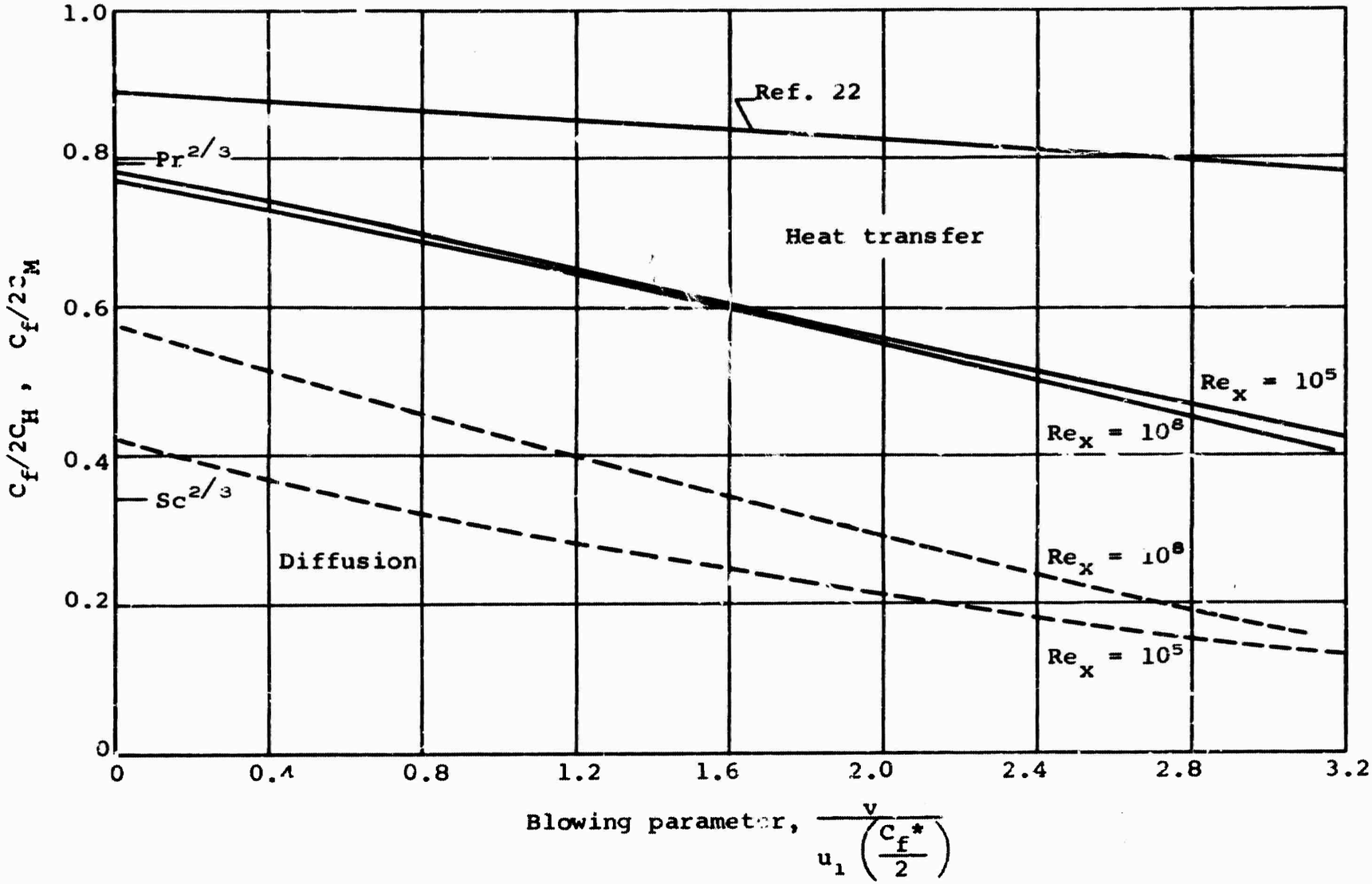

Figure 42.- Reynolds analogy for heat transfer and diffusion.

APPENDIX A

THE ELROD-REICHARDT CRITERION FOR THE DECAY OF TURBULENCE NEAR A WALL

Considerable emphasis has been placed in both the current analysis and other recent analyses on the continuous decay of turbulence as the wall is approached. Theoretically, it is possible to establish at least one constraint with regard to this decay. This criterion, herein referred to as the Reichardt-Elrod criterion (Refs. 41 and 47, respectively), has been derived for the case of the impervious wall and it is well that it be re-examined for the porous wall case.

For the incompressible boundary layer the turbulent shear is represented by $\overline{\rho u'v'}$ and it is the decay of this term in the proximity of the wall that is sought. This will be accomplished by evaluating successive derivatives of the term and noting their values at the wall. One supplemental relation is required, namely, the continuity equation relating the turbulent components of the three velocity vectors

$$\frac{\partial u'}{\partial x} + \frac{\partial v'}{\partial y} + \frac{\partial w'}{\partial z} = 0 \tag{A-1}$$

for constant density flow.

Proceeding with the differentiation yields successively

$$\overline{\frac{\partial u'v'}{\partial y}} = \overline{u' \frac{\partial v'}{\partial y}} + \overline{v' \frac{\partial u'}{\partial y}} \tag{A-2}$$

$$\frac{\partial^2 \overline{u'v'}}{\partial y^2} = \overline{u' \frac{\partial^2 v'}{\partial y^2}} + \overline{v' \frac{\partial^2 u'}{\partial y^2}} + 2 \overline{\frac{\partial u'}{\partial y} \frac{\partial v'}{\partial y}} \tag{A-3}$$

$$\frac{\partial^3 \overline{u'v'}}{\partial y^3} = \overline{u' \frac{\partial^3 v'}{\partial y^3}} + \overline{v' \frac{\partial^3 u'}{\partial y^3}} + 3 \overline{\frac{\partial^2 u'}{\partial y^2} \frac{\partial v'}{\partial y}} + 3 \overline{\frac{\partial u'}{\partial y} \frac{\partial^2 v'}{\partial y^2}} \tag{A-4}$$

The values of these derivatives will depend on certain assumptions with regard to the conditions at the wall. If it is presumed that $u' = v' = w' = 0$ at the wall, the continuity Equation (A-1) requires that $\partial v'/\partial y = 0$. It is immediately evident that first and second derivatives of the turbulent shear must vanish, as well as the first three terms of the expression for the third derivative. The remaining term can be rearranged by use of the continuity equation as follows:

$$\frac{\partial^3\overline{u'v'}}{\partial y^3} = 3\,\overline{\frac{\partial u'}{\partial y}\,\frac{\partial}{\partial y}\left(\frac{\partial v'}{\partial y}\right)} = -3\,\overline{\frac{\partial u'}{\partial y}\,\frac{\partial}{\partial y}\left(\frac{\partial u'}{\partial x}\right)} - 3\,\overline{\frac{\partial u'}{\partial y}\,\frac{\partial}{\partial y}\left(\frac{\partial w'}{\partial z}\right)}$$

$$= -3\,\overline{\frac{\partial u'}{\partial y}\,\frac{\partial}{\partial x}\left(\frac{\partial u'}{\partial y}\right)} - 3\,\overline{\frac{\partial u'}{\partial y}\,\frac{\partial^2 w'}{\partial y\partial z}}$$

$$= -3\,\frac{\partial}{\partial x}\,\overline{\left(\frac{\partial u'}{\partial y}\right)^2} - 3\,\overline{\frac{\partial u'}{\partial y}\,\frac{\partial^2 w'}{\partial y\partial z}}$$

The first term represents the streamwise variation of a mean flow property. At the wall such variations are usually small by comparison with gradients normal to the wall, and certainly will vanish under truly one-dimensional condition, for example, fully developed isothermal pipe flow. The second term represents a correlation between derivatives of u' and w', the two wall parallel components of the velocity. For two-dimensional flow, symmetry arguments indicate that the correlation $\overline{u'w'}$ must vanish. It is invalid, however, to draw any conclusions with regard to the value of the correlation of the derivatives. It can only be concluded that under conditions when variations of mean properties with the streamwise coordinate vanish at the wall and when two-dimensional flow symmetry exists, the third derivative of the turbulent shear may vanish.

It is interesting to consider this result in conjunction with the mixture length hypothesis

$$\overline{u'v'} = \ell^2\,\frac{du}{dy}$$

The first three derivatives of this expression are

$$\frac{d\overline{u'v'}}{dy} = \ell^2\,\frac{d^2u}{dy^2} + 2\ell\,\frac{d\ell}{dy}\,\frac{du}{dy}$$

$$\frac{d^2\overline{u'v'}}{dy^2} = \ell^2\,\frac{d^3u}{dy^3} + 4\ell\,\frac{d^2u}{dy^2}\,\frac{d\ell}{dy} + 2\left(\frac{d\ell}{dy}\right)^2\frac{du}{dy} + 2\ell\,\frac{d^2\ell}{dy^2}\,\frac{du}{dy}$$

$$\frac{d^3\overline{u'v'}}{dy^2} = \ell^2\,\frac{d^4u}{dy^4} + 6\ell\,\frac{d^3u}{dy^3}\,\frac{d\ell}{dy} + 6\ell\,\frac{d^2u}{dy^2}\,\frac{d^2\ell}{dy^2} + 6\left(\frac{d\ell}{dy}\right)^2\frac{d^2u}{dy^2} + 6\,\frac{d\ell}{dy}\,\frac{d^2\ell}{dy^2}\,\frac{du}{dy}$$

$$+ 2\ell\,\frac{d^3\ell}{dy^3}\,\frac{du}{dy}$$

From these expressions it is evident that both ℓ and $d\ell/dy$ must vanish at the wall if either the first two or three derivatives of the turbulent shear stress are to vanish at the wall. Thus, the mixture length hypothesis, by its very formulation, eliminates any option with regard to the value of the third derivative of the shear stress at the wall.

Therefore, the mixing length requirements used here are

$$\lim_{y \to o} \ell \to 0$$

$$\lim_{y \to o} \frac{d\ell}{dy} = 0$$

BLANK PAGE

APPENDIX B

INTERPRETATION OF FRICTION FACTORS FROM PITOT-PROBE READINGS AT AND NEAR THE WALL

It has long been realized that the experimental evaluation of friction factors under conditions of significant surface mass addition is extremely complex. The momentum equation

$$\frac{C_f}{2} = \frac{d\theta}{dx} - \frac{\rho_o v_o}{\rho_1 v_1} \tag{B-1}$$

although a good tool when rates of surface mass addition are low ($\rho_o v_o / \rho_1 v_1 < 0.002$), becomes useless at blowing ratios in excess of 0.003 for available experimental data. The order-of-magnitude differences between friction factors obtained in References 9 and 14 at a blowing ratio of 0.005 are ample demonstration of this fact. At this blowing ratio, the friction factor is less than 4 percent of the axial derivative of the momentum thickness. Thus, three-dimensional and time unsteady effects and errors associated with the differentiation of experimental data becomes excessive relative to $C_f/2$.

Because of this, an alternate technique was attempted in Reference 17. The technique involved the interpretation of total pressure measurements in a region sufficiently close to the wall that the laminar sublayer asserted a significant influence. By evaluation of this influence, friction factors were established hopefully independent of any empirical postulates about the character of turbulent momentum transport.

The basic assumptions involved in this technique in Reference 17 were two, namely:

(1) A pitot probe indicates a pressure equal to the average of the total pressures of the undisturbed incident flow over the frontal area of the probe. That is, if the total pressure distribution of the incident flow is represented by $P_T = f(y)$, then the indicated pitot-probe pressure will be

$$P_P \approx \int_{y_p - d_p/2}^{y_p + d_p/2} P_T \, dy \tag{B-2}$$

where y_p is the distance from the wall to the probe midplane and d_p is the probe thickness.

(2) That the velocity (or total pressure) profile approaches the wall according to the laminar sublayer relation; which for constant property flow is

$$\frac{u}{u_1} = \frac{C_f/2}{v_o/u_1}\left[e^{(v_o/u_1)Re_y} - 1\right] \qquad \text{(B-3)}$$

and that turbulence affects this profile, at increasing distances from the wall, in a well-behaved and reasonably monatonic fashion.

The validity of the first assumption cannot be verified since no exact calculations are known for flow about a probe near a wall. The principle verification is based on experimental results to be presented in a subsequent paragraph of this appendix. The second "assumption" is logically acceptable without further defense based on the experimental evaluations of the turbulent boundary layers reported in References 48 and 49.

In addition to the evaluation of these assumptions, two areas of evaluation remain with regard to the overall technique. These are:

(1) The accuracies of the input measurements, namely, P_p, y_p, d_p, and v_o/u_1, and their effects on the interpreted friction factor.

(2) The sufficiency of the given data and assumptions; that is, given the data and assumptions, is a unique value of the friction factor clearly established?

It is this final point which is the principal concern of the evaluations described in this appendix. In Reference 17, the establishment of the friction factor was based on hand fitting of the data in light of Equations (B-2) and (B-3) (see Figs. 17 through 31 of that ref.). It has been contended that this process is quite arbitrary and thus does not yield any valid measure of friction factor. However, independent application of the technique to the same data by different investigators has resulted in relatively consistent results.

In an effort to further assess the uniqueness of the technique, several <u>analytical</u> relations were postulated for the velocity (or total pressure) profile and the arbitrary constants (including C_f) of these relations were varied over a fairly broad range. For each set of constants the distribution

$$P_T = f(y)$$

was obtained and the right-hand side of Equation (B-2) was evaluated for the probe locations corresponding to experimentally measured values of P_p. The sum of the absolute values of the resultant errors was taken as the measure of merit of the postulated arbitrary constants.

Three functions were postulated. These were:

$$(1)\quad Re_y = \ell n\left(1 + \frac{v_o/u_1}{C_f/2}\cdot\frac{u}{u_1}\right) \qquad 0 < Re_y < Re_{limit} \tag{B-4}$$

$$Re_y = a(P_T - P_s)^3 + b(P_T - P_s)^2 + c(P_T - P_s) + d \qquad Re_y > Re_{limit} \tag{B-5}$$

$$(2)\quad Re_y = \ell n\left(1 + \frac{v_o/u_1}{C_f/2}\,\frac{u}{u_1}\right) + b\left(e^{au} - 1 - au - \frac{a^2u^2}{2} - \frac{a^3u^3}{6}\right) \tag{B-6}$$

$$(3)\quad Re_y = \ell n\left(1 + \frac{v_o/u_1}{C_f/2}\,\frac{u}{u_1}\right) + b\left(e^{au} - 1 - au - \frac{a^2u^2}{2} - \frac{a^3u^3}{6} - \frac{a^4u^4}{24}\right) \tag{B-7}$$

where P_s is the static pressure and $(P_T - P_s) \propto u^2/2$ for constant property flow.[1] For the first relation the first derivative of the profile was made continuous at the laminar limit Reynolds number, Re_{limit}. The last two relations are based on the Spalding postulates (Ref. 53) for describing turbulent velocity profiles and the Elrod constraint described in Appendix A.[2] The set of data in Table B-1 was selected (at random) from Reference 17 for comparison with these relations (Run C-5·10^{-3}-50, Station L). The final point was used as an anchor point for the postulated relations, the other four being used to evaluate the errors for a range of values of the remaining arbitrary constants. For each set of arbitrary constants the errors were determined at each of the four points, and the sum of their absolute values obtained. This sum is plotted in Figures B-1 through B-3 for the three enumerated relations, isolating the arbitrarily assigned values of $C_f/2$ for the abscissa. In each case a relatively distinct minimum is obtained in the range of $C_f/2$ between

---

[1] The u in Equations (B-4) through (B-7) should be considered as equal to $\sqrt{\overline{u}^2}\,(= \overline{u} + \sqrt{u'u'})$. Thus, the constants of the Spalding type relations, for example, would not be expected to be the same as those reported in Ref. 53.

[2] Relations 2 and 3 are consistent with the first two and first three derivatives of the turbulent shear being zero at the wall, respectively.

0.00017 and 0.00019. The value reported in Reference 17 for this station was 0.00018.

Based on the above results it seems valid to accept the technique as providing a unique value of $C_f/2$ independent of the postulated profile relation. Therefore, subsequent evaluations will use only one technique (namely, Eq. (B-6)) for the various tests to be performed.

Rather than continue the rather awkward procedure of cut and try involved in the above technique, a least-square curve fit procedure was devised that automatically and simultaneously evaluated those values of a,b and $C_f/2$ which produced the least-square error of Equation (B-2). The procedure, although iterative, converged rapidly and produced excellent data fits. For the case previously considered, Figure B-4 shows the solution obtained, its integration according to Equation (B-2), and the comparison of this analytical curve with the measured pitot pressures.

A number of tests were performed to demonstrate the sensitivity of the technique to inaccuracies in the requisite experimental parameters. Table B-II summarizes these tests.

It is apparent from Table B-II that no major amplification of the errors in the basic measurements occurs when the friction factor is evaluated. This is in contrast with the momentum equation technique where violent error amplification occurs at high rates of surface mass addition.

Having adopted an analytical expression for the velocity profile the next step in this evaluation study was to reevaluate (with the least-square curve fit program) all the friction factors reported in Reference 17. These values are presented in Table B-III. These values differ only slightly from the originally reported values.

Probably the most significant test of the overall technique is provided by comparison of values of $C_f/2$ obtained without mass addition with those generally reported in the literature and those obtained by use of the momentum equation using the data of Reference 17. This comparison is shown in Figure 16 where it can be concluded that the procedure does indeed perform a creditable job. It is significant to note that with increasing surface mass addition, the total pressure gradient is significantly reduced near the wall and thus the validity of Equation (B-2) becomes <u>less</u> susceptible to question. That is, if the technique, and by inference Equation (B-2), is valid when there is no surface mass addition, it should still be valid when there is surface mass addition.

It would seem, based on the evaluations described above, that friction factors can be obtained through interpretation of pitot-probe measurements at and near the wall, and further, that the technique involved does not degenerate as rates of surface mass addition are increased.

BLANK PAGE

TABLE B-I

DATA USED TO TEST FRICTION EVALUATION PROCEDURES UTILIZING PROFILES (B-4) THROUGH (B-7)

Re_y	$\frac{P_p - P_s}{P_{p_1} - P_s}$
197	0.0086
197	0.0086
270	.0172
393	.0346
516	.0493
761	.0702

TABLE B-II

SENSITIVITY OF FRICTION FACTOR TO INACCURACIES OF PROFILE PARAMETER

Factor		Nominal Value	Perturbation		Friction Factor	
			Value	Change (%)	Value	Change* (%)
v_o/u_1		0.00538	0.006	11.5	0.000168	- 9.2
Probe height		.16	.018	12.5	.000159	-14.1
Scale shift in y		0	.002	--	.000131	-29.2
Probe pressure (in. of heptane) at y_p =	0.008 in.	.007	.009	28.6	.000212	14.6
	.011 in.	.014	.016	14.3	.000207	11.9
	.016 in.	.028	.030	7.1	.000189	2.2
	.021 in.	.040	.042	5.0	.000171	- 7.6
	.031 in.	.057	.059	3.5	.000190	2.7

*Nominal value of friction factor = 0.00185.

TABLE B-III

FRICTION FACTORS INTERPRETED FROM PITOT PRESSURE PROFILES ADJACENT TO THE WALL

Run	Station	$C_f/2$ ($\times 10^3$)		v_o/u_1 ($\times 10^3$)	Re_θ	Re_x ($\times 10^{-6}$)
		From Ref. 17	Least-Square Fit			
C-10^{-4}-50	D	2.5	2.77	0.1098	686	0.130
	E	2.4	2.81	.1192	931	.249
	G	1.75	1.76	.1076	1332	.490
	H	1.95	1.89	.1133	1730	.684
	I	1.6	1.67	.1140	2011	.893
	J	1.75	1.75	.1203	2433	1.083
	K	1.45	1.56	.1203	2820	1.375
	L	1.6	1.58	.1184	3377	1.658
C-10^{-3}-50	E	1.85	2.35	1.129	1063	.248
	G	1.5	1.49	1.122	1573	.490
	I	1.35	1.25	1.129	2416	.887
	I'	1.35	1.30	1.120	2472	.895
	K	1.25	1.17	1.118	3581	1.388
	L	1.25	1.51	1.032	4308	1.678
	M	1.1	1.13	1.080	4873	2.007
	N	1.1	1.08	1.076	5839	2.290
C-2×10^{-3}-50	E	1.47	1.97	2.22	1237	.252
	G	1.21	1.18	2.17	1903	.499
	H	1.1	1.30	2.16	2533	.695
	I	1.05	.92	2.19	2990	.906
	J	.96	1.10	2.15	3704	1.102
	K	.91	.82	2.30	4350	1.312
	L	.89	.94	2.13	5435	1.670
	M	.84	.80	2.19	6314	2.002
	N	.80	.82	2.21	7482	2.304
C-3×10^{-3}-50	E	1.25	1.55/1.61	3.23	1351	.248
	G	1.0	1.18	3.25	2270	.492
	H	.90	.98	3.21	2967	.681
	J	.64	.65	3.27	4510	1.083
	K	.58	.54	3.26	5453	1.381
	L	.58	.63	3.26	6725	1.665
	M	.46	.44	32.5	7886	1.987
	N	.46	.48	3.22	9506	2.230
C-5×10^{-3}-50	E	.68	0.86/0.90	5.43	1740	.254
	G	.41	.49	5.42	2960	.504
	H	.36	.42	5.40	4020	.698
	J	.21	.19	5.57	6170	1.110
	K	.18	.19	5.42	7740	1.410
	L	.18	.19	5.38	9800	1.700
	M	.16	.18	5.37	13900	2.037

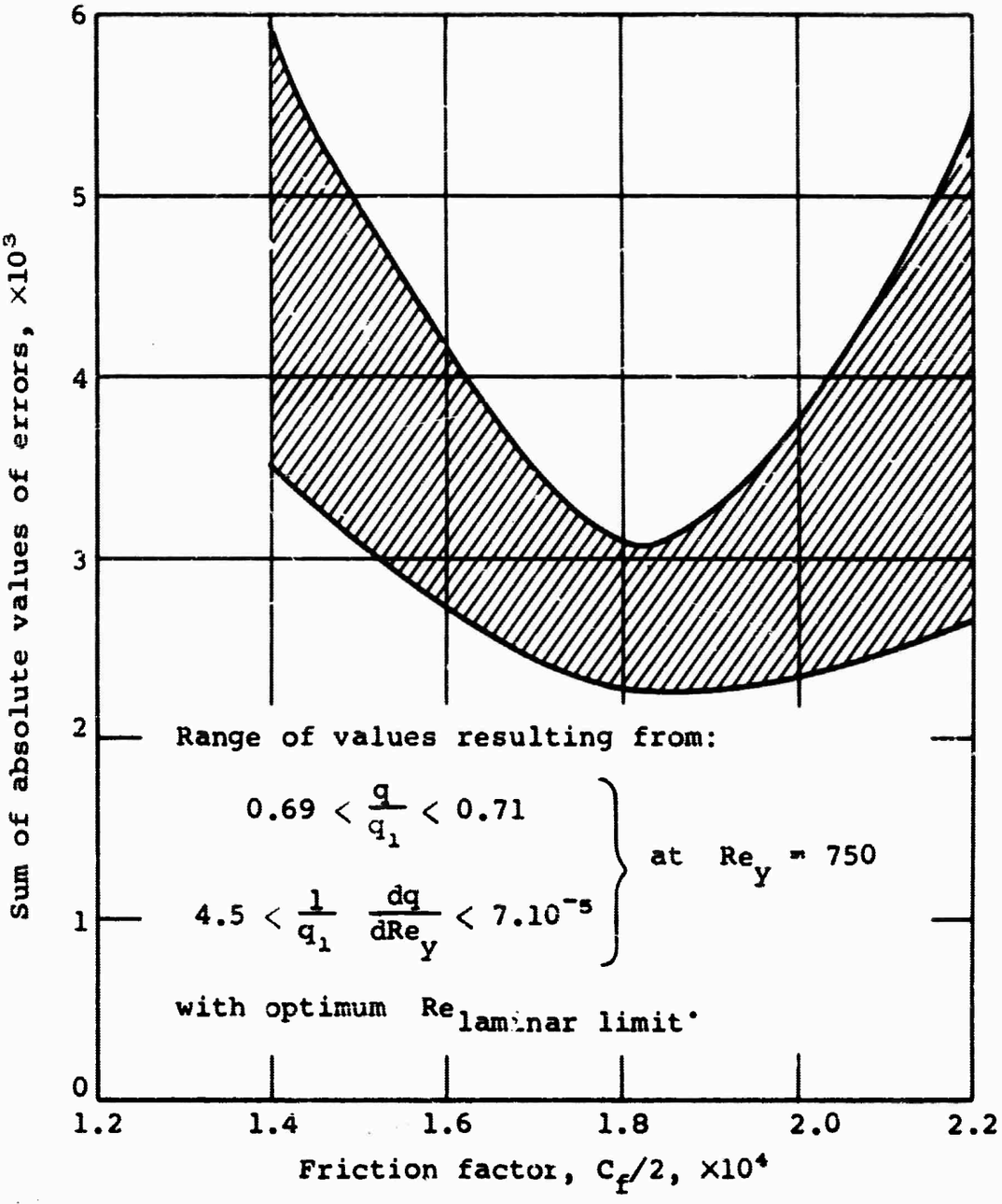

Figure B-1.- Effect of varying arbitrary constants of Equation (B-5) on the resultant error of Equation (B-2) for the measured data points of Table B-1.

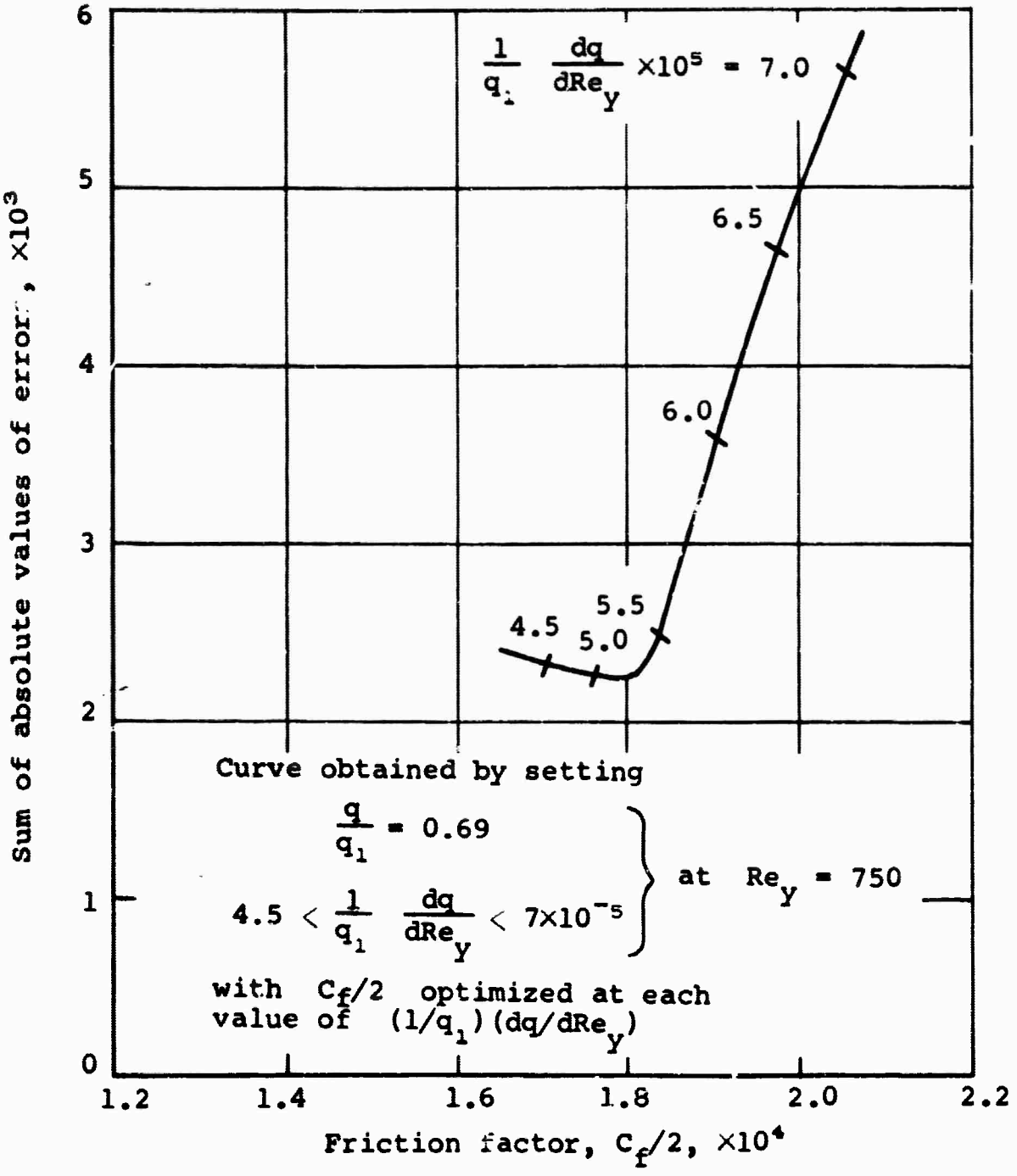

Figure B-2.- Effect of varying arbitrary constants of Equation (B-6) on the resultant error of Equation (B-2) for the measured data points of Table B-1.

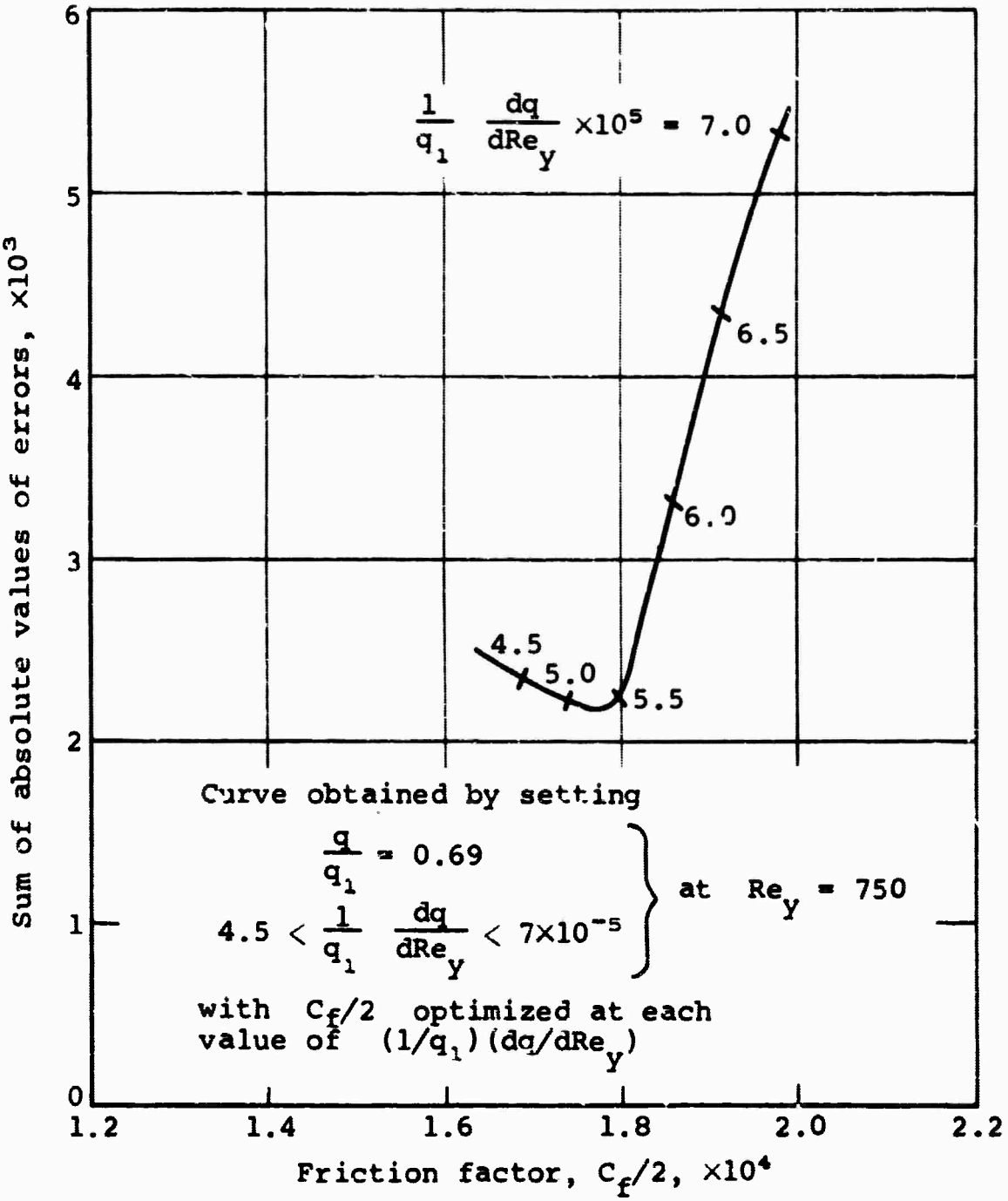

Figure B-3.- Effect of varying arbitrary constants of Equation (B-7) on the resultant error of Equation (B-2) for the measured data points of Table B-1.

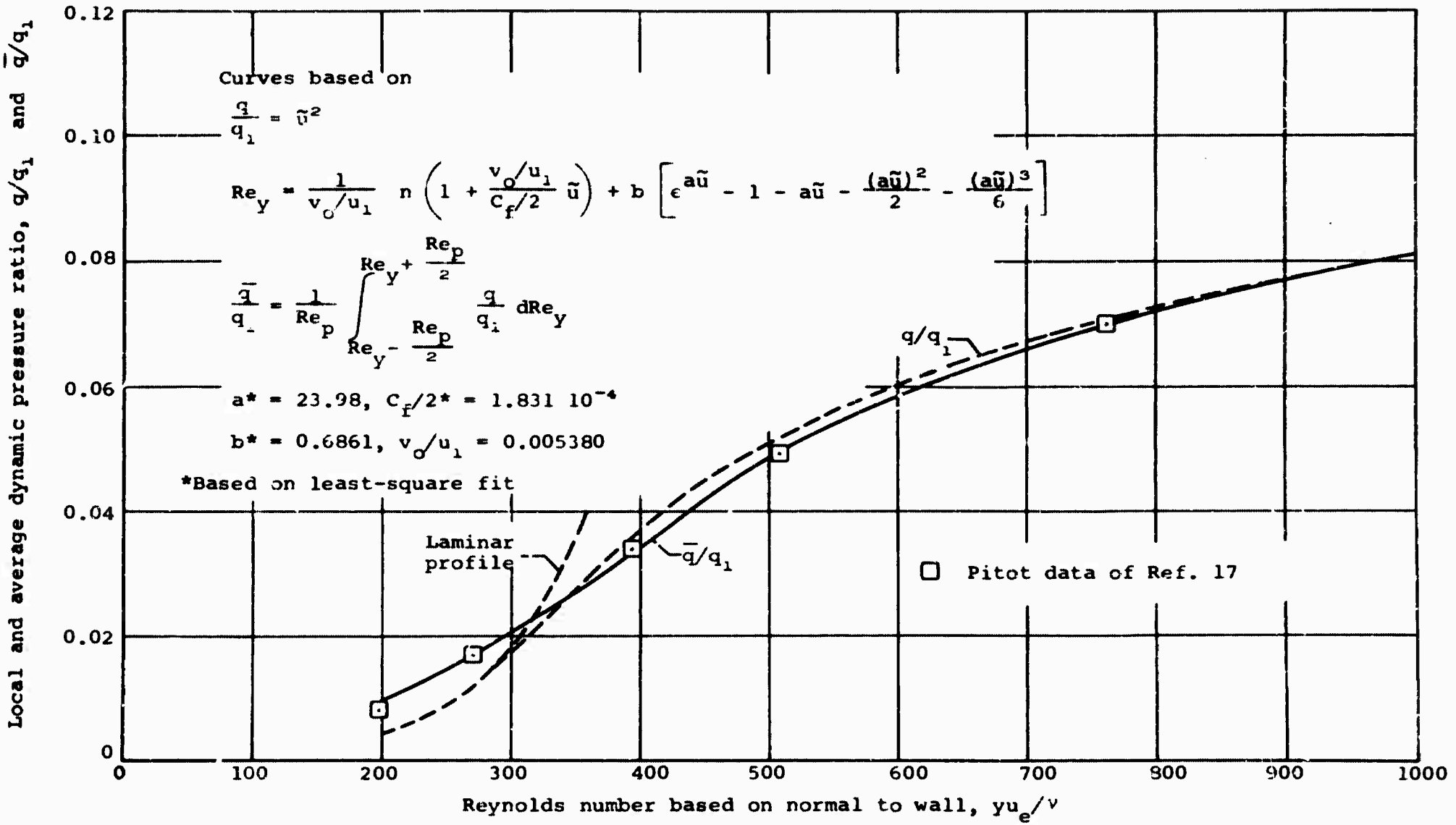

Figure B-4.- Technique for establishing local skin friction from dynamic pressure measurements through least square fit.